A STUDY OF JET IMPINGEMENT ON CURVED SURFACES FOLLOWED BY OBLIQUE INTRODUCTION INTO A FREESTREAM FLOW

SECOND ANNUAL REPORT UNDER NASA

GRANT NGR 43-002-034

VANDERBILT UNIVERSITY

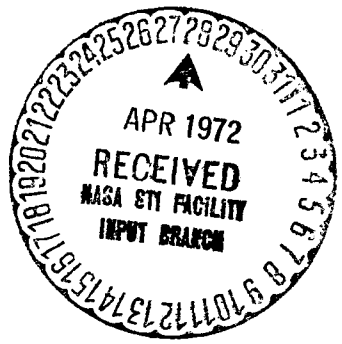

JOHN W. TATOM
NORMAN M. SCHNURR
JOHN W. WILLIAMSON
JOHN H. DUNLAP

DEPARTMENT OF MECHANICAL ENGINEERING
SCHOOL OF ENGINEERING

MARCH 29, 1972

TABLE OF CONTENTS

Title		Page
1.	SUMMARY	1
2.	INTRODUCTION	2
3.	OPPOSING JET STUDY	3
3.1	THE TWO-DIMENSIONAL TRANSVERSE JET	3
3.1.1	Previous Related Studies of the Plane Transverse Jet	4
3.1.2	Experimental Program-General Discussion	5
3.1.3	Equipment	7
3.1.4	Discussion of Results	13
3.1.4.1	General	13
3.1.4.2	The Data-Test Difficulties and Repeatability	13
3.1.4.3	Test Results	16
3.1.4.4	Data Correlation	43
3.1.5	Conclusions	49
3.2	THE DEFLECTED RADIAL PLANE JET	50
3.3	ANALYTICAL INVESTIGATION OF INGESTION - NO CROSSWIND	54
3.4	BLOWN FLAP/THRUST REVERSER MODEL	58
4.	IMPINGING JET STUDY	62
4.1	ANALYTICAL INVESTIGATION	62
4.1.1	The Impingement of a Round Jet on an Axisymmetric Surface of Arbitrary Shape	63

A STUDY OF JET IMPINGEMENT ON CURVED SURFACES FOLLOWED BY OBLIQUE INTRODUCTION INTO A FREESTREAM FLOW

Second Annual Status Report Under

NASA Grant NGR 43-002-034

For Period: February 1, 1971 to January 31, 1972

Submitted by:

John W. Tatom
Assistant Professor
Mechanical Engineering
Vanderbilt University
Principal Investigator

Norman M. Schnurr
Associate Professor
Mechanical Engineering
Vanderbilt University
Faculty Associate

John W. Williamson
Associate Professor
Mechanical Engineering
Vanderbilt University
Faculty Associate

John H. Dunlap
Associate Professor
Mechanical Engineering
Vanderbilt University
Faculty Associate

Date Submitted:

Title		Page
4.1.2	The Effects of Compressibility	64
4.1.3	The Effects of Geometry on Reverser Performance ..	71
4.2	EXPERIMENTAL INVESTIGATION	81
4.2.1.	Experimental Results of the Cascade Reverser/ Blown-Flap Model	81
4.2.2	Experimental Results of the Wedge-Shaped Deflector Model	84
5.	PLANNED FURTHER WORK	97
APPENDIX A	TRANSVERSE JET TEMPERATURE AND VELOCITY DATA	98
APPENDIX B	COMPUTER LISTING AND SAMPLE OUTPUT - CIRCULAR JET IMPINGING ON CURVED SURFACE ..	121
REFERENCES		138

LIST OF FIGURES

Figure No.	Title	Page
3.1	Summary of Test Conditions	6
3.2	Schematic Diagram of Experimental Equipment ...	8
3.3	Electrical Equipment	9
3.4	Model and Probe in the Wind Tunnel	9
3.5	Centerline Temperature Trajectories of 90° Jet ..	18
3.6	Centerline Temperature Trajectories of 120° Jet ..	19
3.7	Centerline Temperature Trajectories of 135° Jet - Effects of Suction	20
3.8	Centerline Temperature Trajectories of 135° Jet - Effects of Inlet-to-Jet Spacing	21
3.9	Centerline Temperature Trajectories of 150° Jet ..	22
3.10	Non-dimensional Temperature Plots for 90° Jet, Without Inlet Suction, VR = 10	24
3.11	Jet Vector Field for 90° Jet, Without Inlet Suction, VR = 10	26
3.12	Isotherms for 90° Jet, VR = 10	27
3.13	Isotachs for 90° Jet, VR = 10	28
3.14	Non-dimensional Temperature Plots for 135° Jet, Without Inlet Suction, VR = 10	29
3.15	Non-dimensional Temperature Plots for 135° Jet, With Inlet Suction, VR = 10	30
3.16	Jet Vector Field for 135° Jet, Without Inlet Suction, VR = 10	31

Figure No.	Title	Page
3.17	Jet Vector Field for 135° Jet, With Inlet Suction, VR = 10	32
3.18	Isotherms for 135° Jet, Without Inlet Suction, VR = 10	33
3.19	Isotachs for 135° Jet, Without Inlet Suction, VR = 10	34
3.20	Flow Visualization Pictures, $\alpha = 90°$, Without Suction	38
3.21	Flow Visualization Pictures, $\alpha = 120°$, Without Suction	39
3.22	Flow Visualization Pictures, $\alpha = 135°$, Without Suction	40
3.23	Flow Visualization Pictures, $\alpha = 135°$, With Suction	41
3.24	Flow Visualization Pictures, $\alpha = 150°$, Without Suction	42
3.25	Correlation of Test Results for 90° Jet	46
3.26	Correlation of Test Results for 135° Jet	47
3.27	Comparison of Data for 90° Jet	48
3.28	The Deflected Radial Plane Jet	51
3.29	Potential Flow Field for Cylindrical Nacelle	59
3.30a	Preliminary Split Flap Model for Balance Checkout	61
3.30b	Balance System Including Blower for Blow Flap/ Reverser Model	61
4.1	Relative Locations of Node Points	66
4.2	Node Points Near the Free Streamline	68

Figure No.	Title	Page
4.3	The Effect of Compressibility on the Pressure Distribution at the Deflector Surface	70
4.4	Jet Impingement Flow Field	72
4.5	Velocity Potential Field for Case A-6	74
4.6	Pressure Distributions for Case A-6	75
4.7	Summary of Analytical Results	76
4.8	The Effect of Jet Exit to Deflector Spacing on Reverser Performance	77
4.9	The Effect of Deflector Width on Reverser Performance	79
4.10	The Effect of Turning Angle on Reverser Performance	80
4.11	Comparison of Analytical and Experimental Results for the Blown Flap Thrust Reverser	82
4.12	Schematic Diagram of the Blown Flap Thrust Reverser	83
4.13a	Three-Dimensional Jet Impingement Rig	87
4.13b	Instrumentation for Jet Impingement Rig	87
4.14	Positioning Variables for the Three-Dimensional Impingement Jet Apparatus	88
4.15	Repeatability of Experimental Measurements Obtained from the Three-Dimensional Jet Apparatus	89
4.16	Effect of Jet Exit Velocity on the Velocity Measurements Obtained from the Three-Dimensional Jet Apparatus	90

Figure No.	Title	Page
4.17	Stagnation Pressure Profiles for the Thrust Reverser with a 90° Included Wedge Angle	92
4.18	Variation of Boundary Layer Thickness as a Function of Included Wedge Angle	93
4.19	Reverse Thrust as a Function of Included Wedge Angle	94
4.20	Similarity of the Normalized Velocity Profiles Obtained from the Three-Dimensional Jet Apparatus	96
A-1	Non-Dimensional Temperature Plots for Test 24 ..	99
A-2	Non-Dimensional Temperature Plots for Test 25 ..	100
A-3	Non-Dimensional Temperature Plots for Test 30 ..	101
A-4	Non-Dimensional Temperature Plots for Test 31 ..	102
A-5	Non-Dimensional Temperature Plots for Test 35 ..	103
A-6	Non-Dimensional Temperature Plots for Test 36 ..	104
A-7	Non-Dimensional Temperature Plots for Test 37 ..	105
A-8	Velocity Vector Feild for Test 24	106
A-9	Velocity Vector Field for Test 25	107
A-10	Velocity Vector Field for Test 30	108
A-11	Velocity Vector Field for Test 31	109
A-12	Velocity Vector Field for Test 35	110
A-13	Velocity Vector Field for Test 36	111
A-14	Velocity Vector Field for Test 37	112

LIST OF TABLES

Table No.	Title	Page
A-1	Test 24, VR = 10, α_J = 135°	113
A-2	Test 25, VR = 5, α_J = 135°	114
A-3	Test 30, VR = 5, α_J = 150°	115
A-4	Test 31, VR = 10, α_J = 150°	116
A-5	Test 35, VR = 5, α_J = 120°	117
A-6	Test 36, VR = 10, α_J = 120°	118
A-7	Test 37, VR = 20, α_J = 120°	119

1. SUMMARY

An investigation directed toward better design of aircraft thrust reversers is being conducted. This is the second yearly report of a three year study of this problem area. The study is divided into two main subdivisions:

(1) A study of jets introduced obliquely into a freestream flow.

(2) A study of jet impingement on curved surfaces.

During the second year, as part of the former study, an experimental investigation of the temperature and velocity fields generated by the two-dimensional transverse jet has been conducted and the results compared with existing data. An approximate analysis of the deflected radial plane jet has been developed. The analytical model of aircraft ingestion discussed in [1] has been extended to include computation of the inlet flow field and should be operational shortly. An investigation of the use of flaps as thrust reversers has been initiated. During the second year, as part of the jet impingement study, analyses of the impingement of a round incompressible and a round compressible jet on a arbitrary axisymmetric surface have been completed. Using these analyses and that for the incompressible plane jet described in [1] a computer study of the effects on performance of thrust reverser geometry has been completed and the results compared with existing data. An experimental investigation of three-dimensional jet impingement on non-plane surfaces has been initiated and some results have been produced.

2. INTRODUCTION

This is the second year report of an investigation supported under NGR-43-002-034. The study is intended to produce basic information concerning, and practical solutions to, the problem of aircraft exhaust ingestion which occurs in reverse thrust operation of fan/jet aircraft during landing or braking. The study is principally directed toward the problem as it affects STOL aircraft for which, because of their high thrust to weight ratio but low landing speeds, reverse thrust operation is especially critical.

The study is divided into two parts, i.e. The Opposing Jet Investigation and The Impinging Jet Investigation. Thus the report has two main sections. For a complete discussion of the program objectives and test philosophy see reference 1.

3. OPPOSING JET STUDY

This study is primarily experimental although some analysis has been included to relate the various parts of the investigation. The work reported here includes:

(1) Results from an experimental investigation of the velocity and temperature fields generated by a hot, transverse two-dimensional jet.

(2) An approximate analysis of the deflected radial plane jet.

(3) A discussion of, and some preliminary results from, a reingestion analysis for a single nacelle operating in reverse thrust.

(4) A brief discussion of an experimental investigation of the use of flaps as thrust reversers.

3.1 THE TWO-DIMENSIONAL TRANSVERSE JET

In [1] the results of an experimental investigation of the flow field and ingestion characteristics of a simulated target thrust reverser engine nacelle system were presented. Since cascade thrust reversers represent a class of reversers as important as target reversers, a corresponding study of their flow fields and ingestion characteristics would provide a logical extension of the work of [1]. Unfortunately, the

construction of a representative cascade reverser-nacelle system was beyond the financial and technical resources of the present study and thus a compromise jet geometry was sought. After some study, the two-dimensional transverse jet was selected as a practical alternative case which has many of the elements of the efflux from the cascade thrust reverser, and can be considered approximately as a cascade reverser rolled out into a plane. An experimental investigation of this jet configuration was conducted. Many of the results of this study are reported in detail in References 2 and 3 and therefore this work is presented here only in an abridged form. There is, however, data from this study which was not reported in [2] and [3] and which is included in Appendix A of this report.

3.1.1 Previous Related Studies of the Plane Transverse Jet

The number of previous studies investigating the round deflected jet is considerable. However, in the case of the two-dimensional jet, the number of studies is limited. And, these investigations have produced only centerline velocities or surface pressures induced by the deflected jets. Generally, the products of these studies are semi-empirical methods for predicting the location of the jet centerline using the limited velocity data collected. After making a survey of these studies. Tatom [4] concludes that all predicted the shape of the centerline to be parabolic. He also observes that the jet trajectories predicted by these semi-empirical methods show considerable variation.

The only known previous sources of experimental data for the plane transverse jet are the works by Ivanov [5] and Heyser and Maurer [6]. Neither of these papers are concerned with temperature data. Major emphasis was on the jet (centerline) trajectory with no information reported concerning local conditions in the overall jet field. The report by Heyser and Maurer is concerned with high Mach Number flow and thus, is not as relevant to many of the transverse jet applications as the study by Ivanov which was conducted at a low subsonic condition.

3.1.2 Experimental Program-General Discussion

The study deals with the two-dimensional hot-air jet introduced into a uniform freestream flow at angles of 90, 120, 135 and 150 degrees (the angles being measured from the direction of the freestream flow). The velocity ratio, i.e. the ratio of the jet velocity to the freestream velocity, was set at values of 5, 10 and 20. These velocity ratios were selected to simulate the relatively wide range of conditions encountered in practice and yet to remain within the capabilities of the test facility. Figure 3.1 contains a list of all tests reported and their boundary conditions.

In the testing, which, with one exception, was conducted at a nearly constant jet temperature, the 135° jet was operated both with and without inlet suction, and the effects of inlet-to-jet spacing were also investigated. All the other jets were operated without inlet suction. All testing was conducted in the Vanderbilt low speed induction wind tunnel

Fig. 3.1. Summary of Test Conditions

Test Number	α_J Jet Angle Degrees	Velocity Ratio	Inlet Suction ?	Jet Temperature °F	Ambient Temperature °F	Jet Velocity fps	Ambient Velocity fps	Jet-to-Inlet Spacing (jet widths)
0	90	5	No	100	87	63.2	12.6	6.88*
11	90	5	No	201	85	122.5	24.5	6.88
12	90	10	No	200	81	120	12	6.88
13	90	20	No	204	83	155.2	7.78	6.88
14	135	5	No	216	88	126.9	25.4	6.88
15	135	10	No	215	86	126.7	12.5	6.88
16	135	20	No	197.5	90	126.7	6.34	6.88
17	135	5	Yes	213	86	126.9	25.4	6.88
18	135	10	Yes	219.5	83	126.7	12.7	6.88
19	135	20	Yes	212	82	126.7	6.34	6.88
24	135	10	Yes	202	80	126.7	12.67	22.5
25	135	5	Yes	199	84.5	126.7	25.34	22.5
30	150	5	No	202	80.5	124.5	24.9	6.88
31	150	10	No	210	85	124.5	12.5	6.88
35	120	5.0	No	203	83	122.4	24.5	6.88
36	120	10	No	205	83	122.4	12.24	6.88
37	120	20	No	213	83	122.5	6.13	6.88

*This particular inlet-to-jet spacing represented the minimum spacing possible with the jet model. It is probably somewhat larger than that corresponding to modern fan jet aircraft, especially those with a short duct design, but is perhaps representative of long duct designs.

modified with a false bottom. This false bottom contained the jet model and blowing box, an inlet suction section and a boundary-layer removal section. Data were taken by traversing in the vertical center plane of the wind tunnel. All traverses were made into the opposing freestream flow at fixed heights above the false bottom. During the tests, both velocity and temperature data were recorded.

3.1.3 Equipment

A schematic diagram of the equipment arrangement is presented in Figure 3.2. In this figure the coordinate system shown designates the positive x direction as directly opposite the freestream flow and the positive y direction toward the top of the wind tunnel. The origin of the coordinates is located at the center of the jet exit area.

The equipment used in this study included the following:

(1) An induction wind tunnel.

(2) A blowing box with an 0.102 inch jet.

(3) An inlet suction section.

(4) A boundary-layer removal section.

(5) A hot air generator.

(6) A traversing mechanism.

(7) Electronic equipment related to the temperature compensated hot wire anemometer (Figures 3.3 and 3.4).

(8) An x-y plotter.

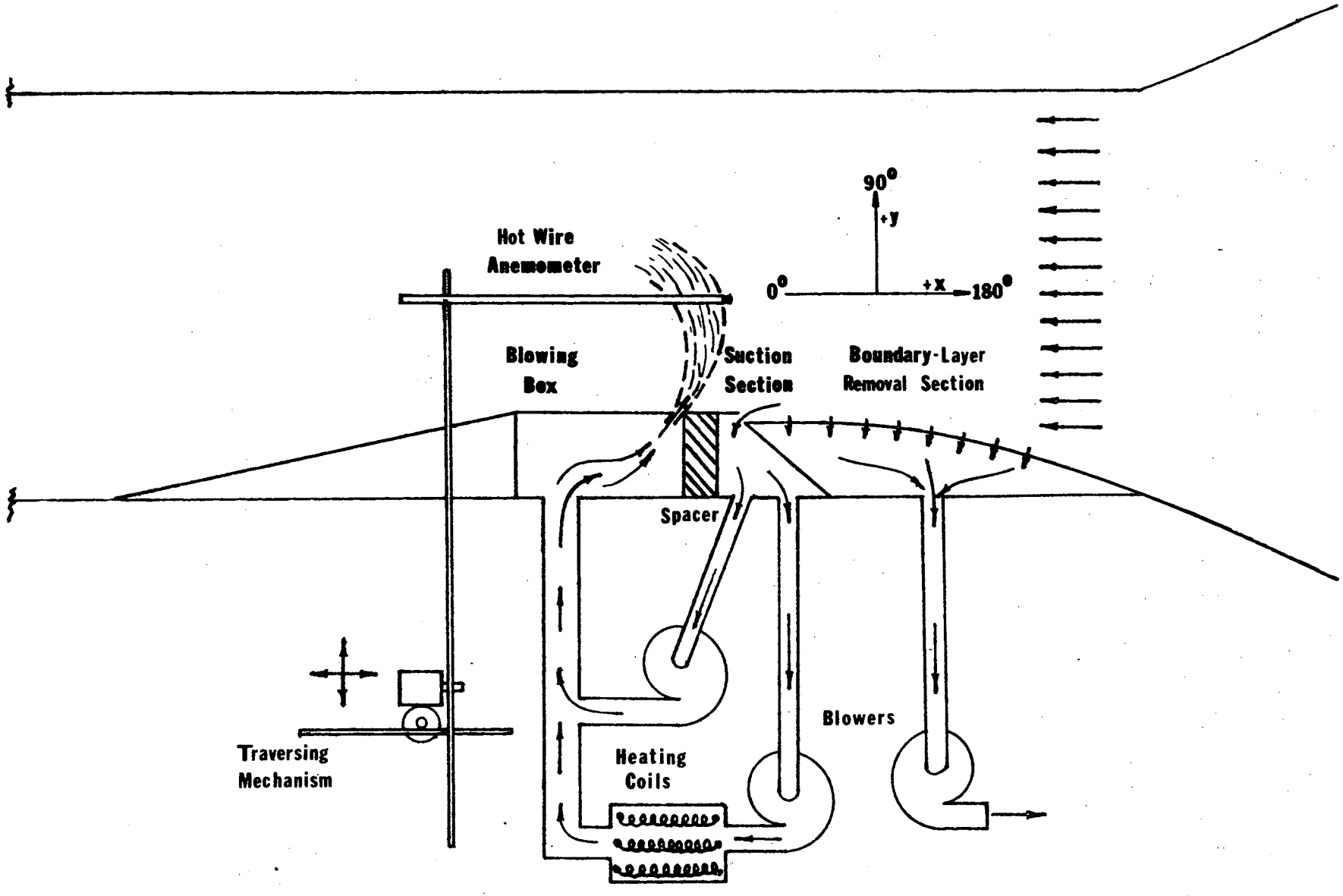

Fig. 3.2. Schematic Diagram of Experimental Equipment

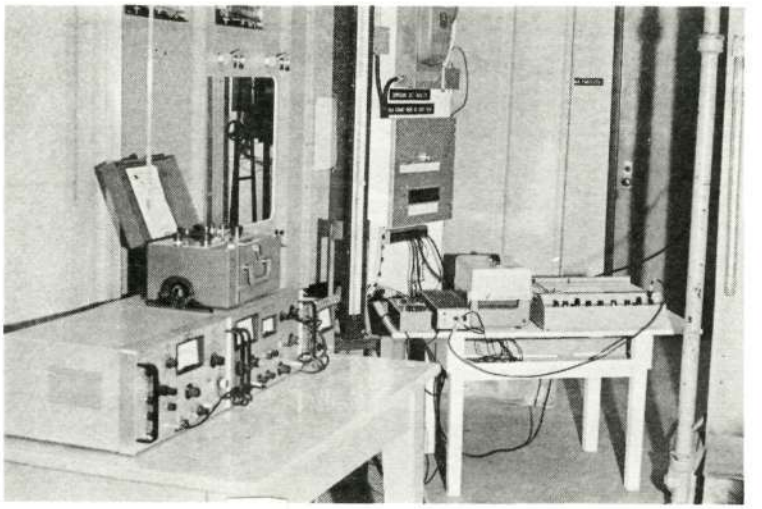

Figure 3.3 Electrical Equipment

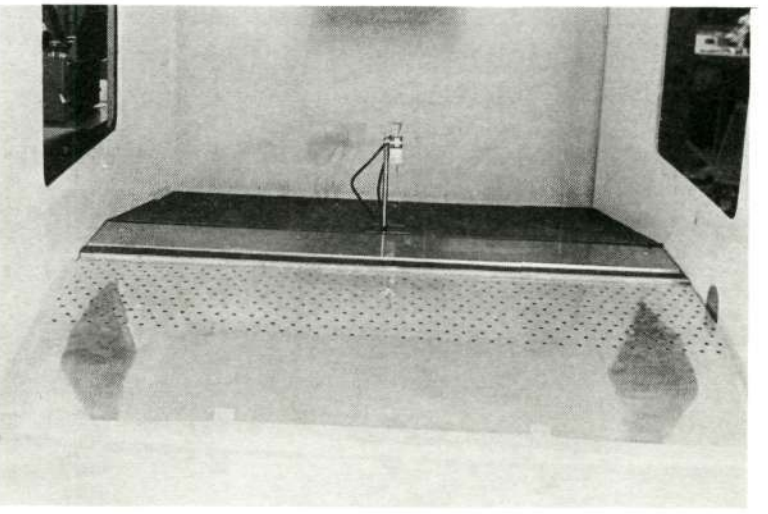

Figure 3.4 Model and Probe in the Wind Tunnel

A Zumwalt and Darby, Inc., induction wind tunnel was used in the testing. This wind tunnel had two test sections; a high speed section and a low speed section. All tests were conducted in the low speed section. This section was 40 inches square and produced a velocity which could be varied from 0 to approximately 40 feet/second. The measured turbulent fluctuations in this section were less than four percent of the tunnel velocity for all test cases. In order to produce a truly two-dimensional jet, it was necessary to install in the tunnel a false bottom which enclosed the jet blowing box, the inlet suction section and the boundary layer removal section. Figure 3.4 shows the false bottom in the wind tunnel. This bottom reduced the height of the tunnel but did not cause any increase in the turbulence level.

The blowing box was made from quarter inch aluminum plate. Aluminum was used as the construction material since it provided the necessary strength to maintain the tolerances required of the 0.102 inch wide jet slot. The box was 40 inches long, 3.5 inches high and 7.5 inches wide. This provided a plenum cross-sectional area large in comparison with the effective jet slot area. The top and front plates of the box were removable. Different pairs of plates were used to change the angle of the jet. These plates were machined to a tolerance of 0.001 inch to insure the accuracy of the jet dimensions. At the bottom of the box, a 5 X 8 inch duct supplied the hot air to the plenum. The combination of the large duct

and the large cross-section of the plenum resulted in low velocities and a pressure variation across the blowing box of less than 2 percent in the most extreme case. With this slight variation in delivery pressure, the jet was assumed to have a constant velocity over its entire length. The small width of the slot made it impossible to measure the jet exit velocity profile. However, the velocity profile was determined to be essentially square by using the analytical method presented by H. Schlicting [7] in the case of developing channel flow.

Since the temperature of the suction section was near ambient and the pressure was low it was constructed of plywood. A 0.20 inch inlet width was maintained by gluing spacers along the slot. In calibration tests, the maximum pressure variation across the suction section was found to be less than 4 percent of the sub-ambient head. Therefore, the intake velocity was regarded as essentially uniform.

The boundary-layer removal section, besides removing the low energy air adjacent to the model, provided a fairing from the floor of the wind tunnel to the suction section. The boundary-layer removal section consisted of a plywood frame covered with sheet metal perforated with quarter inch diameter holes. A check for uniformity of velocity through these holes using the hot wire anemometer revealed that the variation of velocity was less than 5 percent. Using an analytical solution for boundary-layer suction again taken from Schlicting [7], the displacement

thickness of the boundary-layer at the suction inlet was determined to be less than 0.004 inch.

The hot air generator, described in [1], produced pressures in the blowing box of approximately 2.9 inches of water and a delivery temperature of about 200°F for the testing reported here. At this pressure and temperature, a jet velocity of approximately 125 feet/second was obtained.

The traversing mechanism was powered by two constant speed motors mounted so that the probe could be translated in a vertical plane both horizontally and vertically. Calibrations showed that the rate of traverse was 1.0 millimeter/second.

The primary sensor employed in this experiment was a Thermo-Systems, Inc., Model 1330, temperature compensated hot wire anemometer with a single sensor element and associated electrical components. This system had the capability of measuring a single velocity component (i.e., either $\vec{u}$ or $\overrightarrow{u+v}$) in a variable temperature environment on one bridge circuit and temperature on another bridge circuit. Outputs of the bridges were separate; thus it was necessary to switch bridge circuits, and to rotate the probe 90° for the velocity measurements in order to obtain the individual responses. Hence both velocity and temperature could not be monitored simultaneously. In the temperature measuring mode, the probe operated as a resistance thermometer. Any change in the environmental

temperature caused a corresponding change in the resistance of the sensor. The sensor was a platinum film on a 0.006 inch diameter glass rod. It has a frequency response of around 15,000 hertz. The probe was calibrated in situ both in temperature and velocity prior to testing.

3.1.4 Discussion of Results

3.1.4.1 General

The information obtained in the investigation was in several forms, e.g.

(1) Temperature traverses at various heights above the jet model.

(2) Velocity ($\vec{u}$ and $\overrightarrow{u+v}$) traverses at various heights above the jet model.

(3) Flow visualization pictures taken through use of an ammonia-sulfur dioxide smoke generator which made deflected jet visible.

The temperature and velocity data were recorded in a rectangular region whose vertical boundaries were chosen to include as much as practical of the deflected jet trajectory. Because the jet temperature and momentum rapidly diffused and therefore became difficult to measure, the breadth of this region was usually not more than 40 jet widths and the height was usually less than about 60 jet widths.

3.1.4.2 The Data-Test Difficulties and Repeatability

There were numerous difficulties at the outset in getting the

anemometer to operate correctly in the temperature mode, mainly because of problems in obtaining a proper ground. Once it was calibrated and working properly, however, few problems were encountered during the testing. The temperature data reduction was relatively straightforward. Getting the anemometer to operate in the velocity mode, however, was never any problem but some difficulties were encountered during the testing and in the subsequent data reduction. The problem arose because the anemometer was designed to measure, flows in one general direction.

In the complex flow field generated by the transverse jet and the freestream, there are regions in the jet and behind the jet where the air velocity has an u component opposite to that of the freestream. The probe was mounted facing the freestream; thus if the u component was very large in comparison to the v component and opposing the freestream, the probe support assembly generated a wake in which the sensor was located. This produced erroneous readings in the $\vec{u}$ and $\overrightarrow{u+v}$ traverses which could not be detected until the data reduction process was completed. However since the flow angles were obtained by taking the arc cosine of the ratio $|\vec{u}/\overrightarrow{u+v}|$ it was usually clear in these cases when something was amiss, since the $|\vec{u}/\overrightarrow{u+v}|$ ratio would be computed to be greater than unity. In such cases, the data was thrown out, and therefore there are regions, behind the jet primarily, where no velocity data is reported and where some inaccuracies are present.

In the region immediately in front of the jet, especially near the jet exit where the velocities were large, the flow experienced an abrupt change in direction as the external air was entrained into the jet which was in turn directed into the freestream. Hence in this region it was not always clear whether the u component was directed upstream or downstream, (or the v component upwards or downwards), since the anemometer provided only the magnitude of the velocity components. Through use, however, of the flow visualization pictures and the temperature data it was usually possible to determine the proper flow directions without resort to any subjective processes. Fortunately, the majority of the velocity data was not affected by these difficulties and was reduced without problem.

In general the data was found to be repeatable to a satisfactory degree although some variations were observed. Detailed discussions of repeatability are found in [2] and [3]. The major reason for variations in the data between repeated tests is believed to be the sensitivity of the flow to the jet-to-freestream velocity ratio and problems in reestablishing the test boundary conditions, since rerun traverses within a given test always showed negligible variations both in temperature and velocity. Analysis of the temperature data from a number of repeat test traverses indicated that the maximum variation occurred with a 2.5% difference in the location of the maximum non-dimensional temperature, a 24% difference

in the magnitude of the maximum and a 12% average deviation. The minimum variation occurred with a negligible difference in the location of the maximum non-dimensional temperature point and in the magnitude of the maximum and with a 3.6% average deviation. A corresponding analysis of velocity data revealed that the maximum variation occurred with a difference of 4 percent in maximum velocity location, and an average variation of 16% in the $\overrightarrow{u+v}$ data. The minimum occurred with a negligible variation in maximum velocity location and a 1% average variation in the $\overrightarrow{u+v}$ results.

3.1.4.3 Test Results

The temperature and velocity data* obtained from the anemometer traverses were reduced to the non-dimensional forms:

(a) $\left(\frac{T-T_a}{T_j-T_a}\right)$ as a function of x/d_J and y/d_J

and

(b) $\left(\frac{\vec{u}}{U_\infty}\right)$, $\left(\frac{\overrightarrow{u+v}}{U_\infty}\right)$ and α as functions of x/d_J and y/d_J

Typical data from these traverses are presented here in several ways. These include:

(a) Jet centerline trajectory plots.

(b) Non-dimensional temperature plots.

(c) Velocity vector plots.

(d) Isotherm plots.

(e) Isotach plots.

---

*The complete data for tests 0 and 11 through 19 are presented in [2] and [3]. The data for the remaining tests are located in Appendix A.

The jet centerlines were obtained by determining the locus of points where the temperature and the velocity was a maximum. Comparison of the temperature centerlines and the velocity centerlines revealed the not too surprising result that the curves were essentially coincident, although some small deviations were occasionally present, especially at large distances* from the jet exit where the temperature and velocities were near that of the freestream. Thus for simplicity and convenience, in the following discussion only the temperature centerlines are utilized.

Presented in Figures 3.5 through 3.9 are centerline temperature trajectories for the 90°, 120°, 135°, and 150° jets at jet-to-freestream velocity ratios of 5, 10 and 20. In the case of the 135° jet, Figures 3.7 and 3.8 also illustrate the effects of inlet suction and jet-to-inlet spacing on the centerlines. It was found that without inlet suction the 150° jet became attached to the jet model assembly at velocity ratios above 10 (and occasionally at lower velocities). It was also found that inlet suction resulted in jet attachment at all velocity ratios for the 150° jet. Thus because the attached flow was extremely turbulent and because of the problems that were encountered with the anemometer in situations where the sensor was located in the probe wake, it was not practical to measure the flow characteristics in the attached 150° jet. Therefore data for

---

*In these regions there did appear to be a tendency for the temperature centerlines to be slightly above and in front of the velocity centerlines although there were frequent occasions when the reverse occurred. Considering the difficulty in locating a maximum in these regions since the curves experienced considerable fluctuations and were very flat, it is not clear whether this tendency has any physical significance.

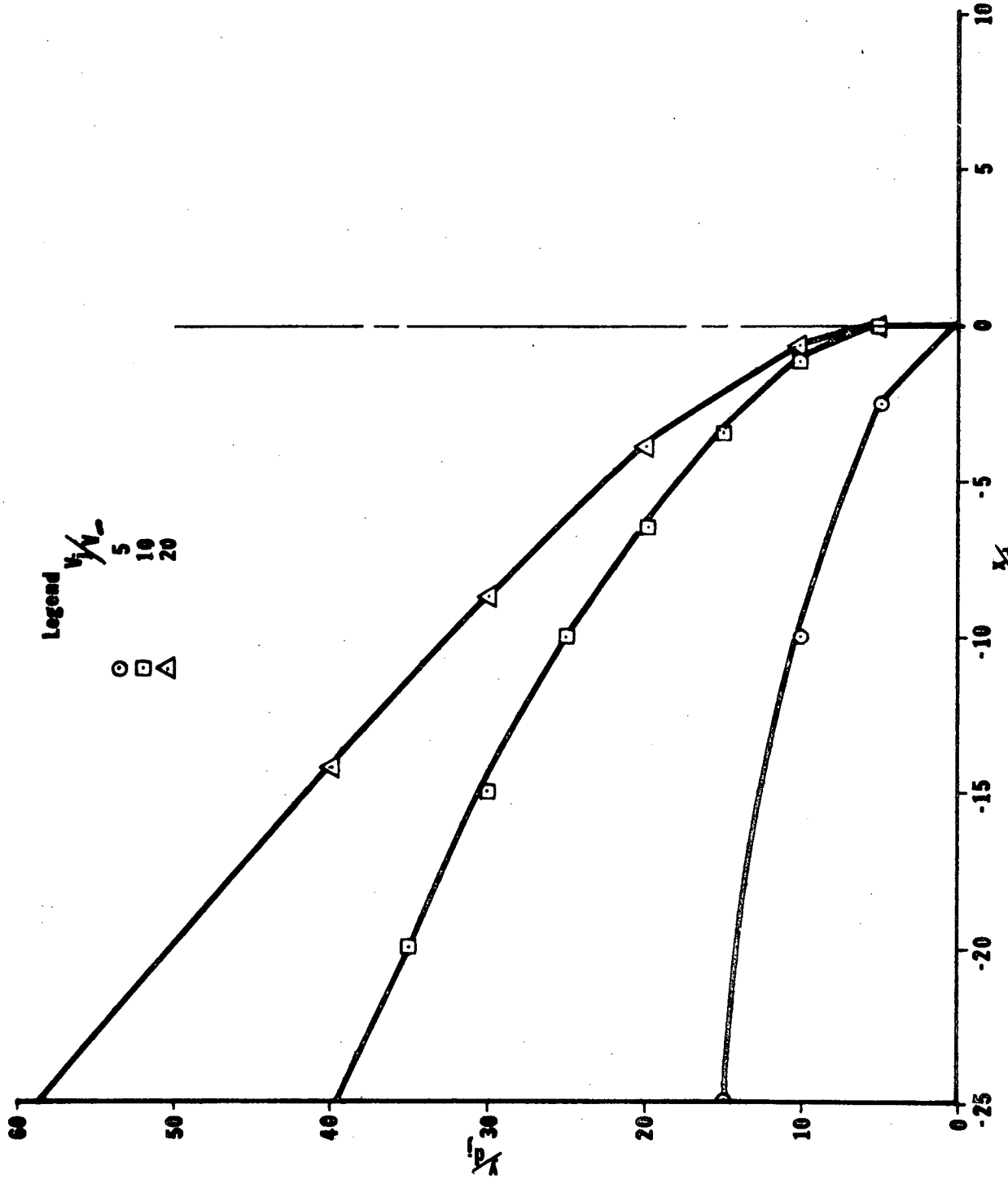

Fig. 3.5 Centerline Temperature Trajectories of 90° Jet

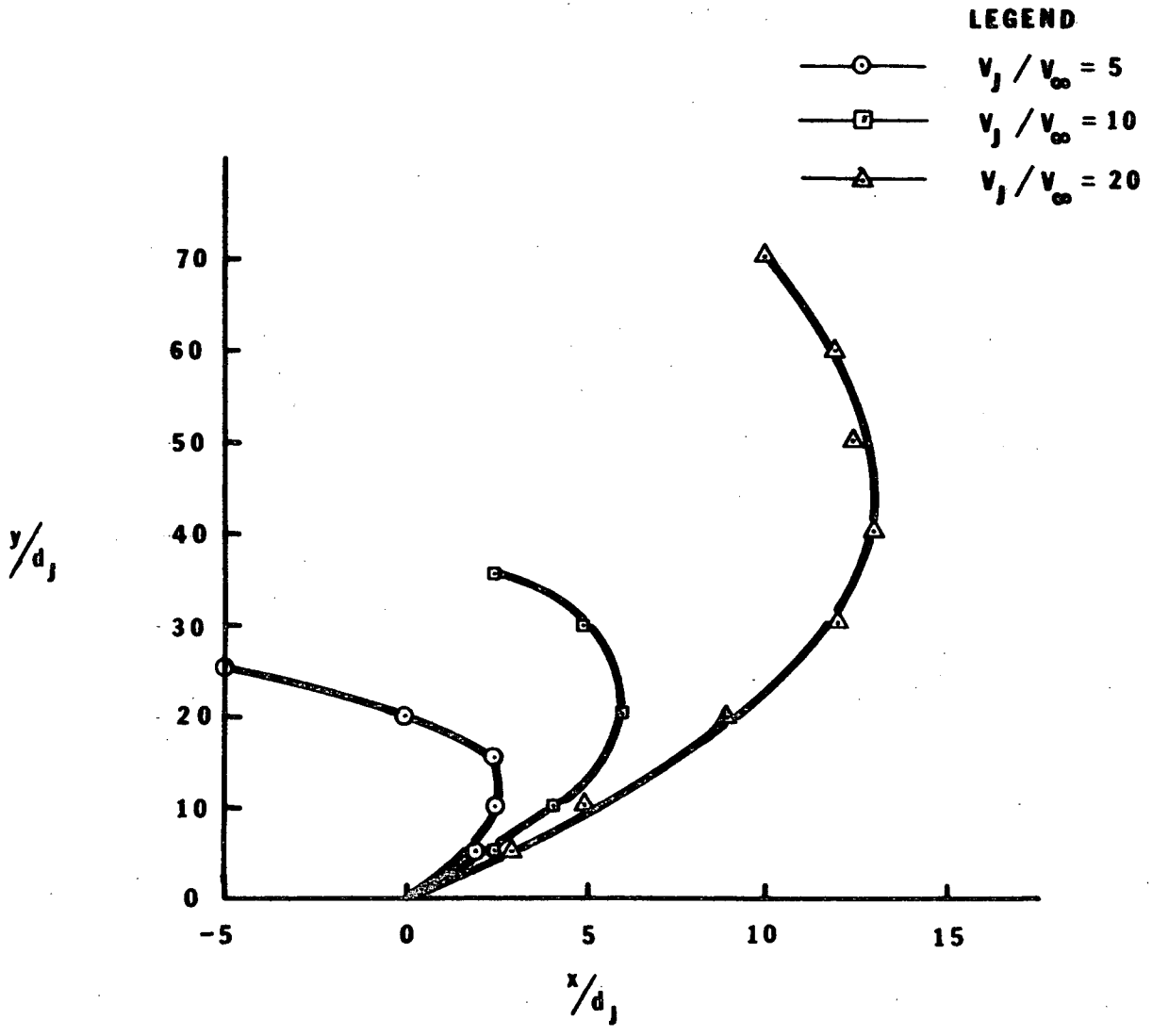

Fig. 3.6. Centerline Temperature Trajectories for 120° Jet

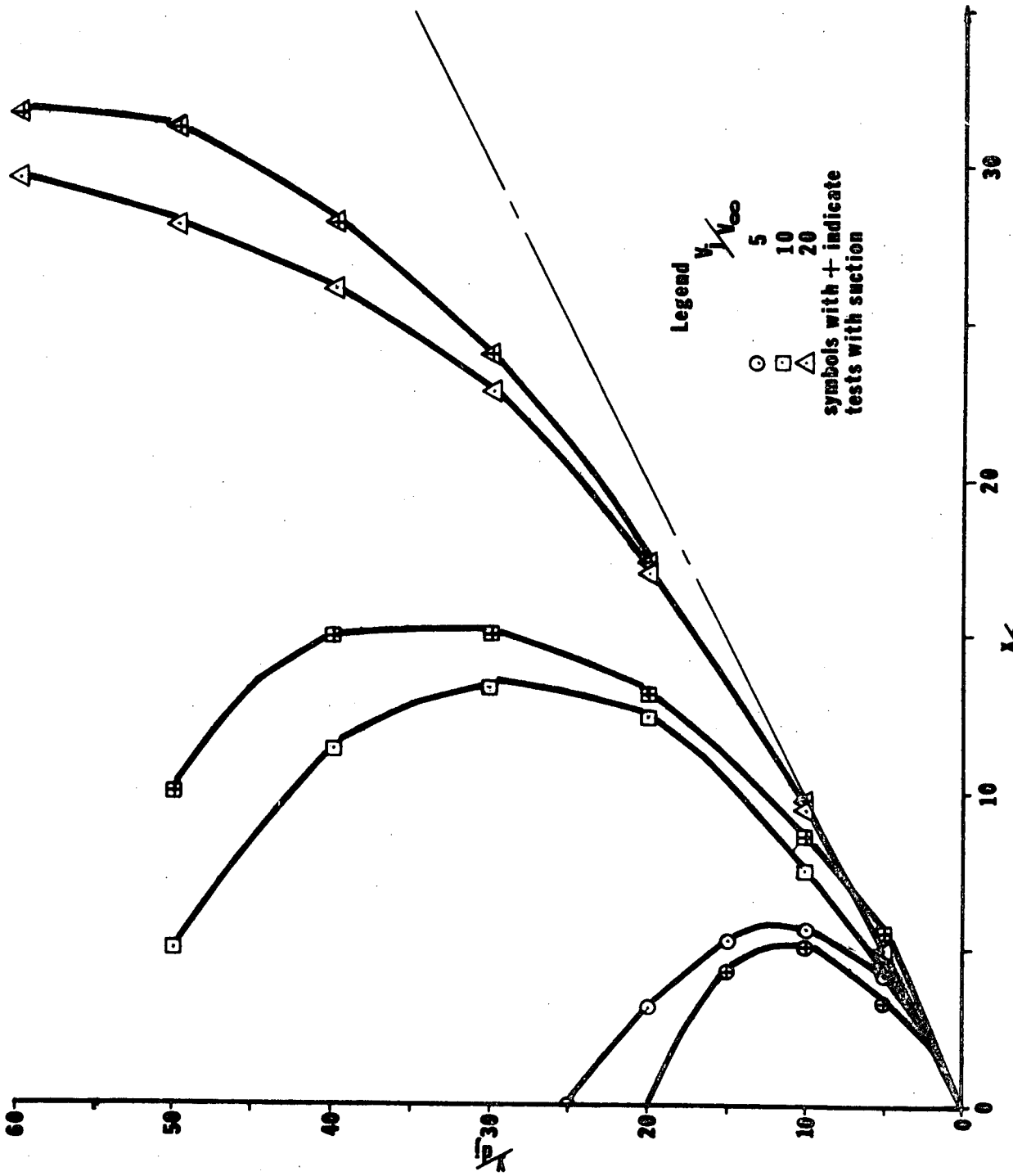

Fig. 3.7. Centerline Temperature Trajectories of the 135° Jet

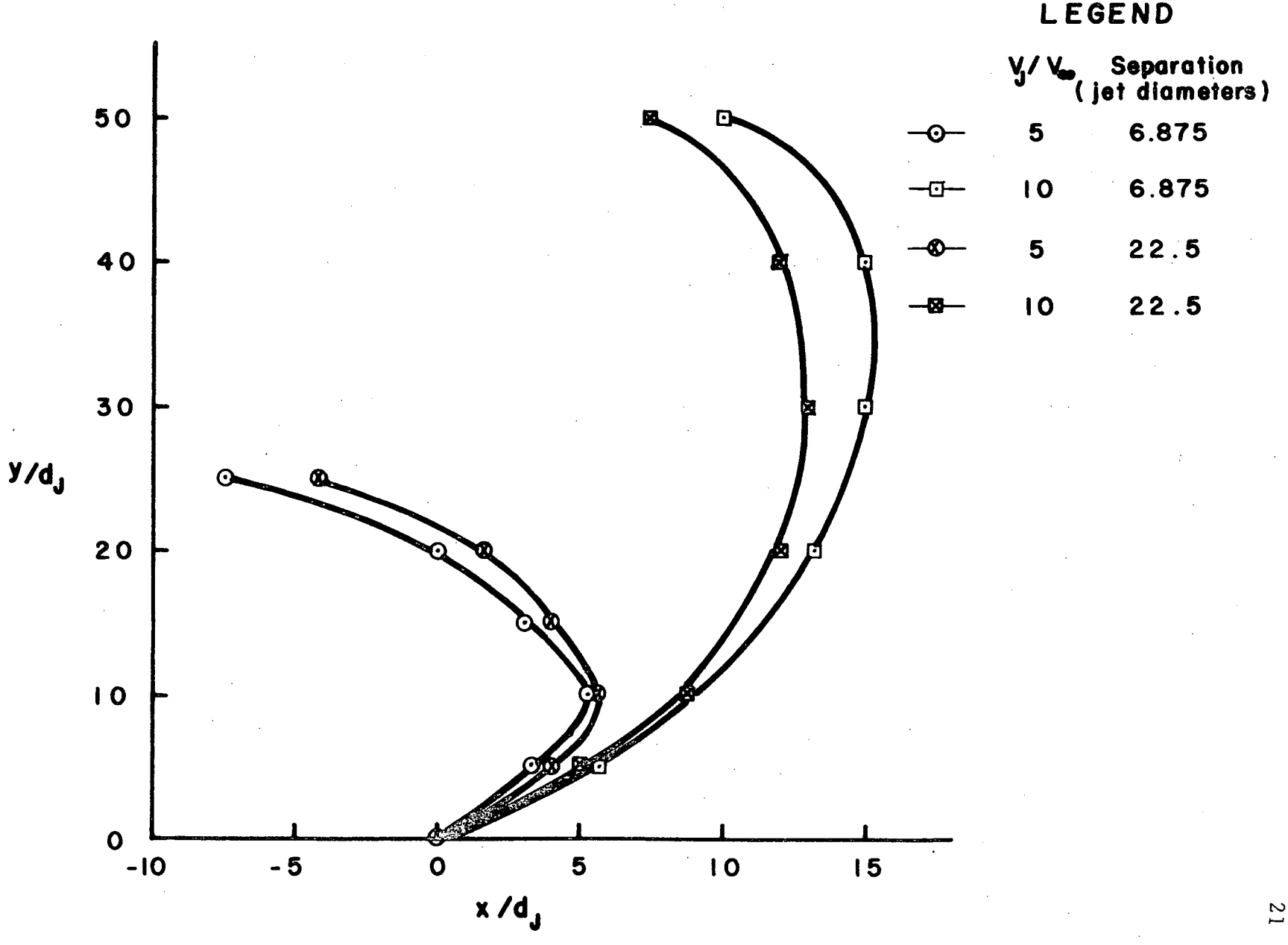

Fig. 3.8. Centerline Temperature Trajectories of 135° Jet - Effects of Inlet-to-Jet Spacing

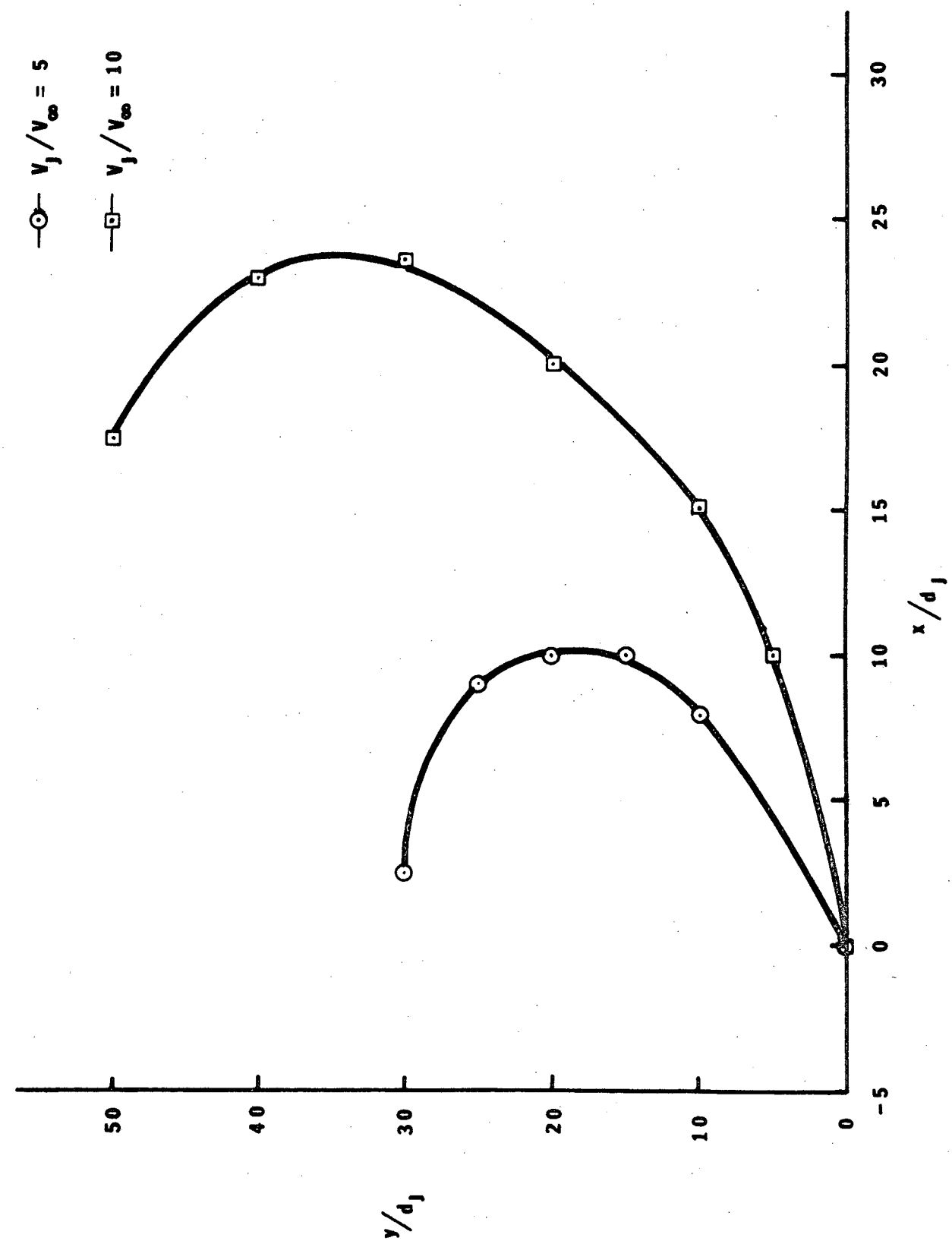

Fig. 3.9. Centerline Temperature Trajectories of 150° Jet

this case is limited to velocity ratios of 5 and 10 without inlet suction.

Study of the deflected jet centerline data revelas that the vertical penetrations of the 120° and 135° jets are considerably greater than those for the 90° and 150° jets. It also appears that the effects of inlet suction and jet-to-inlet spacing are small for the 135° jet although the trajectories with suction do tend to lay slightly in front of and above those without suction. This is a particularly interesting result since it allows considerable simplifications when applied to the analytical model of ingestion. This is discussed in Section 3.3. In general the centerline plots appear to be consistent with expectations and contain no surprises.

Of the jet geometries investigated, the 90° and the 135° jets are perhaps the configurations of most interest and for that reason more detailed data for these two cases are presented. Curves for the 90° jet at a velocity ratio of 10 are shown in Figures 3.10 through 3.13. Plots of the non-dimensional temperature rise as a function of x/d_J and y/d_J are presented in Figure 3.10. The figure demonstrates a rapid decay of the jet temperature and deflection of the centerline by the freestream. Of interest is the fact that the temperature in the region behind the jet does not return to ambient but remains at a significant level above it. This is evidence of the presence of a large vortex behind the jet in which a portion of the heated air in the deflected jet turns back and fills in the separated flow region behind the jet.

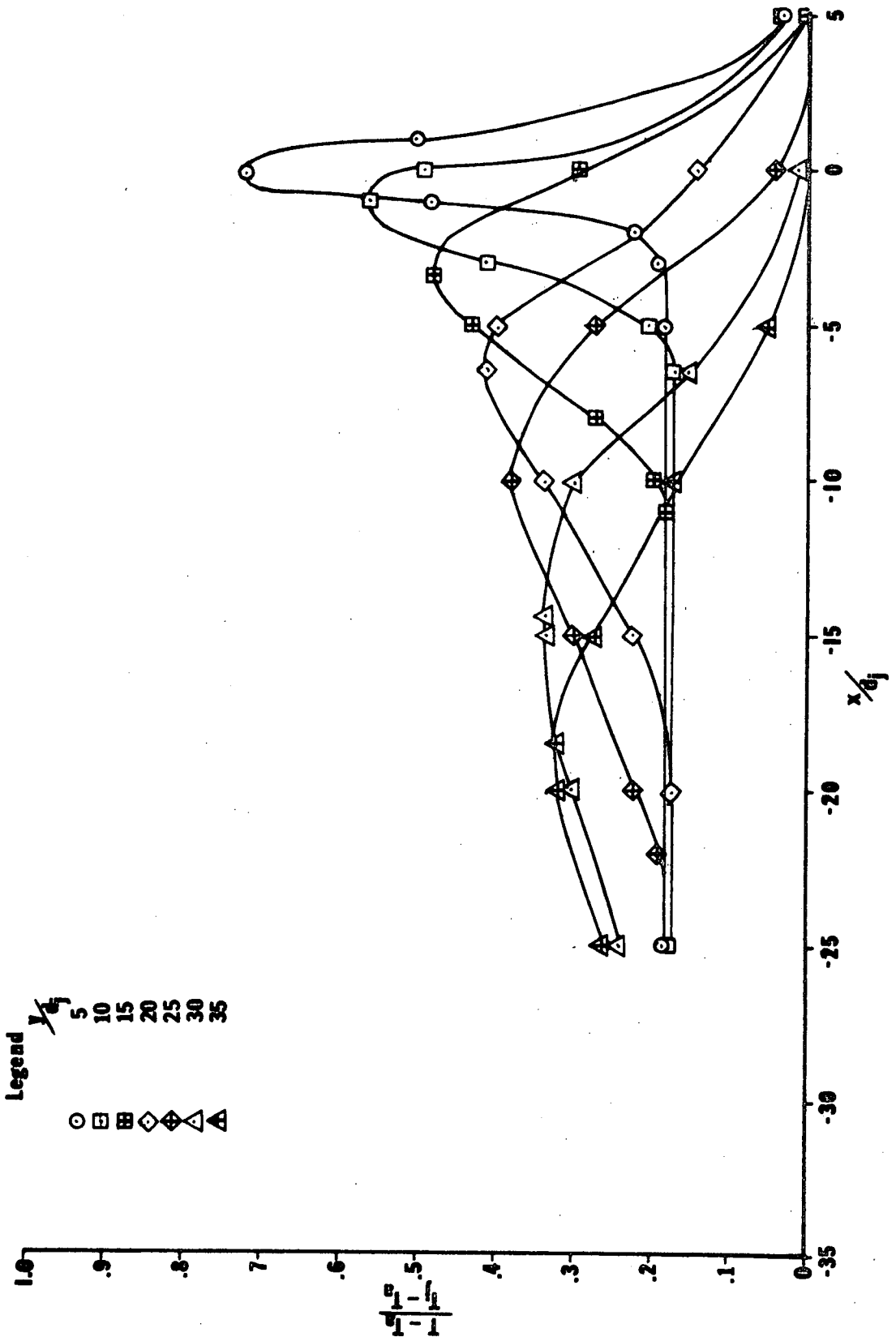

Fig. 3.10. Non-dimensional Temperature Plots for Test 12, $\alpha = 90°$, VR = 10 without inlet suction, $T_j - T_a = 119°F$

Figure 3.11 presents a velocity vector field plot for the 90° jet. This figure demonstrates the rapid entrainment and relatively minor deflection of the freestream by the jet. Also shown is evidence of recirculation behind the jet. Plots of the jet isotherms and isotachs are presented in Figures 3.12 and 3.13. These figures provide a further picture of the character of the jet field and demonstrate the strength of the extra shearing forces present.

The 135° jet, because it was the largest turning angle jet tested for which attachment was not a problem, was perhaps the most interesting case investigated, especially so far as thrust reverser applications are concerned. To illustrate in detail the temperature and velocity data obtained for this geometry, Figures 3.14 through 3.19 are presented. In all these figures the jet-to-freestream velocity ratio is fixed at a value of 10. Besides demonstrating the character of the temperature and velocity fields these figures also show the relative insensitivity of the deflected jet properties to the presence of inlet suction.

The non-dimensional temperature traverses shown in Figures 3.14 and 3.15 show substantial agreement not only in the location of the maximum temperature points but in their relative magnitudes. There are clearly some differences in these two families of curves but the similarities far outweigh the discrepancies. Both figures indicate the presence of a region of heated air behind the jet just as in the case of the 90° jet and

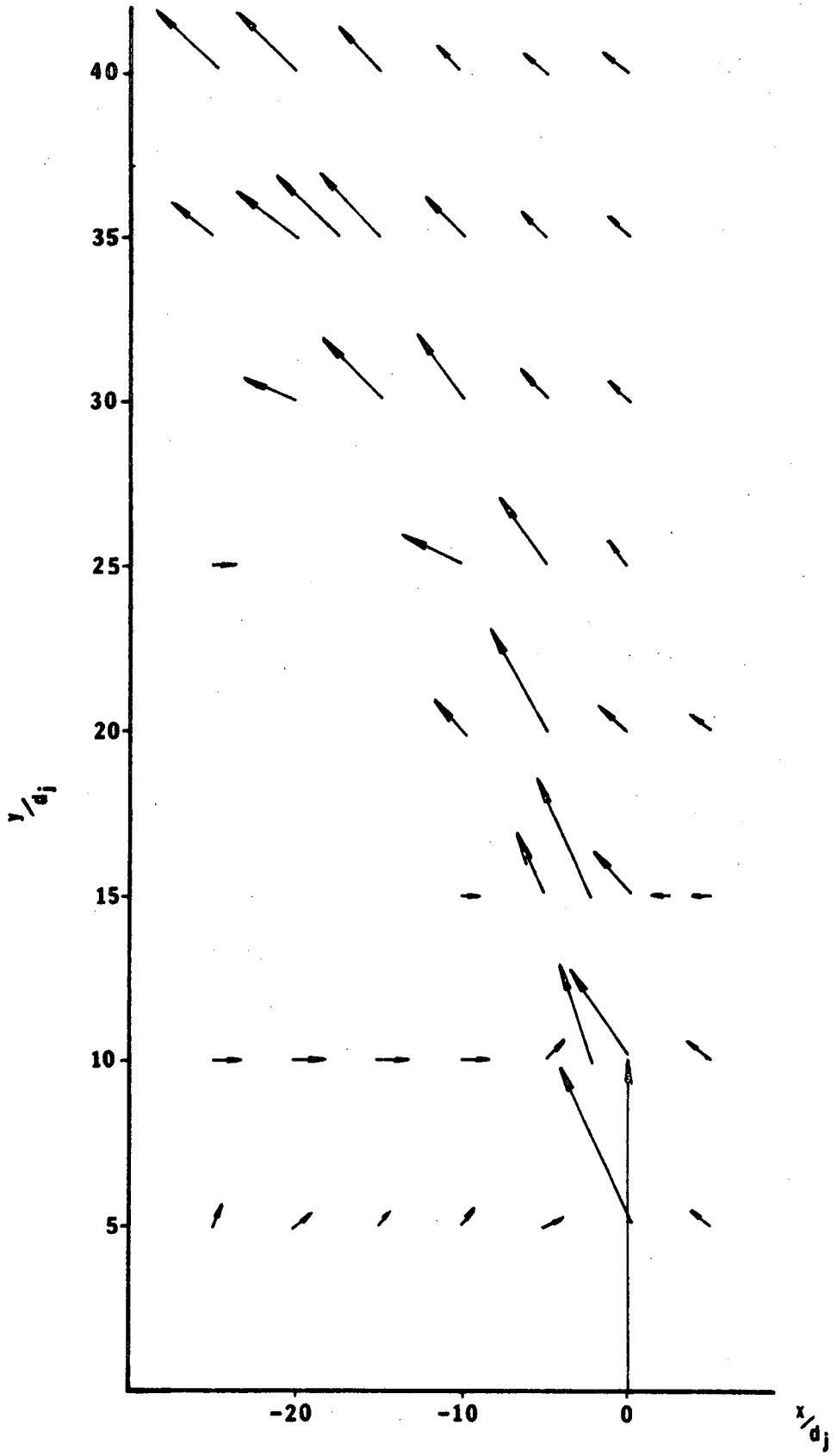

Fig. 3.11. Jet Vector Field, Test 12, $\alpha = 90°$, VR = 10 without Inlet Suction

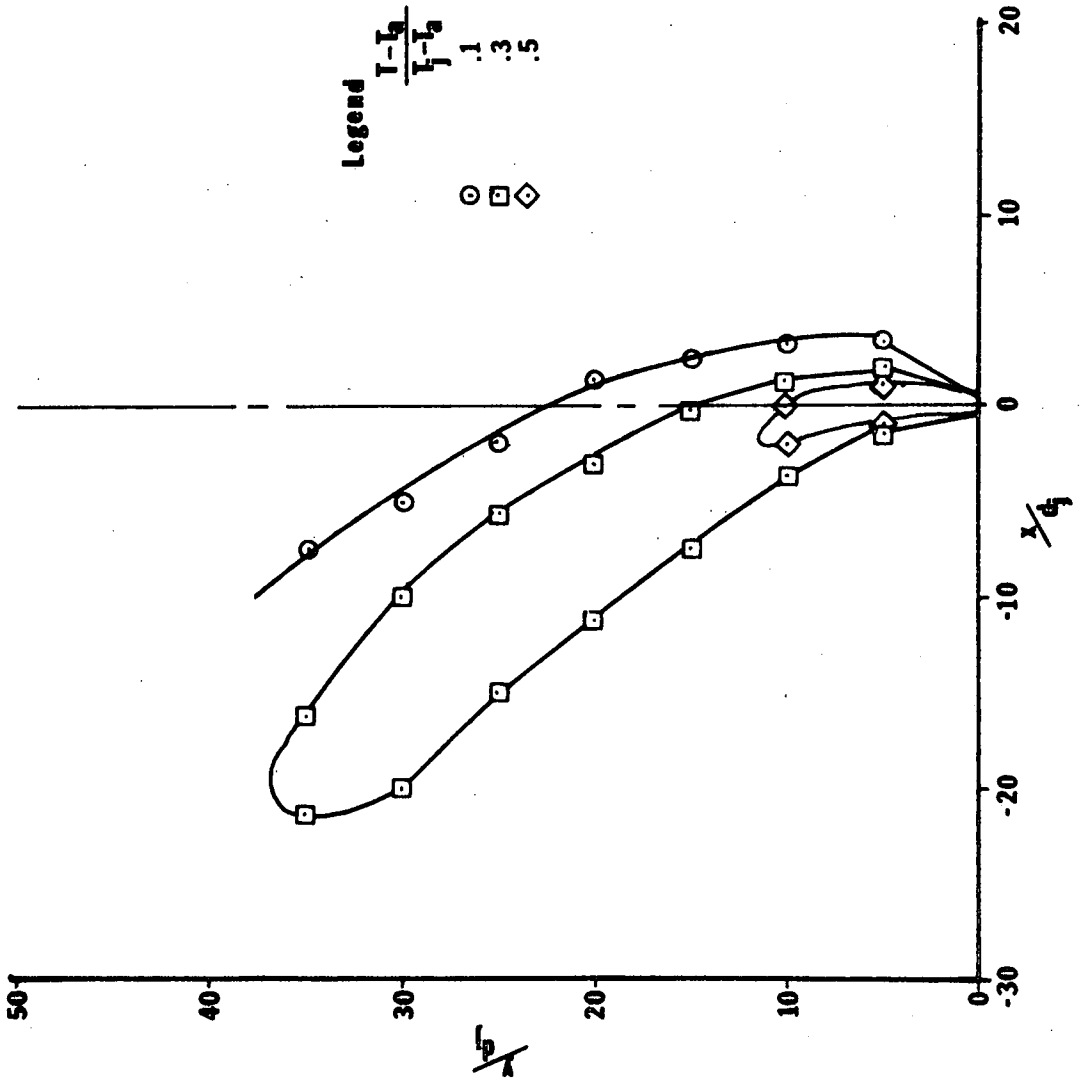

Fig. 3.12. Jet Isothermal Boundaries for Test 12

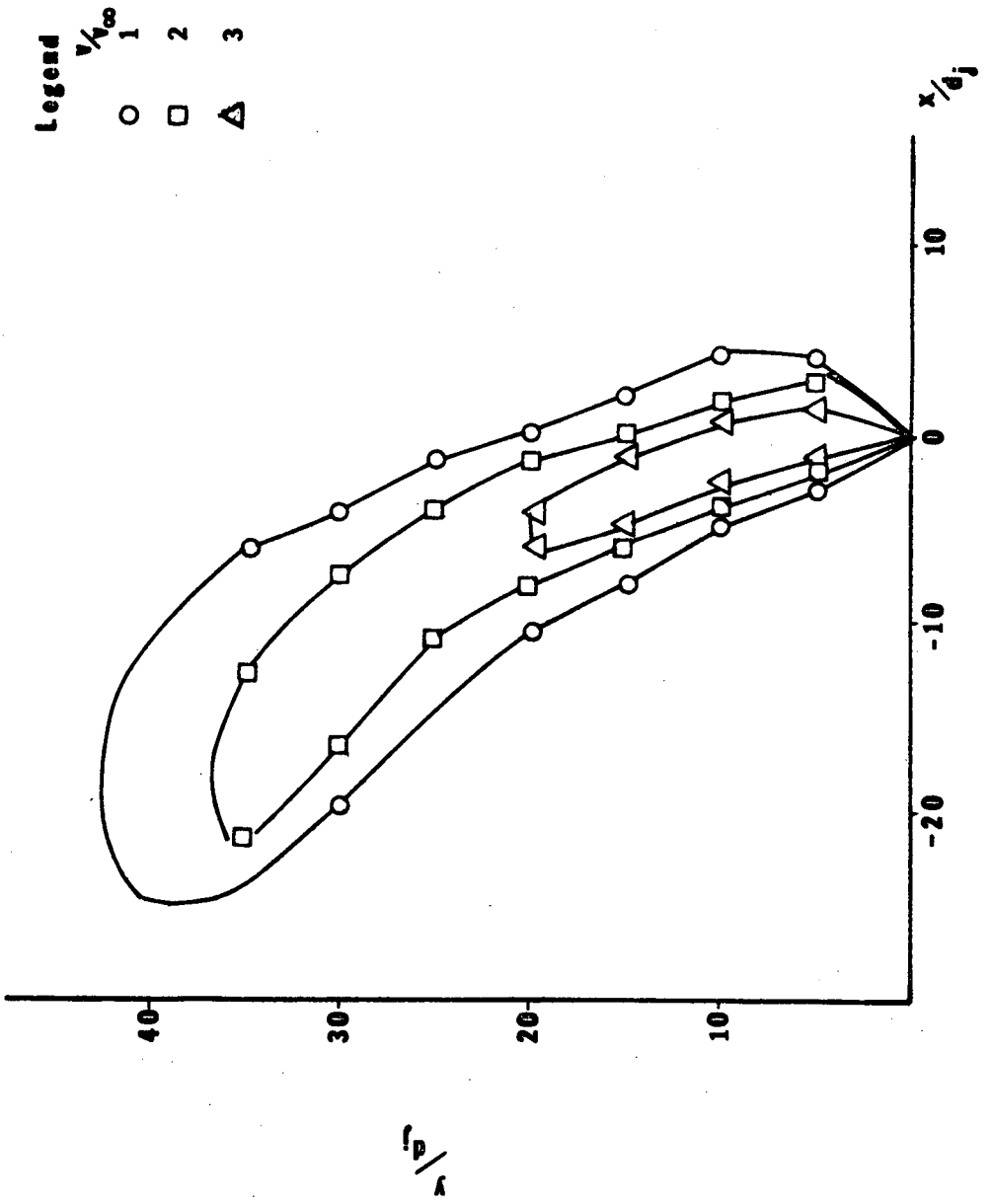

Fig. 3.13. Isotachs for Test 12

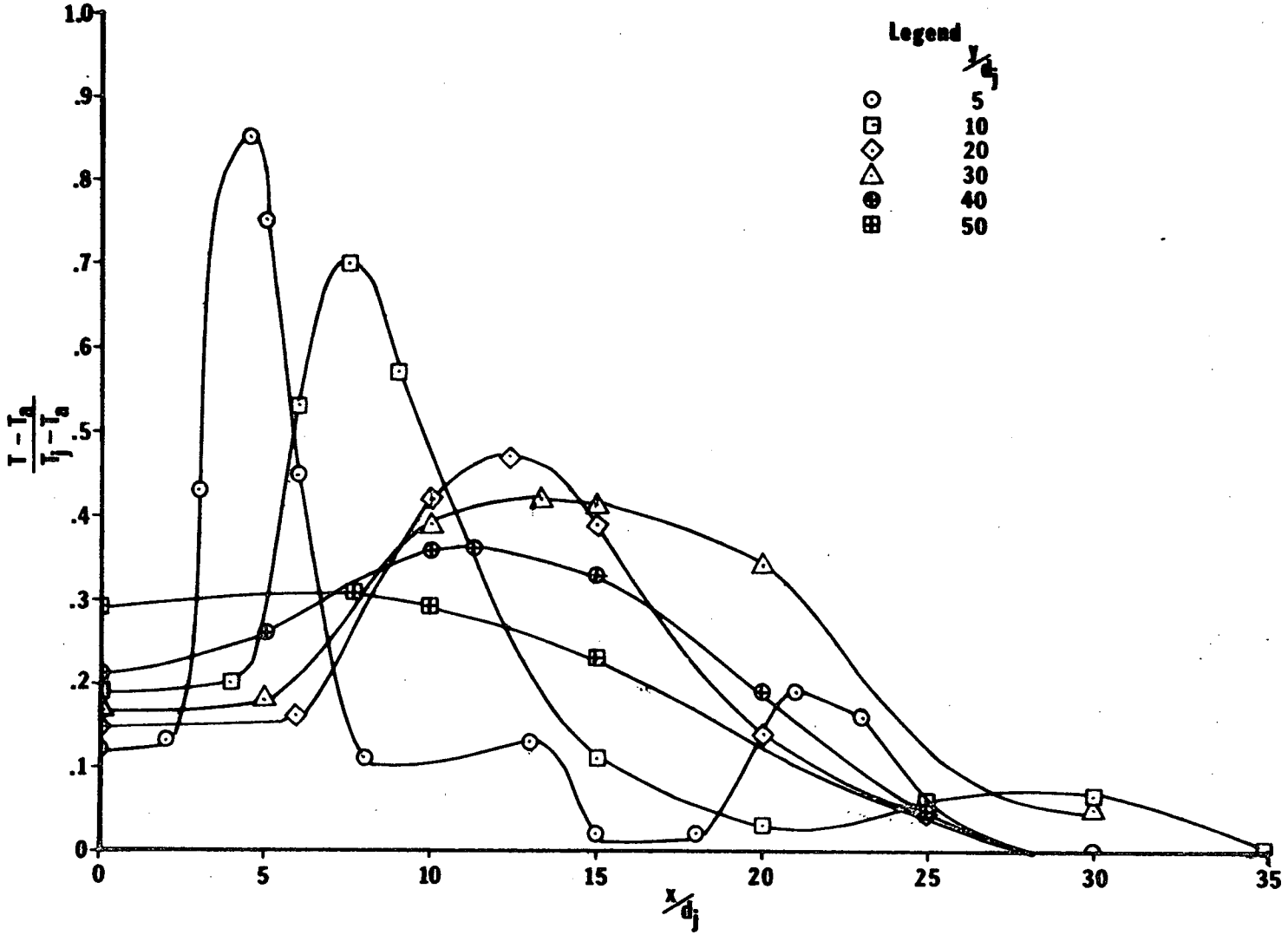

Fig. 3.14. Non-dimensional Temperature Plots for Test 15, $\alpha = 135°$, VR = 10, without inlet suction, $T_j - T_a = 119°F$

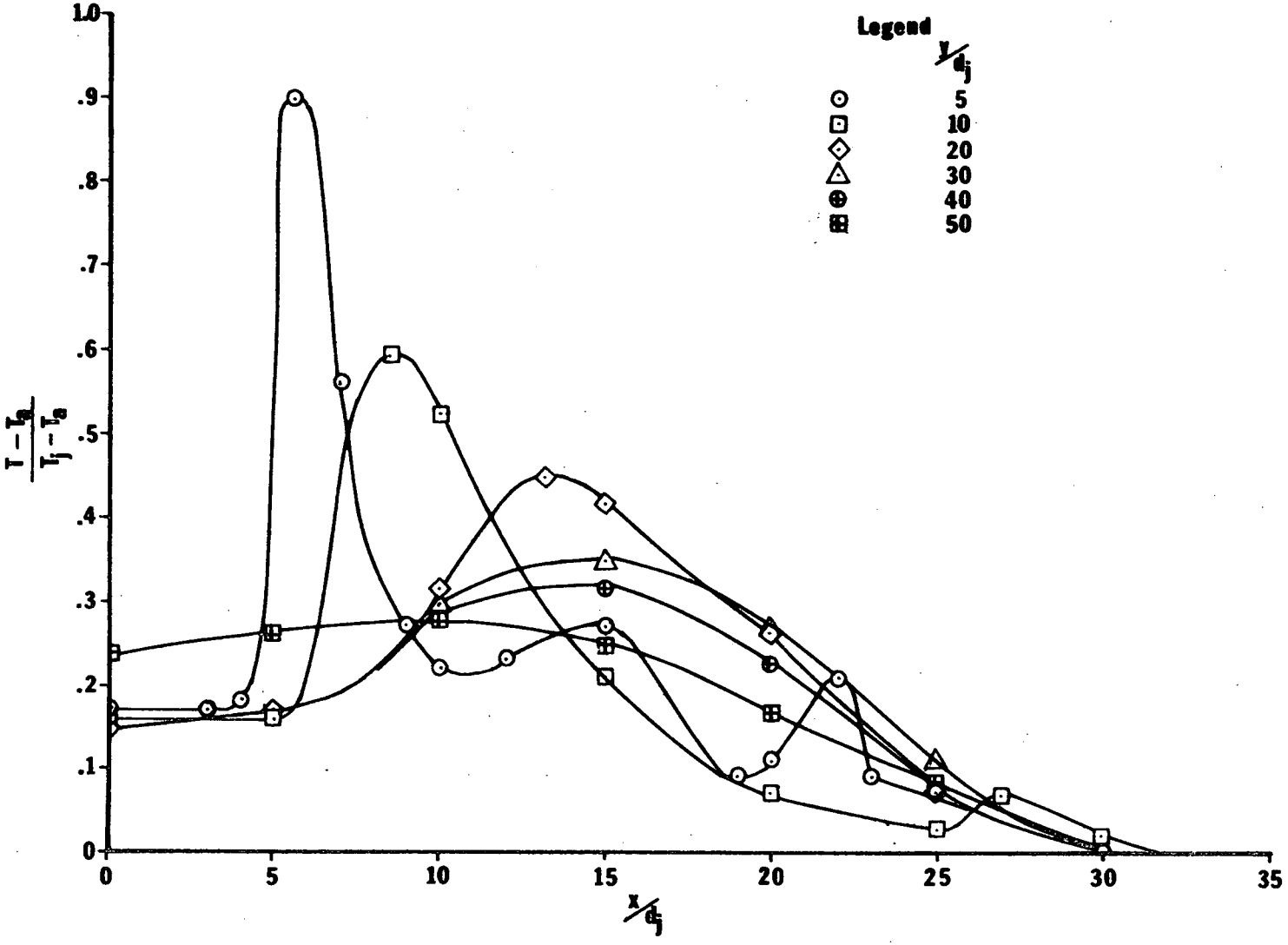

Fig. 3.15. Non-dimensional Temperature Plots for Test 18, $\alpha = 135°$, VR = 10 with inlet suction, spacing - 6.88 jet widths, $T_j - T_a = 118°F$

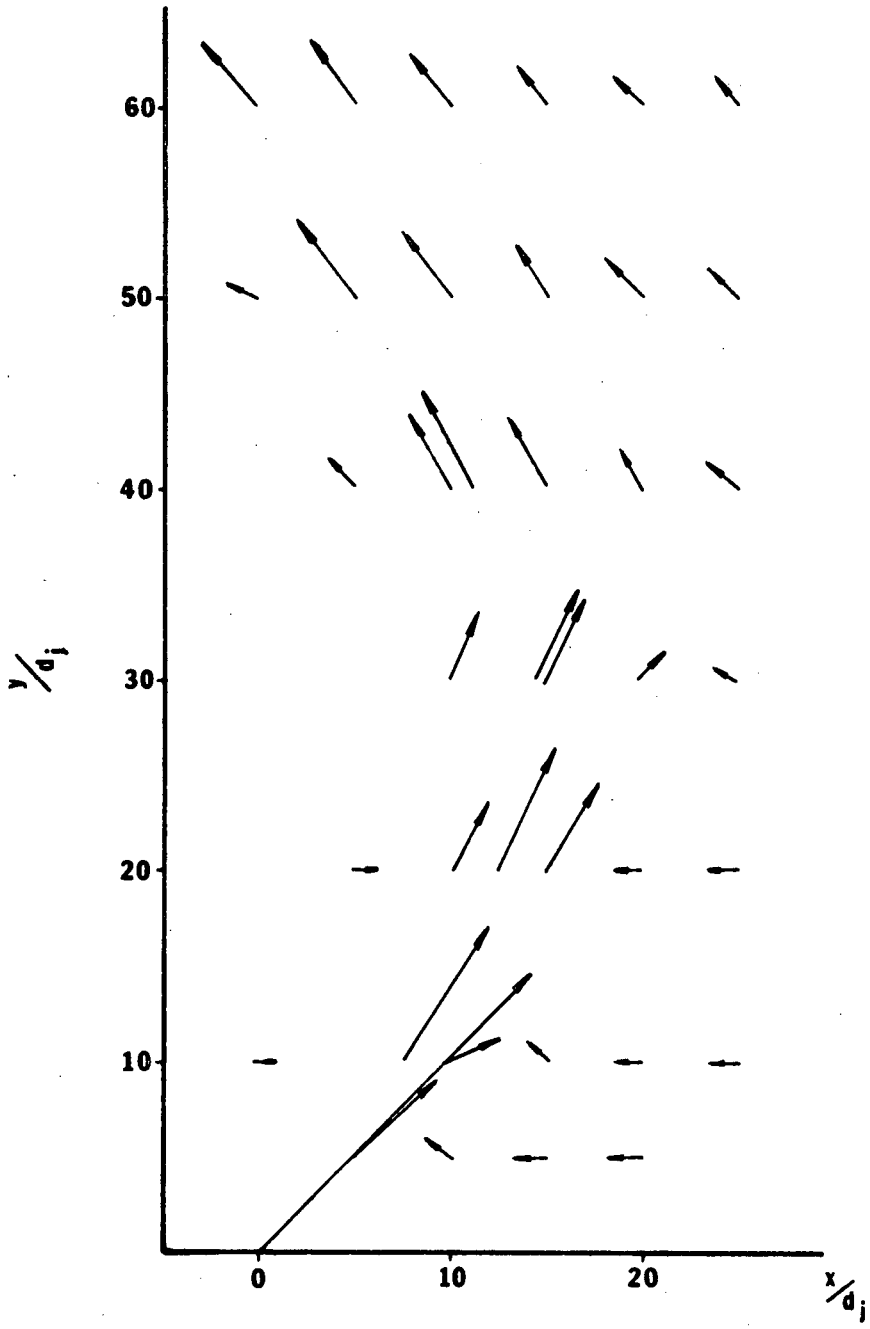

Fig. 3.16. Jet Vector Field, Test 15, No Suction

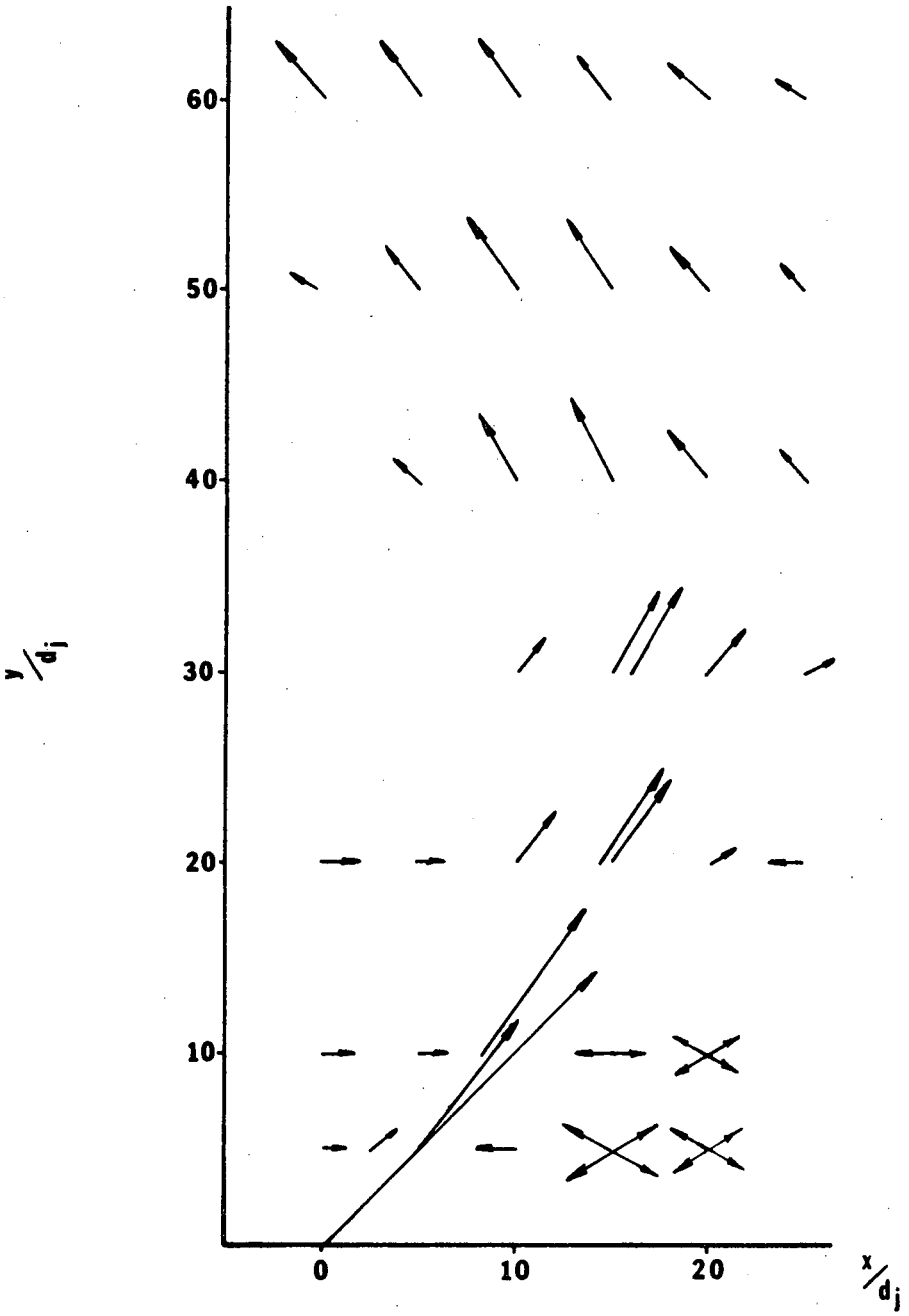

Fig. 3.17. Jet Vector Field, Test 18, with Suction

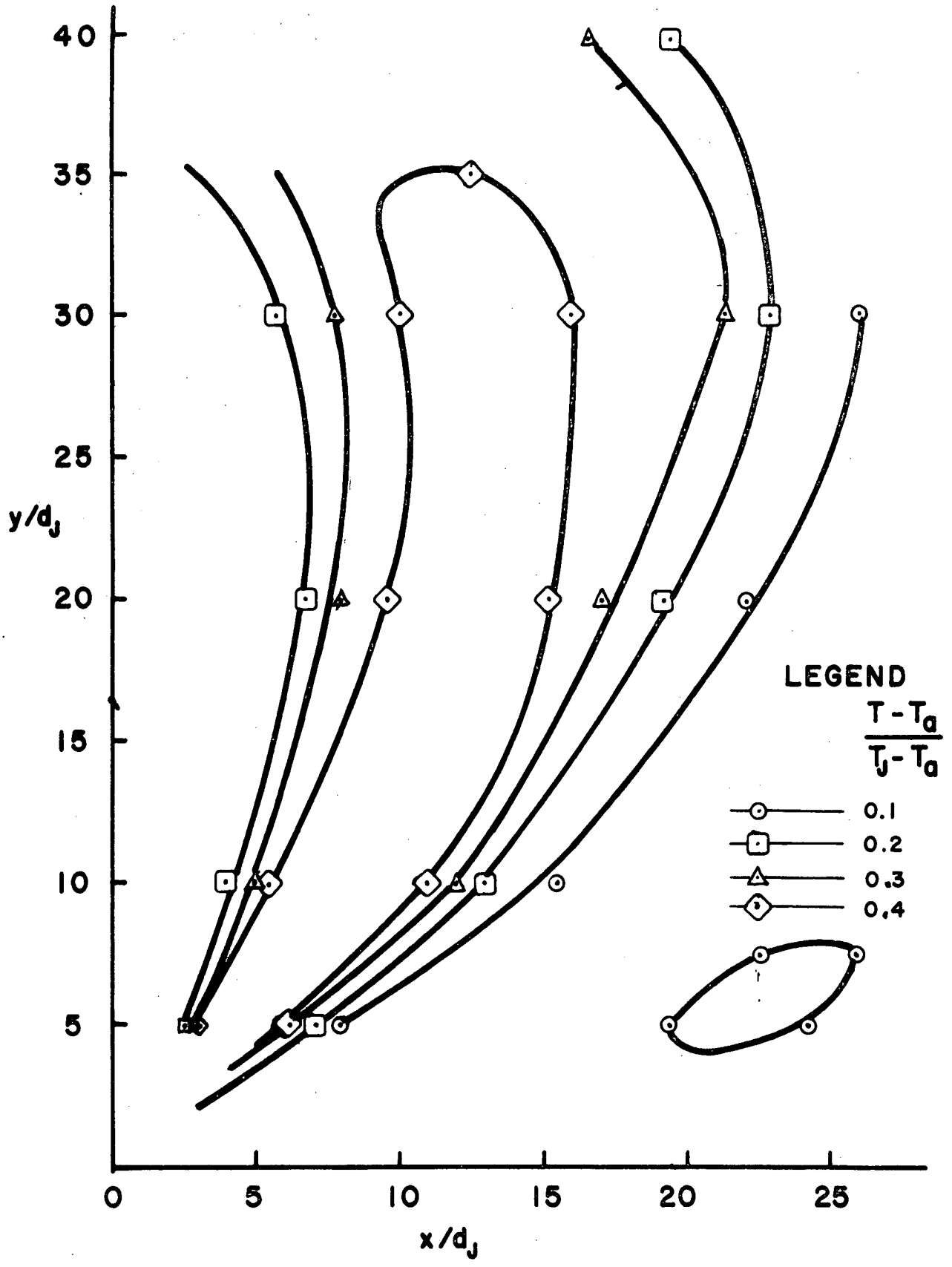

Fig. 3.18. Jet Isothermal Boundaries for 135° Jet - No Suction

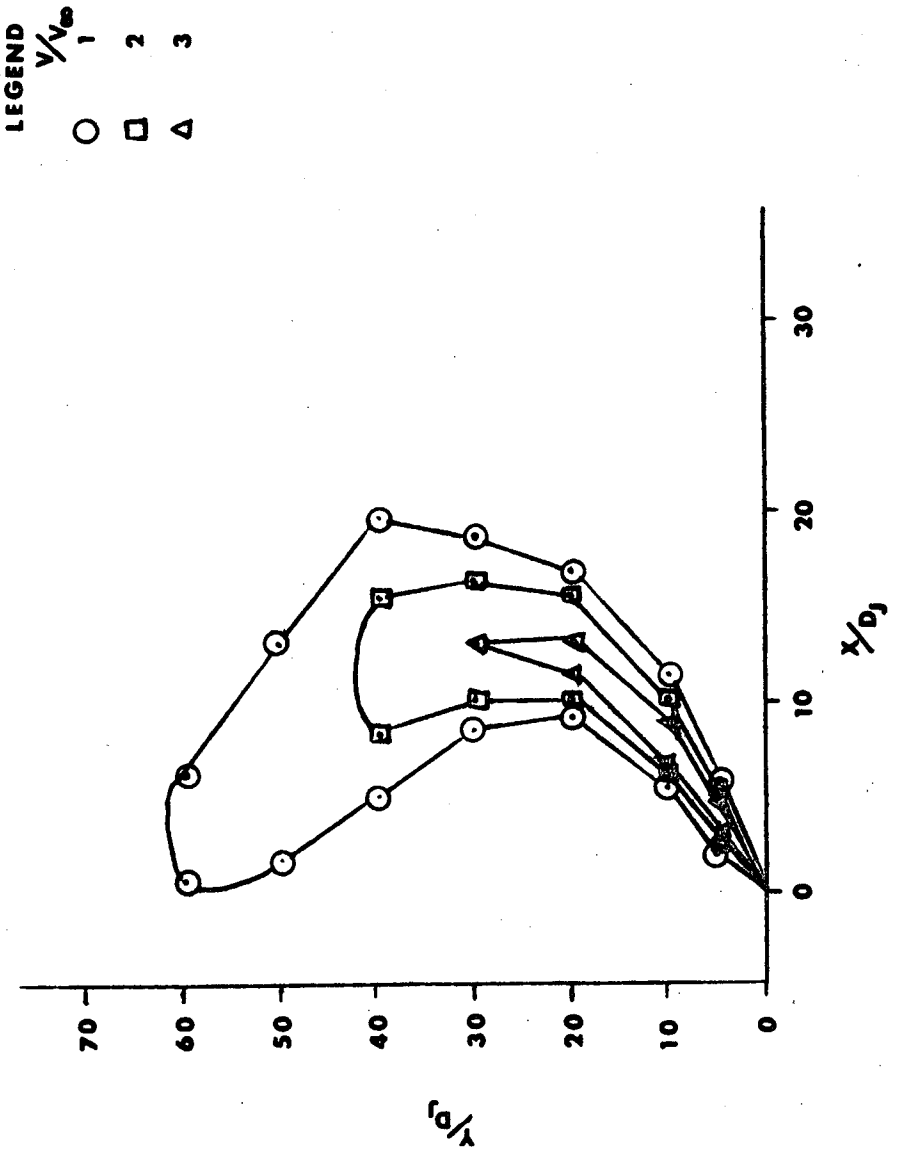

Fig. 3.19. Jet Isotachs for 135° Jet – No Suction

suggest the presence of separated flow. An intriguing result, shown in both figures at y/d_J values of 5 and 10, is a significant temperature rise between 20 and 30 widths ahead of the jet. The fact that this temperature rise (the presence of which was verified by numerous repeat traverses and rerun tests) occurs for tests both with and without inlet suction and is located far ahead of the inlet suggests that it is a property of the transverse jet flow field. Tatom [4] speculates on the presence of a clockwise vortex system ahead of the transverse jet. Such a vortex could carry relatively warm air from the jet forward into a region ahead of the jet exit. This is the only explanation for this peculiar result presently offered. It should be noted, however, that this anomalous temperature rise was not observed at 90°, 120° nor 150° so it appears to be peculiar to the 135° jet.

Presented in Figures 3.16 and 3.17 are velocity vector plots for the 135° jet with and without inlet suction. Examination reveals that, contrary to the temperature data, the velocity vectors exhibit almost complete agreement. An interesting result, verified later in the flow visualization study and shown in these figures is the direct entrainment of the freestream air in the region up to 20 to 30 widths above the jet exit. This illustrates the insensitivity of the external flow to the presence of the jet and again is important to the analysis of ingestion discussed in Section 3.3. Examination of the flow in the region where the anomalous

temperature rises of Figures 3.14 and 3.15 occur reveals in Figure 3.17 some misbehavior of the velocity vectors. Since the x and y velocity components could be either positive or negative and since the presence of the vortex is a possibility, these vectors are plotted in the four orientations allowed. With some imagination the presence of a vortex can be seen, although from the data shown its presence is clearly not established. Shown also in these two figures are vectors behind the jet illustrating the back flow and entrainment into the jet from the rear. They also provide some indication of the presence of a large vortex or separated flow region behind the jet.

Figures 3.18 and 3.19 correspond to the 135° jet without suction and are useful in demonstrating the shape of the deflected jet. The figures also illustrate the very rapid diffusion of temperature and momentum that occurs within the deflected jet due to the large shearing mechanisms present.

Finally, as part of the transverse jet investigation a flow visualization study was conducted. In this study hydrogen sulfite smoke, generated by the reaction of ammonia and sulfur-dioxide, was introduced into the freestream at two upstream points and injected at a single point in the jet itself, and the flow field was then photographed. Initially the pictures were taken sometime after the smoke generator had been turned on. It was found, however, that the three-dimensional

properties of the vortex downstream of the jet were such that this region, which extended from one side of the tunnel to the other, became completely filled* with smoke. The photographic result was not very useful in visualizing the fluid motion in this region since the vortex appeared as a large bright circular blur, and so it was decided to try to take the pictures as shortly as possible after the smoke was turned on in the hope of catching the circular flow while discrete elements of the vortex were still visible. The pictures shown in Figures 3.20 through 3.24 were all taken using this latter technique. Inspection of these photographs reveals that unfortunately, with only one or two exceptions, they do not provide a really good presentation of the recirculation region behind the jet either and that often they suffer from a lack of smoke. Besides the smoke problem one of the difficulties which contributed to a degradation of the photographic quality of the pictures was the problem of lighting, and film and shutter speed. Too much light tended to blind the camera to reflections from the tunnel surfaces and so the best compromise was to use moderate lighting and a film with as high an ASA speed as possible. Thus Kodak Tri X was used in all the pictures. Unfortunately, this film was still not fast enough to allow operation of the camera at a shutter speed sufficient to freeze the motion. Hence a considerable amount of blurring is present.

---

*An interesting sidelight to this condition was the persistence of the smoke; even after the generator had been shut off the vortex continued to remain visible for perhaps 5 to 10 seconds. This provided evidence that fluid in the separated region behind the jet tended to be trapped there for some period and was reentrained into the jet numerous times.

VR = 5

VR = 10

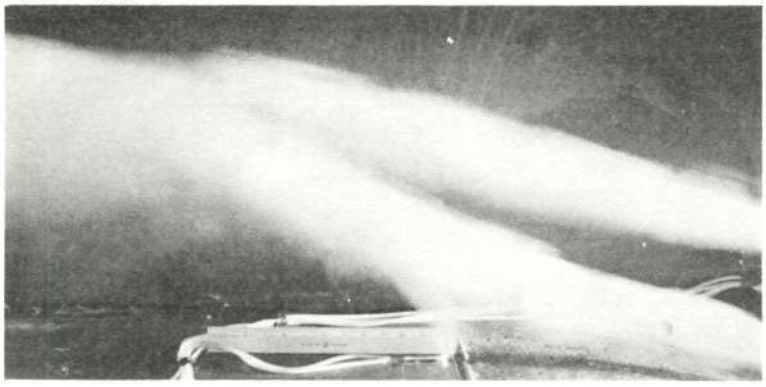

VR = 20

Figure 3.20 Flow Visualization Pictures; $\alpha = 90°$ without suction

VR = 5

VR = 10

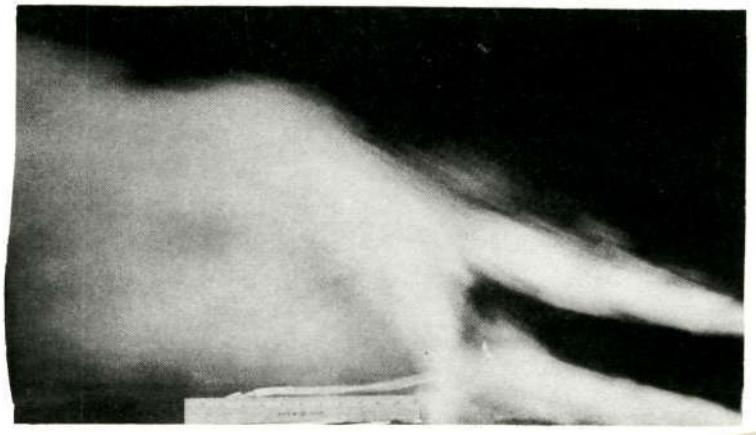

VR = 20

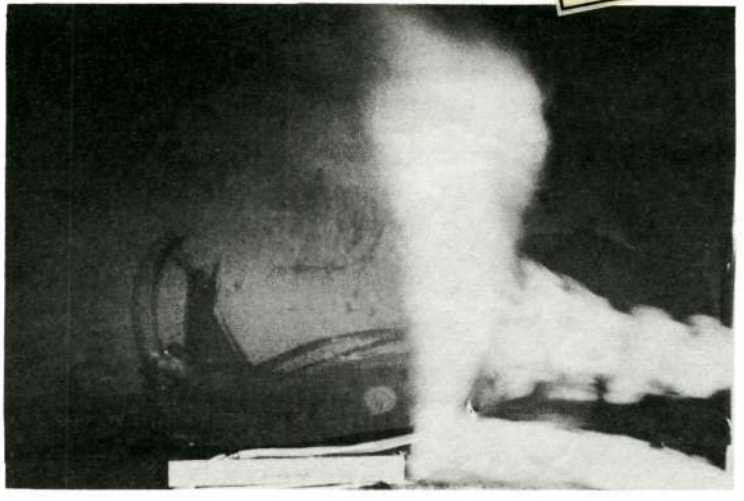

Figure 3.21. Flow Visualization Pictures; $\alpha = 120°$, without suction

VR = 5

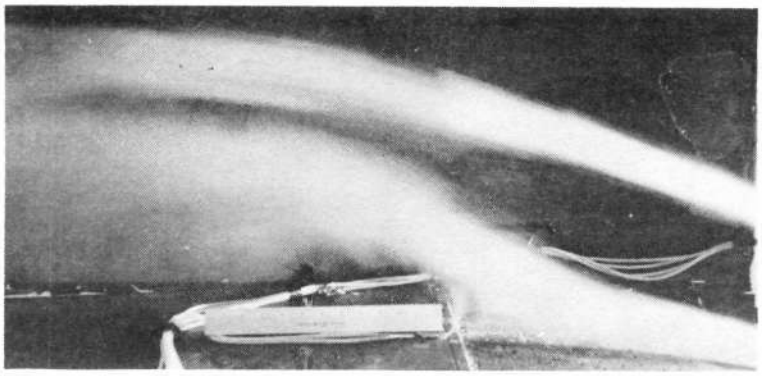

VR = 10

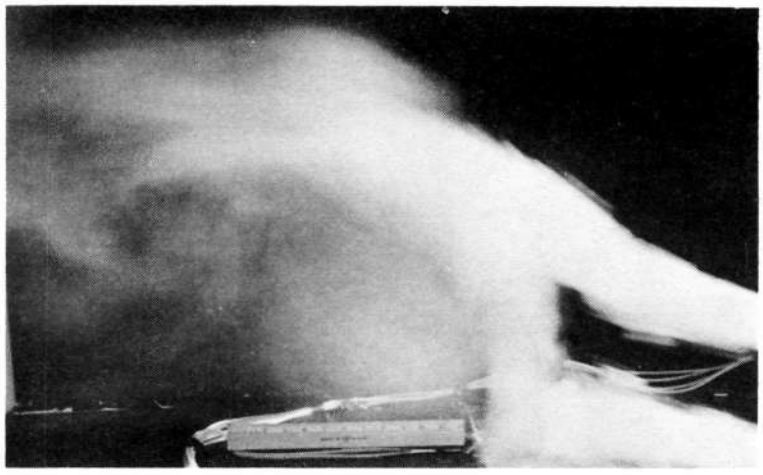

VR = 20

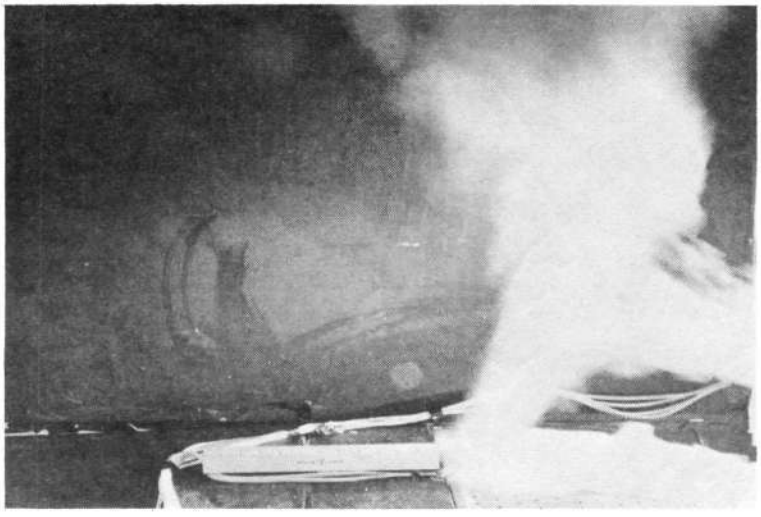

Figure 3.22 Flow Visualization Pictures; $\alpha = 135°$ without suction

VR = 5

VR = 10

VR = 20

Figure 3.23 Flow Visualization Pictures; $\alpha = 135°$ with suction

VR = 5

VR = 10

Figure 3.24. Flow Visualization Pictures; $\alpha = 150°$, without suction

Even with these shortcomings the pictures provide a valuable means for observing the properties of the flow. Besides showing the vortex behind the jet, the photographs illustrate the significant entrainment at all jet angles of the freestream by the jet, a condition which results in a relatively minor deflection of the external air, especially near the jet exit and at the larger velocity ratios. The 135° jet pictures also demonstrate the relatively minor effects that inlet suction had on the overall flow field. Figure 3.24 presents a view of the attached 150° jet at a jet-to-freestream velocity ratio of 10. It appears that the jet penetrates approximately 100 jet widths before it detaches from the model. This would be a disastrous length if it were applied to a realistic engine nacelle cascade reverser. Thus it seems clear that the 150° jet, without some drastic means to prevent attachment, is not suitable for cascade reverser applications. Finally, no evidence of the presence of vortices in front of the 135° jet is seen in the figures. Because of the blurring which occurs in the region where vortices might be expected due to the rapid fluid motion, their apparent absence is not believed to be conclusively established however. Clearly some closer further study of this region would be desirable.

3.1.4.4 Data Correlation

As mentioned earlier, only limited data concerning the plane transverse jet were found in a search of the literature. This, of course, limits the amount of data correlation that can be done. However, there

is the report by Ivanov [5] showing the centerline trajectories of two-dimensional jets resulting from velocity data and in the empirical equation by Vizel and Mostinskii [8] derived using Ivanov's data. During testing it was observed that the temperature peaks occur at approximately the same position as the velocity maximums. Thus a correlation between the trajectories predicted by the equation formulated by Vizel and Mostinskii using the velocity data of Ivanov and the temperature and velocity trajectories resulting from the present tests at 90° and 135° was made. The equation used is the following:

$$x/d_j = \frac{1}{4} C_x \rho_\infty V_\infty^2 \left(\rho_j V_j^2 \sin\alpha_J\right)^{-1} \left(y/d_j\right)^2 + \left(y/d_j\right) \cot \alpha_J$$

where:

x and y = horizontal and vertical coordinates,

d_j = width of the jet,

ρ = density of the fluid,

V_∞ = ambient velocity,

V_j = initial velocity of the jet,

α_J = angle of the jet, and

C_x = entrainment or drag coefficient.

The entrainment or drag coefficient is dependent upon the angle and velocity ratio. Using data from Ivanov, Vizel and Mostinskii found the value of C_x to be about 5 for a 90° jet angle. However, it

should be noted that in [8] there was substantial deviation of the predicted curve using $C_x = 5$ from Ivanov's data at a velocity ratio of approximately 10. In the present investigation, mean values of C_x were calculated by solving the above equation for C_x at several points along the trajectory and then averaging the results. This method produced average values of C_x as shown in Figures 3.25 and 3.26. For the 90° angle tests, the values of 4.32, 4.80 and 12.97 were found for the velocity ratios of 5, 10 and 20, respectively. For the 135° jet, corresponding values of 2.27, 4.62 and 7.42 were obtained. Although there are differences between the present C_x values at 90° and those from [8], the jet trajectories do fall nicely along parabolas as predicted. One explanation for the variation in C_x values may be the differences between the initial jet velocity shape factor for the present work and that of Ivanov.

To further compare the results of this investigation with prior work, including the recent analytical investigation by Tatom [4], Figure 3.27 is presented. Plotted in this figure are experimental velocity vector data from Ivanov [5] and from test (0) of the present study together with the computed results from [4]. In general the three families of vectors show good agreement. One main difference between the predicted data and that measured was the extent of the region of separated flow behind the jet. The analytical results predict a much smaller region than

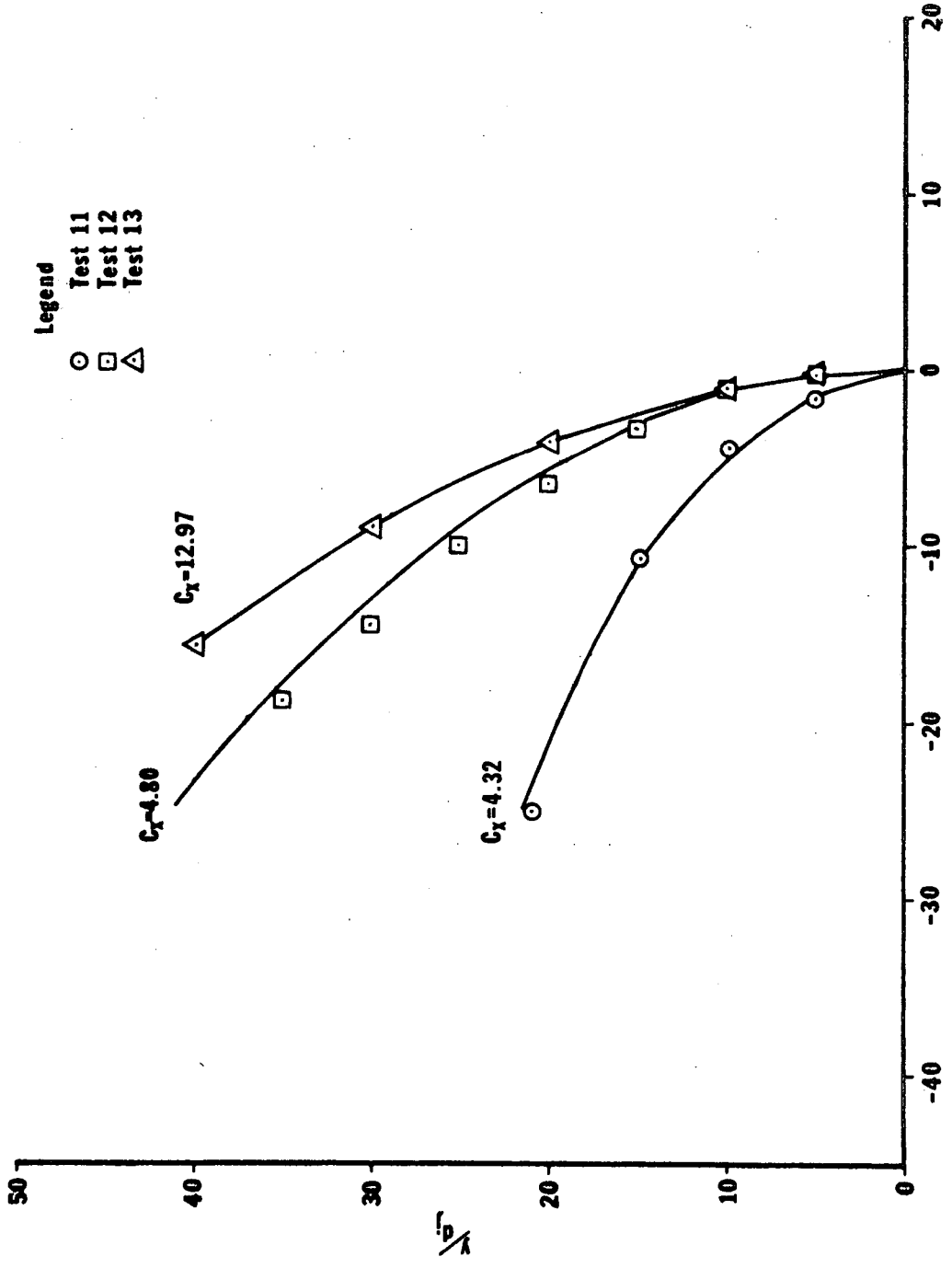

Fig. 3.25. Correlation of Results for 90° Jet

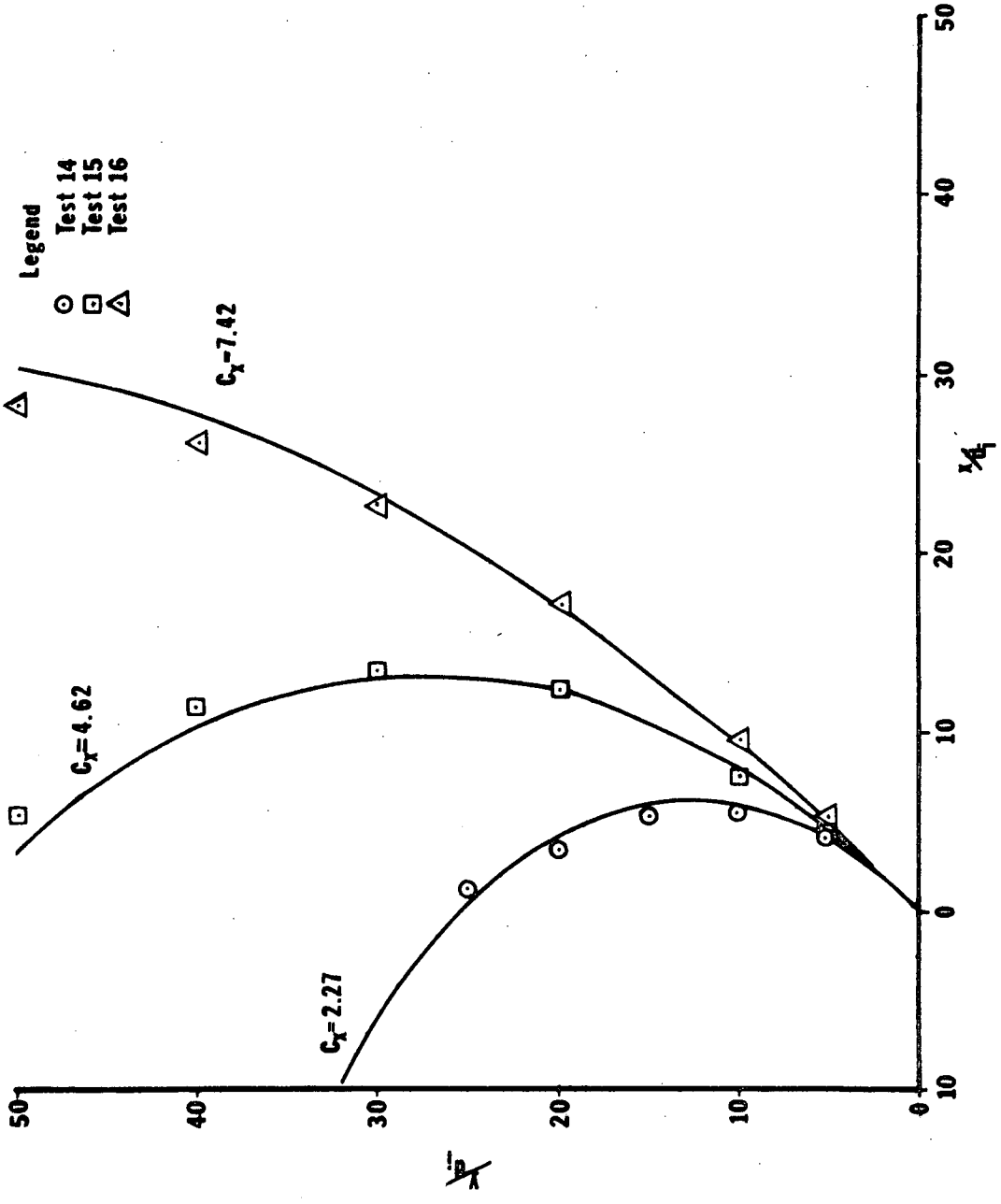

Fig. 3.26. Correlation of Results for 135° Jet without suction

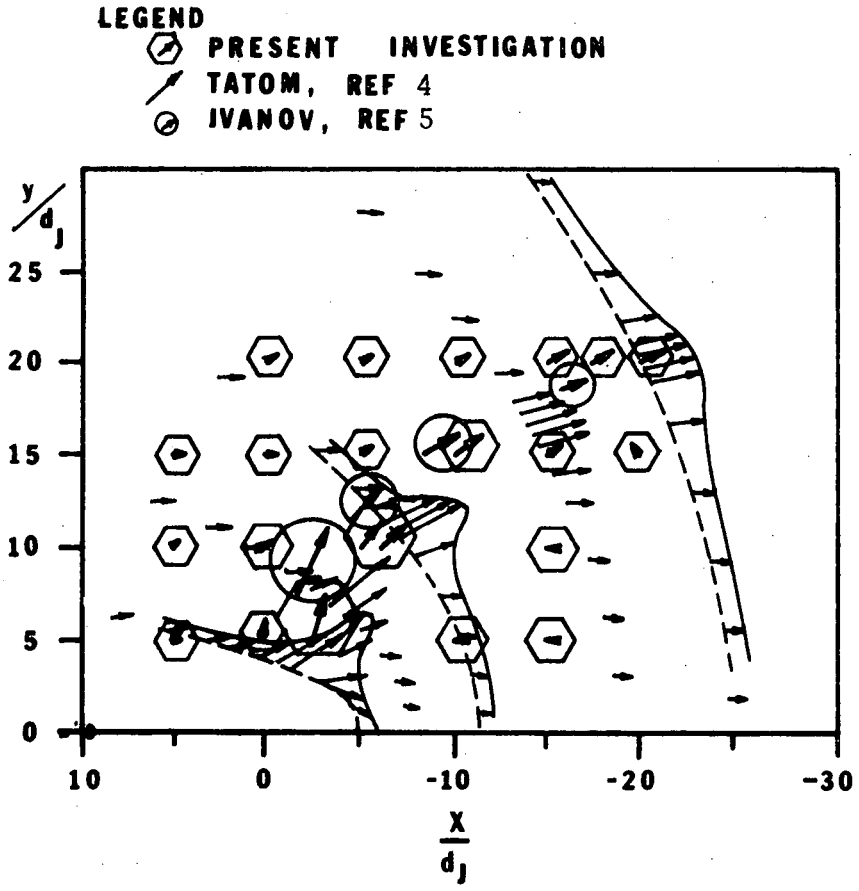

Fig. 3.27. Comparison of Results for 90° Jet

observed. It is believed, however, that if additional time for convergence had been available in the analysis of [4], better agreement would have resulted, since the size of the separated flow region was increasing when the computations were terminated.

3.1.5 Conclusions

From the results of this investigation, the following conclusions can be drawn:

1) A large, relatively high temperature region of separated flow lies downstream of the hot two-dimensional transverse jet.

2) Entrainment of the freestream by the jet results in a minor deflection of the freestream ahead of the jet and especially near the jet exit.

3) The effects on the deflected jet flow field of inlet suction and jet-to-inlet spacing are small, so long as jet attachment does not occur.

4) At large turning angles, jet attachment frequently occurs and in these cases the presence of inlet suction can cause great changes in the character of the flow field.

5) The presented results appear to be consistent with available information.

3.2 THE DEFLECTED RADIAL PLANE JET

The two-dimensional transverse jet study discussed in Section 3.1 has as its primary justification the cascade thrust reverser. Yet, clearly there is a difference between the efflux from a cascade reverser and the plane transverse jet. Knowledge of this difference is needed before the data of Section 3.1 can be applied most effectively to the cascade reverser. The following approximate analysis* is presented then in an effort to determine this difference and, hopefully, to provide a bridge by which the available test data can be applied to the cascade reverser.

Consider an incompressible isothermal radial plane jet of initial thickness δ_o exhausting at an angle α_o from the surface of a cylinder of radius R_o and, for the moment, into still air (see Figure 3.28). Assume that, like its plane-two-dimensional counterpart and also the round jet, once fully developed turbulence is present the following relation holds:

$$\left(\frac{u}{u_m}\right)^2 = f(y/b(x)) = f(\xi) \qquad (3.1)$$

where: u = local jet velocity

u_m = maximum jet velocity at a station x

y = distance transverse to jet centerline

$b(x)$ = jet semi-thickness

$f(\xi)$ = universal jet velocity distribution.

---

*This analysis in a slightly different form was developed for General Dynamics, San Diego, as part of a short investigation supporting their work. It is reproduced here for completeness with their permission.

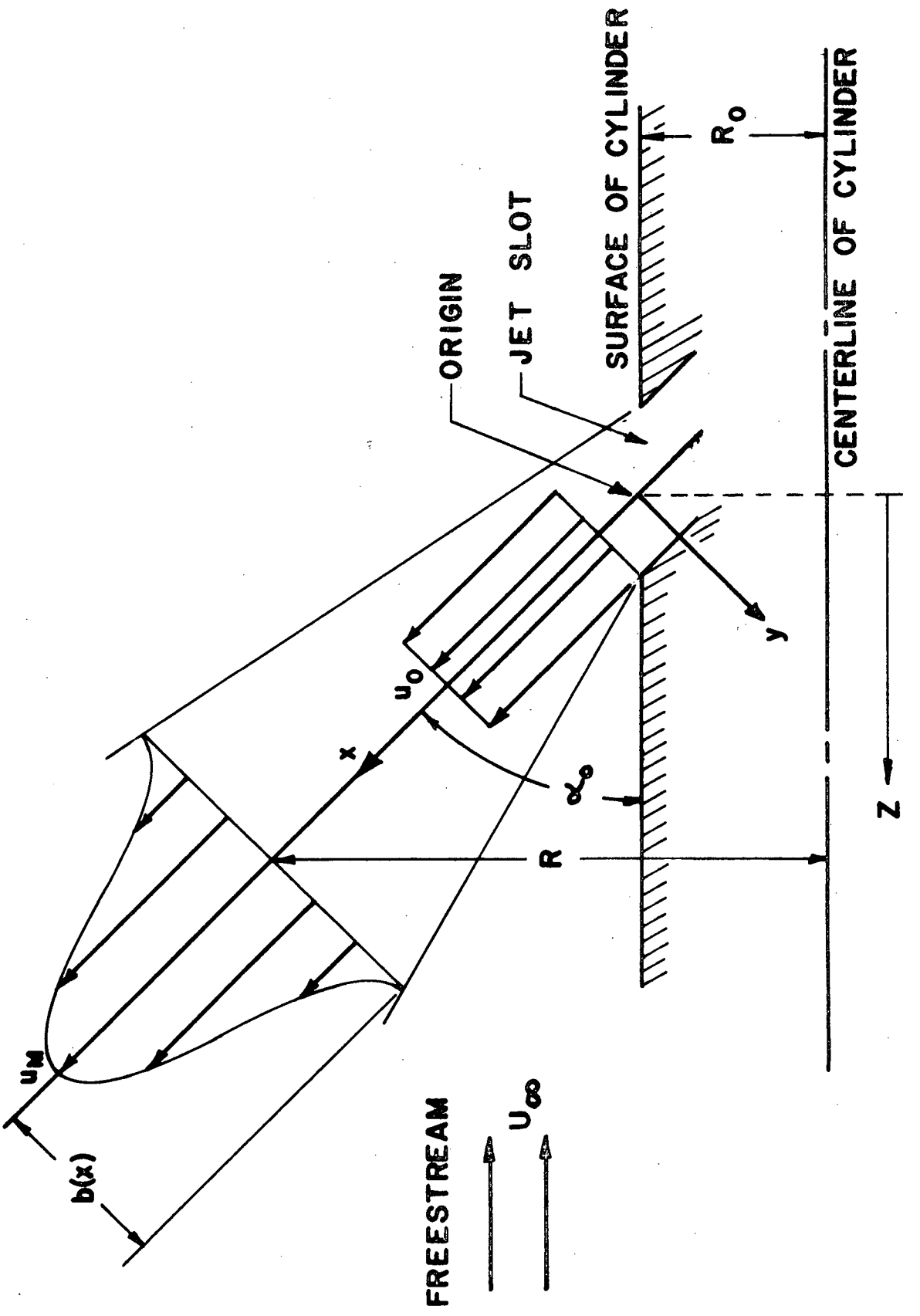

Fig. 3.28. The Deflected Radial Jet

2-3

Now the total jet momentum flux, M_x, is conserved. Hence at a given x location:

$$M_x = 2\rho_o u_o^2 \delta_o \pi R_o = \int_o^b 4 \rho_o u^2 \pi R dy \qquad (3.2)$$

where ρ_o = jet density
u_o = jet exit velocity
R_o = jet exit radius
R = R_o x sin α_o

Applying the assumed universal velocity distribution relation, it can readily be shown that

$$\frac{u_m^2}{u_o^2} = \frac{R_o \delta_o}{b(x)(R_o + x \sin \alpha_o)\, 2J} \qquad (3.3)$$

where $J = \int_o^1 f(\xi)\, d\xi$

Again from the results for the plane and the round jet, take

$$b = kx = k \frac{(R - R_o)}{\sin \alpha_o} \qquad (3.4)$$

where k is an unknown constant.

For round jets $k_o \tilde{=} .072$, for plane-two-dimensional jets $k \tilde{=} .050$.

Thus

$$\frac{u_m}{u_o} = \frac{\delta_o}{x} \left\{ \frac{1}{\left[\frac{\delta_o}{x} + \frac{\delta_o \sin \alpha_o}{R_o} \right] 2kJ} \right\}^{1/2} \qquad (3.5)$$

Now consider the radial plane jet exhausting at some angle α_o from the surface of a cylinder into a freestream at velocity U_∞. Following the approximate approach of Abramovich (Ref. 9) in his discussion of the air curtain, assume: (1) the dependence of the jet average radial velocity, component on distance from the origin remains the same as that in still air, but (2) the axial component of the average jet velocity is summed up algebraically with the velocity of the crosswind. In addition, (3) assume that the local jet angle α is approximately equal to α_o for the portion of the jet trajectory of interest.

Write:

$$\frac{dR}{dt} = \bar{u} \sin \alpha_o = v_r \tag{3.6}$$

$$\frac{dz}{dt} = U_\infty + \bar{u} \cos \alpha_o = v_z \tag{3.7}$$

Thus:

$$\frac{dz}{dR} = \frac{U_\infty}{\bar{u} \sin \alpha_o} + \cot \alpha_o = \frac{v_z}{v_r} \tag{3.8}$$

Applying the first assumption and treating the term under the radical in in (3.5) as a constant χ, approximately*, write:

$$\frac{\bar{u}}{\bar{u}_o} \simeq \frac{\chi}{\bar{x}} \tag{3.9}$$

where:

$$\bar{x} = \frac{x}{\delta_o} \tag{3.10}$$

and

$$x = \frac{(R - R_o)}{\sin \alpha_o}$$

---

*The approximate character of the analysis justifies this simplification.

Thus

$$\frac{d\bar{z}}{d\bar{R}} = \frac{U_\infty (\bar{R}-\bar{R}_o)}{\bar{u}_o \chi \sin^2 \alpha_o} + \cot \alpha_o \qquad (3.11)$$

where: $\bar{z} = z/\delta_o$ and $\bar{R}_o = \frac{R_o}{\delta_o}$

$\bar{R} = R/\delta_o$

Integrating and applying the boundary condition $z(\bar{R}_o) = 0$ gives the desired result

$$\bar{z} = \frac{U_\infty}{2 u_o \chi \sin^2 \alpha_o} (\bar{R}-\bar{R}_o)^2 + (\bar{R}-\bar{R}_o) \cot \alpha_o \qquad (3.12)$$

It is interesting that the corresponding two-dimensional solution taken from [9] (and which checks the data nicely) is in nearly identical form, i.e.,

$$\bar{x} = \frac{2 U_\infty \bar{x}^{3/2}}{3 \bar{u}_o \chi \sin^{3/2} \alpha_o} + \bar{y} \cot \alpha_o \qquad (3.13)$$

Clearly these two equations provide a convenient means for relating the available two-dimensional data to the radial plane jet case.

3.3 ANALYTICAL INVESTIGATION OF INGESTION - NO CROSSWIND

The outline of an analytical method which allows prediction of the onset of ingestion in the case of a single nacelle operating in reverse thrust and located within an axisymmetric freestream was presented in [1]. In this analysis, a basic assumption was the independence

of the inlet and the reversed jet flow fields. Thus, so far as this analysis is concerned, one of the more significant results of the two-dimensional jet testing is the apparent insensitivity of the jet flow field to the presence of inlet suction. Further, it appears that the freestream flow is not affected significantly by the jet's presence. Now since the two-dimensional jet is much more sensitive to the external flow than a round jet [9], it is quite justifiable to assume that a discrete reversed jet (round or otherwise) will not be affected by inlet suction either and is predominantly influenced by the freestream. The freestream, however, is not especially influenced by the jet presence.* This provides then, a verification for the above assumption and thus the basis for a great simplification in the analysis of ingestion.

Referring to [1], the remaining task in the analysis, once the independence of the inlet and the jet flow fields is determined, is to locate the pre-entry streamline and to determine whether the maximum penetration point of the reversed jet lies inside or outside this streamline. To locate the pre-entry stream tube requies a mathematical solution of the potential flow field around an aircraft engine nacelle operating in the presence of a freestream. Since the reversed jet trajectories involve strongly turbulent flow and are to be determined from test correlations independently of the potential flow calculations, the nacelle is considered to be ingesting but not exhausting any freestream air. In addition, since

---

*Keffer and Baines [10] observed in the case of the round deflected jet "The external flow is affected very little by the presence of the jet".

the primary emphasis is on the flow some distance from the nacelle and since this flow should be relatively independent of the exact nacelle shape, it is assumed that the actual nacelle can be represented by a right circular cylinder with the same aspect ratio. Thus the problem reduces to finding the pre-entry streamline corresponding to a cylinder with an inlet facing into the freestream.

There are several ways to develop the desired potential flow field [11], most of which involve the use of a system of distributed sources and sinks. The basic problem (i.e., the Neuman Problem) is determining the strength of the various singularities used to generate the nacelle. While standard computer routines [12] have been developed to generate aerodynamic surfaces such as engine nacelles, none is presently available at the Vanderbilt Computer Center and it was felt more expedient and informative to develop a method rather than try to obtain, debug and become familiar with an existing program.

The method* chosen for determining the strength of the singularities used to generate the nacelle is basically iterative. The fundamental idea is that the normal velocity at the surface of the nacelle must be zero and the strength of the singularities must be adjusted until this velocity vanishes. The computational procedure operates as

---

*The basic principle of the computation procedure for calculating the source/sink distribution presented here arises partially from the analysis of [13]. However, the method of iteration, indeed, the need for an iterative procedure was developed as part of this investigation.

as follows:

1) The flow field generated by the inlet (which is taken as a disc sink of uniform strength) and the freestream is calculated, and the normal velocities induced at selected points along the representative cylinder and end cap are determined.

2) Singularities which induce velocities equal and opposite to those induced by the inlet-freestream combination are added at the appropriate points and then the normal velocity induced at each point by all the other points is calculated.

3) The strength of each singularity is then adjusted to compensate for the induced velocity at that point by all the other singularities and the process continued until the normal velocity at each point is reduced to some prescribed value.

Using a convergence criteria of one percent of the freestream velocity with a system of 21 cylindrical points and 21 end cap points, this process converges within about 10 iterations and two minutes on the Vanderbilt Sigma 7 computer.

Once the potential field for the system is determined, the location of separate streamlines is found by applying the condition that

along any streamline the Stokes stream function is constant. The procedure involves taking derivatives of the velocity potential with respect to axial and radial position and solving numerically the ordinary differential equation which must be satisfied by each streamline. This is not a simple operation, however, since the streamlines can have rather complex shapes. An example of the preliminary results of this program is presented in Figure 3.29, where several streamlines are shown for a typical cylindrical nacelle.

A complete description of this potential flow computation method combined with the jet analysis of [1] is presented in [14] and typical predicted results using the method are shown.

3.4 BLOWN FLAP/THRUST REVERSER MODEL

The flap system for an externally blown STOL aircraft represents a structural assembly which has many of the characteristics required of a thrust reverser. It is strong, capable of a high temperature environment, is located immediately behind the engine exhaust and can be rapidly deployed. Because of these simularities the question of whether it can be used as a thrust reverser arises; the idea being that the jet exhaust could be captured and deflected forward and upward through a slot in the wing by the flaps. Not only would such an arrangement utilize already required hardware, it would exhaust the jet into a flow region where because of the wing presence, engine ingestion would be

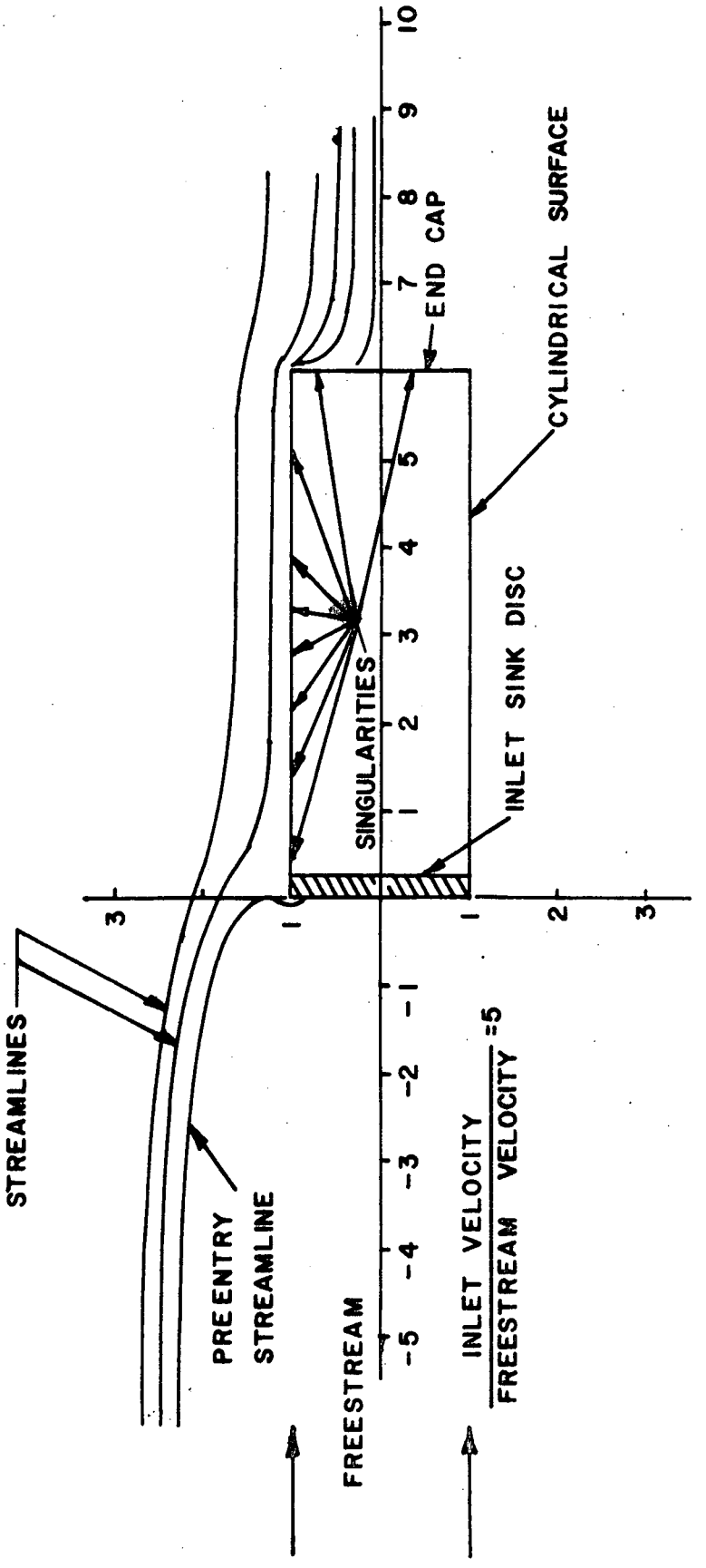

Fig. 3.29. Potential Flow Field for Cylindrical Nacelle

extremely unlikely to occur. In addition the upward and forward moving jet should provide some spoiling of the wing aerodynamics with the associated increase in drag.

To investigate such a system, work has begun on a semi-span wing model to be tested in the low speed section of the wind tunnel. Because no force balance is available for this tunnel section, a ball bearing supported, moment balance system including a viscous damper has been constructed and a preliminary split flap wing section has been built to test it. This model and the balance are shown in Figures 3.30a & b. Present indications are made that the balance system operates very well.

Construction of the flap reverser model has been initiated but fabrication is incomplete at this writing. To avoid the problem of tailoring the jet impingement on the flap reverser system, the model to be tested will be hollow. Air will be supplied at one end and will be exited from a span wise slot in the aft section of the wing. Thus the model will resemble a thrust reverser for an Augmentor Wing type STOL aircraft. Total drag plus reverse thrust measurements will be made at various jet-to-freestream velocity ratios. A flow visualization study is also planned.

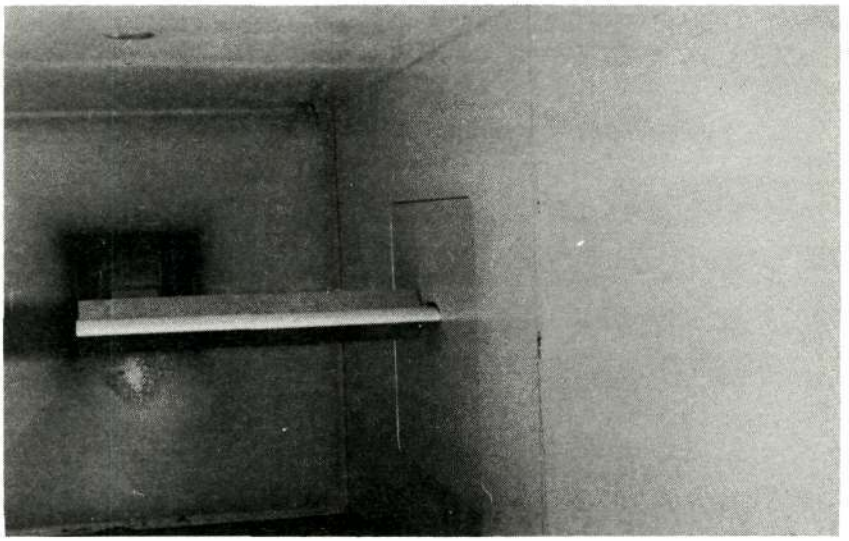

Figure 3.30a. Preliminary Split Flap Model for Balance Check Out

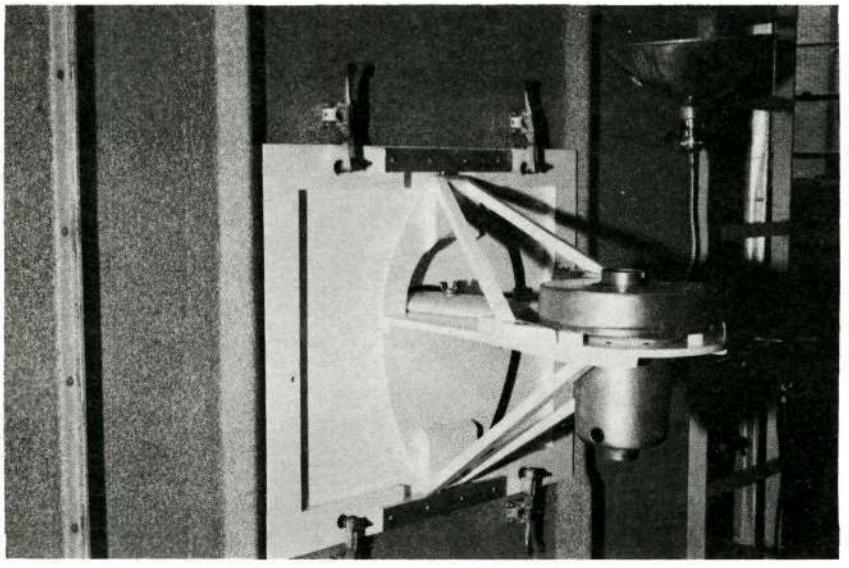

Figure 3.30b. Balance System Including Blower for Blown Flap/Reverser Model

4. IMPINGING JET STUDY

This study is directed toward providing a means for analysis of the flow fields generated by jet impingement on and/or deflection by thrust reverser surfaces. The study is divided into an analytical and an experimental investigation. At the outset the emphasis in this study was analytical, with the experimental program providing a means for check of the analysis. However, it has become increasingly apparent that mathematical solution to the general three-dimensional jet impingement problem may be beyond the presently available resources of this study. This is due primarily to the difficulty in locating the three-dimensional deflected jet freestream surface. In [1] this problem and its solution are discussed for the case of the plane impinging jet where locating the freestream line is the principal difficulty. The problem is greatly compounded, however, when non-symmetric three-dimensional jet impingement is considered. As an alternative approach it has, therefore, been decided that a generalized jet impingement study should be conducted experimentally with the aim of not only providing useful test data but also with the hope of finding means, perhaps semi-empirical or approximate, by which the impinging jet analysis can be later extended.

4.1 ANALYTICAL INVESTIGATION

The following analytical work was accomplished during the

second year of the investigation:

1) An analysis of a round jet impinging on an axisymmetric deflector of arbitrary shape was developed.

2) The round jet solution was extended to include the effects of compressibility.

3) The effects of geometry on reverser performance were systematically investigated for both the round and the plane jet.

Each of these areas is discussed.

4.1.1 The Impingement of a Round Jet on an Axisymmetric Surface of Arbitrary Shape

The numerical solution of a circular jet impinging on an axisymmetric surface was developed largely through revision of the plane jet solution discussed in [1]. One significant change, however, was to use the finite difference form of the Laplace equation in cylindrical coordinates instead of cartesian coordinates. It was also necessary to revise the calculations of flow rates and reverse thrust to account for the circular cross-section of the jet and deflector. The final change was the introduction of a variable grid spacing. This was necessary because the deflected jet beomes quite thin as radial distance from the stagnation point increases. If a sufficient number of node points is used in the relatively thin outer region, using a constant grid spacing,

this produces a very large number of node points in the region nearer the jet centerline, a condition which results in excessive computation time. This difficulty was overcome by using a coarse grid in the region near the jet centerline and a finer grid for the outer portion of the jet.

A sample output and statement listing for this program are included as Appendix B. Examination of this listing reveals many similarities with that for the plane jet presented in [1].

4.1.2 The Effects of Compressibility

One of the basic assumptions in the analysis has been to neglect compressibility effects. However, because the jet exhaust velocity for many aircraft engines is quite large, it was considered important to determine the Mach number range for which this assumption does not cause significant error. This was done by solving the compressible flow equations in the round jet program for a limited number of cases.

The compressible flow problem is solved in exactly the same way as the incompressible case with the one exception of a change in the finite difference equation used. There were some difficulties in using the compressible flow equation in finite difference form, however, so some discussion of the details of this aspect of the work are included.

The compressible potential flow equation in cylindrical coordinates is

$$\left(1 - \frac{(\partial\phi/\partial r)^2}{c^2}\right) \frac{\partial^2\phi}{\partial r^2} + \left(1 - \frac{(\partial\phi/\partial z)^2}{c^2}\right) \frac{\partial^2\phi}{\partial z^2}$$

$$- \left(2 \frac{(\partial\phi/\partial z)(\partial\phi/\partial r)}{c^2}\right) \frac{\partial^2\phi}{\partial z \partial r} + \frac{\partial\phi/\partial r}{r} = 0 \qquad (4.1)$$

The local sonic velocity can be computed from the equation

$$c^2 = c_o^2 - \frac{k-1}{2} \left((2\phi/\partial r)^2 + (\partial\phi/\partial z)^2\right) \qquad (4.2)$$

Equation 4.1 is converted to finite difference form by using the approximations listed below. The relative location of the node points is shown in Figure 4.1.

$$\frac{\partial\phi}{\partial r} = \frac{\phi_{I,J+1} - \phi_{I,J-1}}{2\Delta r} \qquad (4.3)$$

$$\frac{\partial\phi}{\partial z} = \frac{\phi_{I+1,J} - \phi_{I-1,J}}{2\Delta z} \qquad (4.4)$$

$$\frac{\partial^2\phi}{\partial r^2} = \frac{\phi_{I,J+1} + \phi_{I,J-1} - 2\phi_{I,J}}{\Delta r^2} \qquad (4.5)$$

$$\frac{\partial^2\phi}{\partial z^2} = \frac{\phi_{I+1,J} - \phi_{I-1,J} - 2\phi_{I,J}}{\Delta z^2} \qquad (4.6)$$

$$\frac{\partial^2\phi}{\partial r\, \partial z} = \frac{\phi_{I+1,J+1} - \phi_{I+1,J-1} + \phi_{I-1,J-1} - \phi_{I-1,J+1}}{4\, \Delta r\, \Delta z} \qquad (4.7)$$

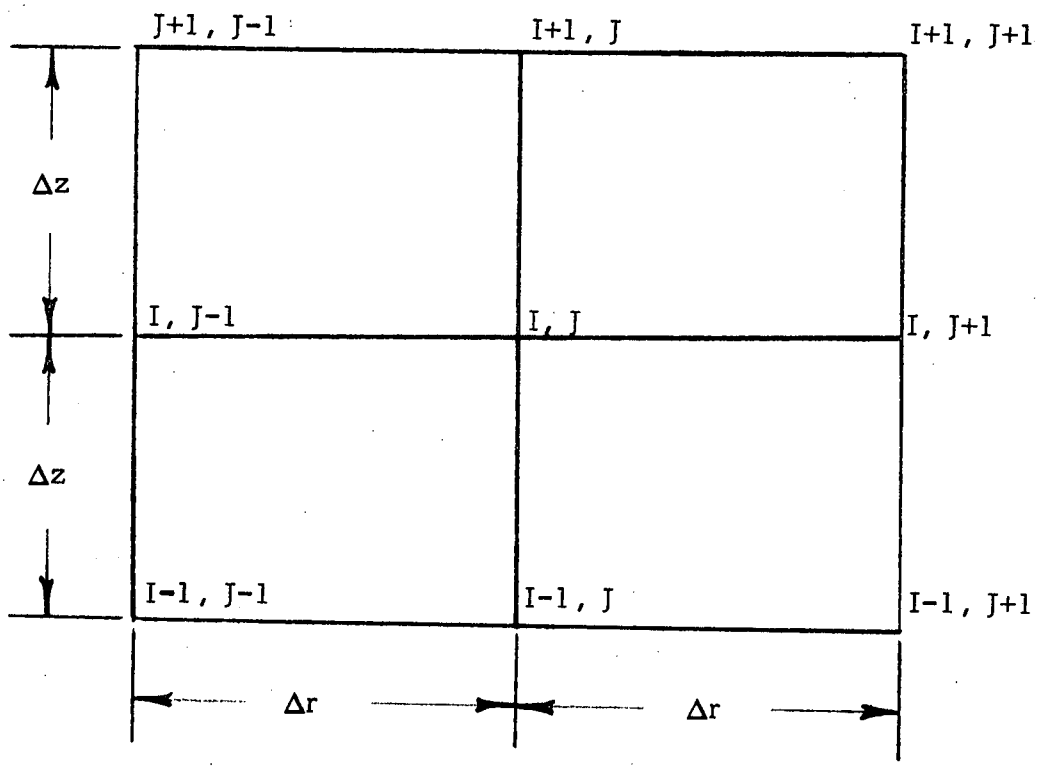

Fig. 4.1. Relative Locations of Node Points

where $$A_1 = \left(1 - \frac{\phi_r^2}{c^2}\right) = 1 - \frac{\left(\phi_{I,J+1} - \phi_{I,J-1}\right)^2}{4\Delta r^2 c^2}$$

$$A_2 = \left(1 - \frac{\phi_z^2}{c^2}\right) = 1 - \frac{\left(\phi_{I+1,J} - \phi_{I-1,J}\right)^2}{4\Delta z^2 c^2}$$

and $$A_3 = \frac{\phi_r}{r} - 2\frac{\phi_z \phi_r}{c^2} = \phi_r \left(1 - 2\frac{\phi_z}{c^2}\right) = \frac{\phi_{I,J+1} - \phi_{I,J-1}}{2\Delta r}$$

$$\left[1 - \frac{\left(\phi_{I+1,J} - \phi_{I-1,J}\right)}{\Delta z\, c^2}\right]$$

Substituting equations 4.3 through 4.7 into equation 4.1 and rearranging gives an explicit expression for the potential at point I, J of the form

$$\phi_{I,J} = \left(\frac{\Delta z^2}{2A_2} + \frac{\Delta r^2}{2A_1}\right)\left[A_1 \frac{\left(\phi_{I,J+1} + \phi_{I,J-1}\right)}{\Delta r^2} + A_2 \frac{\left(\phi_{I+1,J} + \phi_{I-1,J}\right)}{\Delta z^2} + A_3\right] \tag{4.8}$$

It should be noted that $\phi_{I,J}$ can be obtained in explicit form only if Δr and Δz are the same on both sides of the node point in question. This condition is not generally satisfied for the node points near the deflector or near the free streamline or for those node points along the line where the grid spacing changes. This difficulty is handled by defining additional node points which will yield an even spacing and assigning their ϕ value by linear interpolation between adjacent node points. This is illustrated by Figure 4.2.

The points represented by an x are the auxiliary points added. The velocity potential at these points is determined by linear interpolation between surrounding points. Note, however, that one of the node points falls outside the flow field and cannot be computed in this way. This point would normally be used only in the cross derivative term. The procedure used here is to ignore that point and use a different (slightly less accurate) formulation for the cross derivative

$$\frac{\partial^2 \phi}{\partial r \partial z} = \frac{\phi_{I,J} - \phi_{I,J-1} + \phi_{I-1,J-1} - \phi_{J-1,J}}{\Delta z\ \Delta r} \tag{4.9}$$

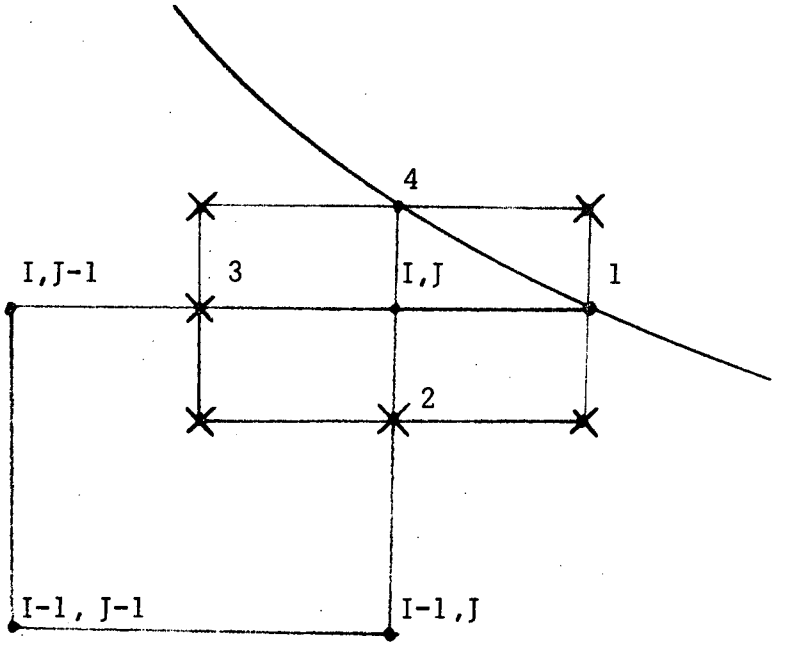

Fig. 4.2. Node Points Near the Free Streamline

All other derivatives are computed using point I, J and points 1, 2, 3 and 4. This revision changes the A_3 term in equation 4.8 since the cross derivative now includes a $\phi_{I,J}$ term. That term can be transferred to the left side of equation 4.8 so that $\phi_{I,J}$ can still be found explicitly.

The compressible solution is now carried out as follows. A shape for the free streamline and the Mach number[1] along the free streamline are specified. The free streamline velocity is then computed

---

[1]The most convenient Mach number to specify is that along the free streamline. It is approximately equal to the Mach number at the exit for cases where back pressuring effects are small.

based on a total pressure of one atmosphere and an arbitrary total temperature.[2] This free streamline velocity is used to compute the values of velocity potential along the assumed freestream boundary and the potential at all node points is then determined using the relaxation procedure with the compressible flow equations. It is necessary to determine the r and z velocity components at each point in the flow field so that the local sonic velocity can be found using equation 4.2. The freestream boundary is then adjusted to the correct shape in the manner discussed in [1].

The computation time is greatly increased due to the complexity of the finite difference equations, the use of the extra node points and the necessity of constantly recomputing the local sonic velocity at each node point. Therefore, only four runs were made for one fixed geometry at freestream Mach numbers of .1, .5, .8, and .95. Presented in Figure 4.3 is a plot of the calculated static pressure distribution along the deflector surface for the cases M = 0.1, 0.5 and 0.8. These plots indicate a negligible Mach number effect up to M = 0.8. Upon consideration it is not too surprising that the

---

[2] In the cases investigated, the total temperature was taken arbitrarily as 530°R. Selection of specific values of temperature and pressure is necessary because the solution is carried out in dimensional form. Non-dimensional results such as reverser effectiveness are not limited to these specific values, however.

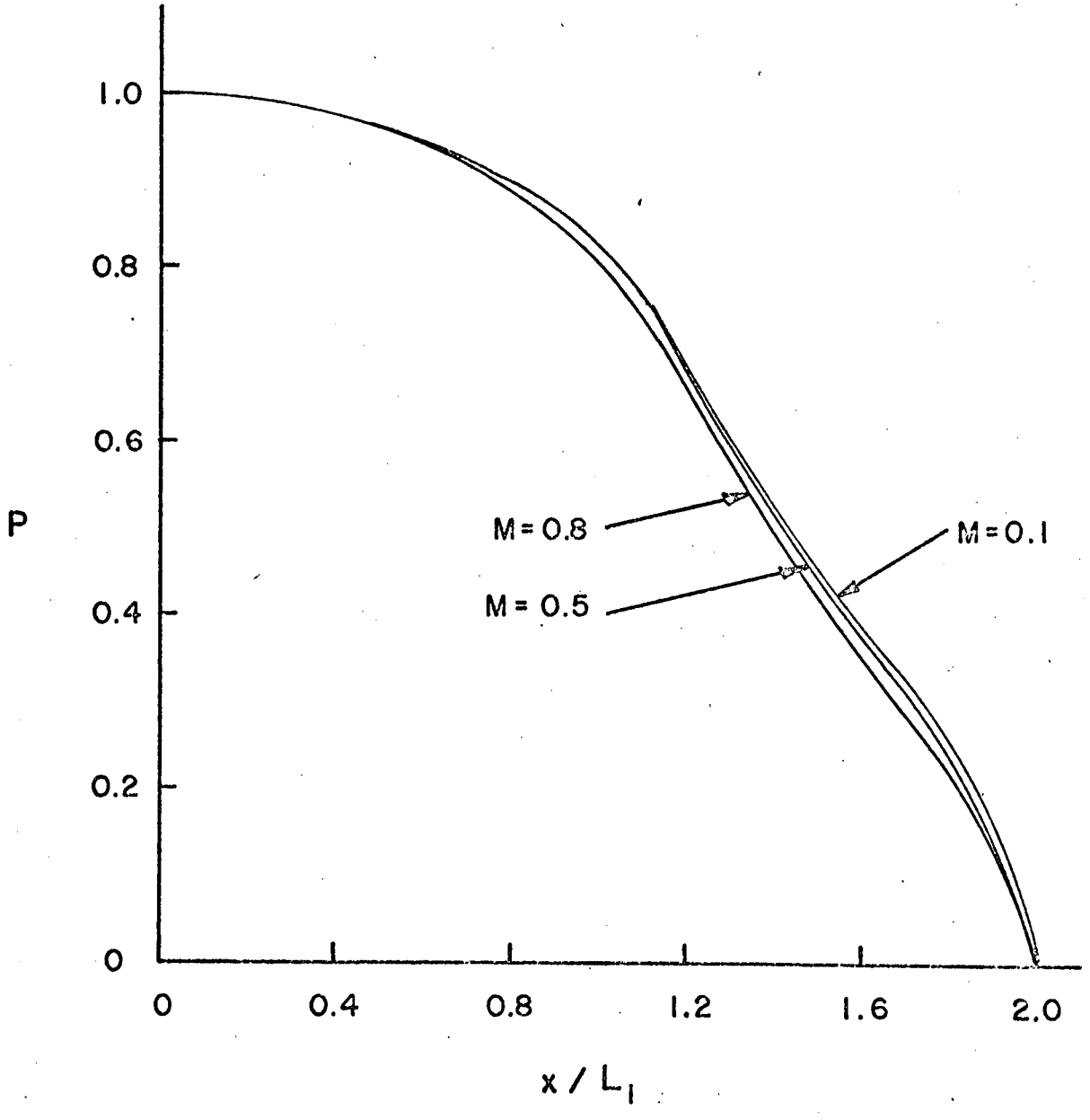

Fig. 4.3. The Effect of Compressibility on the Pressure Distribution at the Deflector Surface

compressibility effects are not significant for free streamline Mach numbers up to .8, because the maximum velocity occurs on the free streamline and the Mach numbers throughout most of the region are much smaller.

The M = .95 case did not converge satisfactorily and, therefore, no results are presented. This is probably due to the fact that the coefficients in equation 4.1 approach zero as Mach number approaches unity; a condition causing an accuracy problem which is somewhat compounded by the approximations made in the analysis.

It is nevertheless safe to conclude that the incompressible flow analysis gives quite satisfactory results for freestream Mach numbers less than about .8.

4.1.3 The Effects of Geometry on Reverser Performance

Solutions were obtained for a variety of plane jet and circular jet cases for the purpose of determining the effect of various geometrical parameters on performance. These parameters include the dimensionless depth h/L_1 and the angle θ. (See Figure 4.4). The shape selected for the cross-section of the deflector was an ellipse having its center on the jet axis and passing through points F and E.

The results obtained for each case and illustrated in Appendix B, included the free streamline location, the velocity potential field, the velocity vector at each node point, the pressure distribution

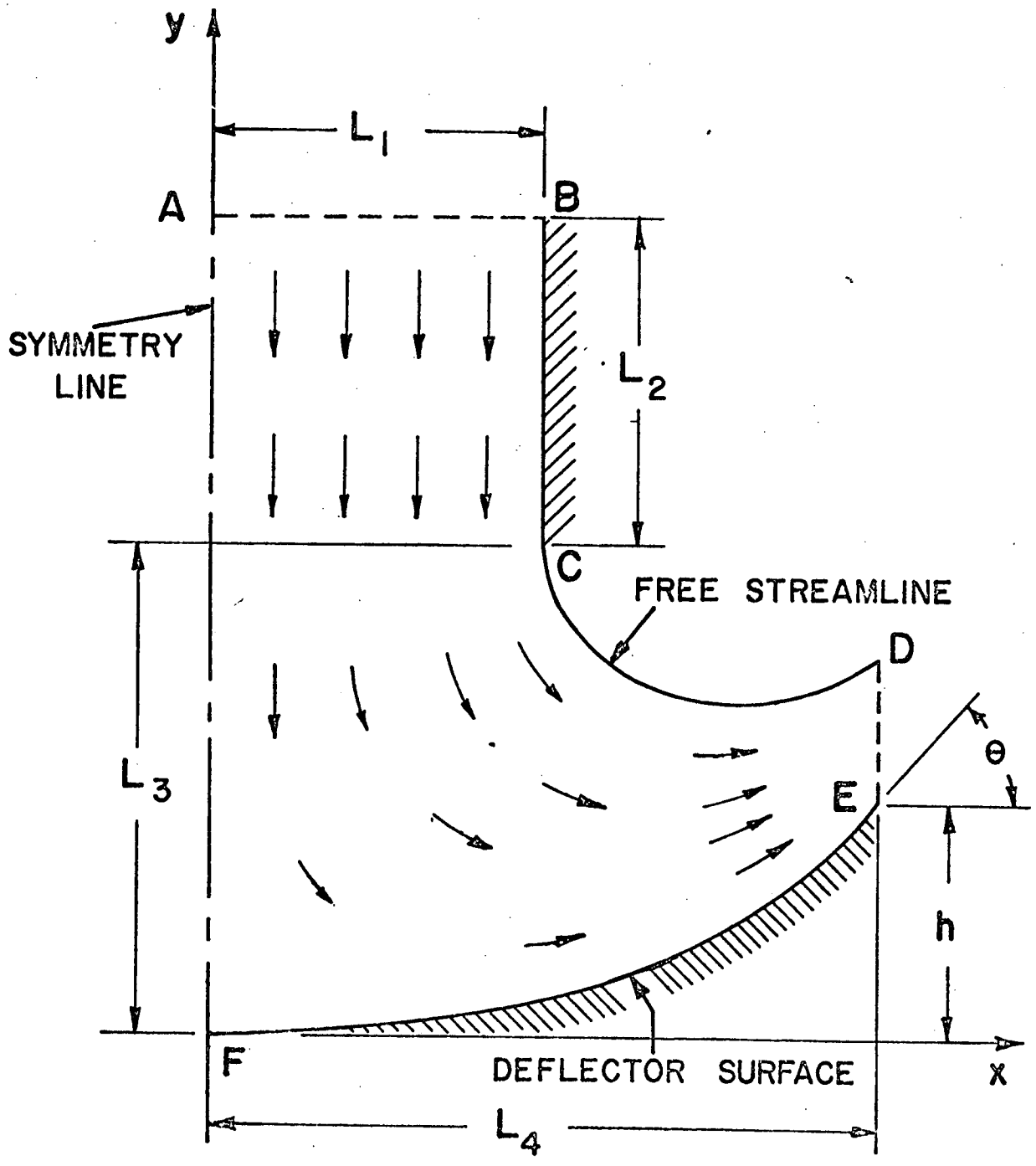

Fig. 4.4. Jet Impingement Flow Field

along the deflector surface and jet centerline, the turning effectiveness η_T and the reverser effectiveness, η.* The velocity potential field and pressure distributions for a typical case for a circular jet are shown in Figures 4.5 and 4.6.

A series of runs was made for both the plane and circular jet cases to investigate the effects of geometry on performance. The results for all cases are summarized in Figure 4.7.** Since the jet exit-to-deflector spacing has the greatest effect on reverser performance it is perhaps of most interest. The effect of this parameter on reverse performance is shown in Figure 4.8 for the round jet case. The turning effectiveness increases with decreasing jet to deflector spacing as expected since "spillage" is decreased. There is, however, an accompanying decrease in mass flow rate with decreased spacing causing an eventual decrease in reverser effectiveness. Note than an optimum

---

*The turning effectiveness, η_T, is defined as the ratio of reverse thrust to the momentum flux measured at the cross section a distance L_2 upstream of the jet exit. It may be calculated by simply determining the angle through which the flow is turned. Comparison of actual turning effectiveness with the ideal turning effectiveness which would result if the flow left the deflector exactly parallel to the deflector surface is an indication of the spillage. The reverser effectiveness, η, is the ratio of reverse thrust to the momentum flux which would exist at the jet exit cross section in the absence of back pressuring effects (i.e., if the deflector were not present). It, therefore, includes the loss in thrust associated with a reduced flow rate caused by the back pressuring effect.

**The complete computer output for these 23 cases has been placed on file at the Joint University Library in Nashville, Tennessee and is available under the title "Two-Dimensional Jet Impingement Data Under NGR-43-002-034".

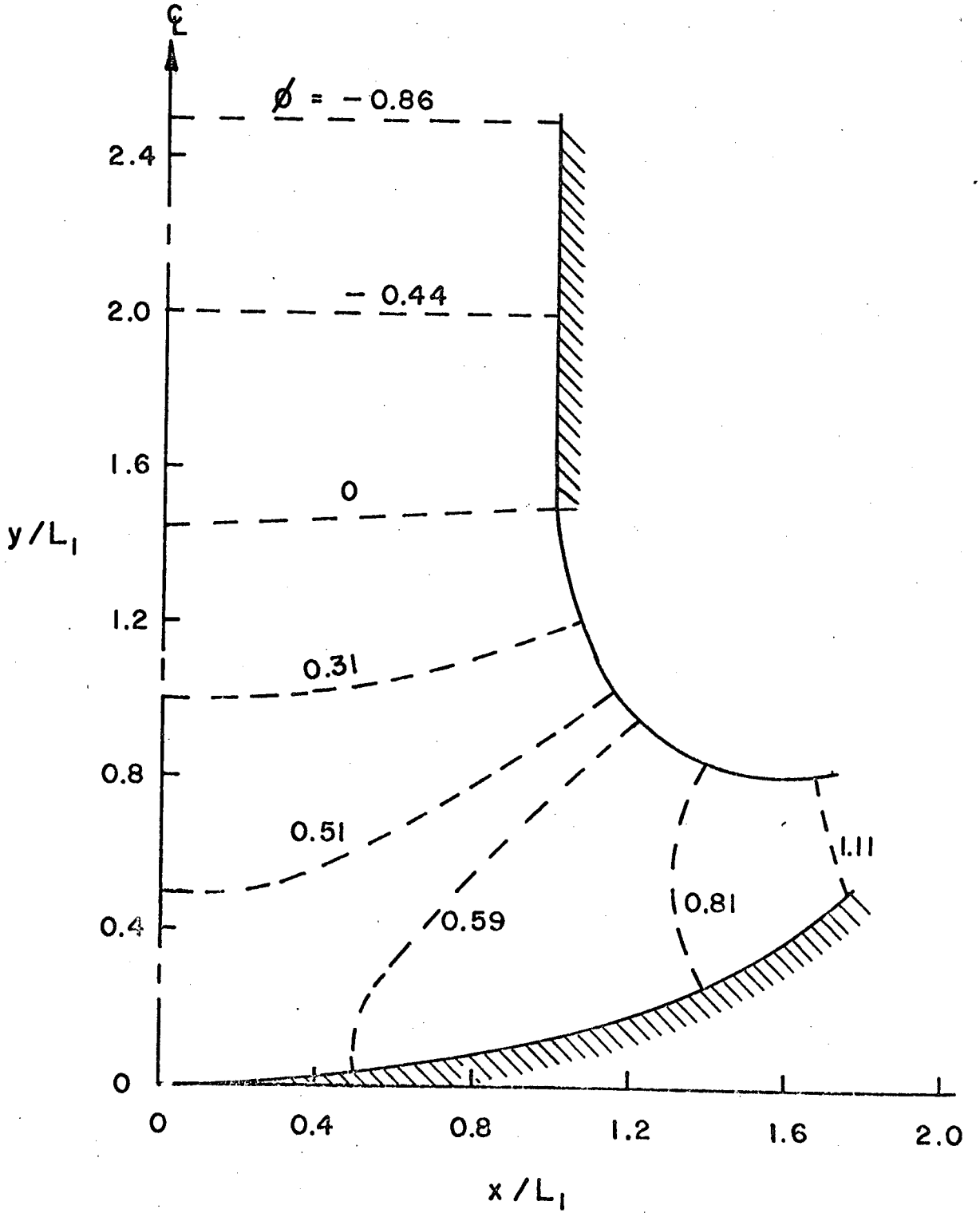

Fig. 4.5. Velocity Potential Field for Case A-6

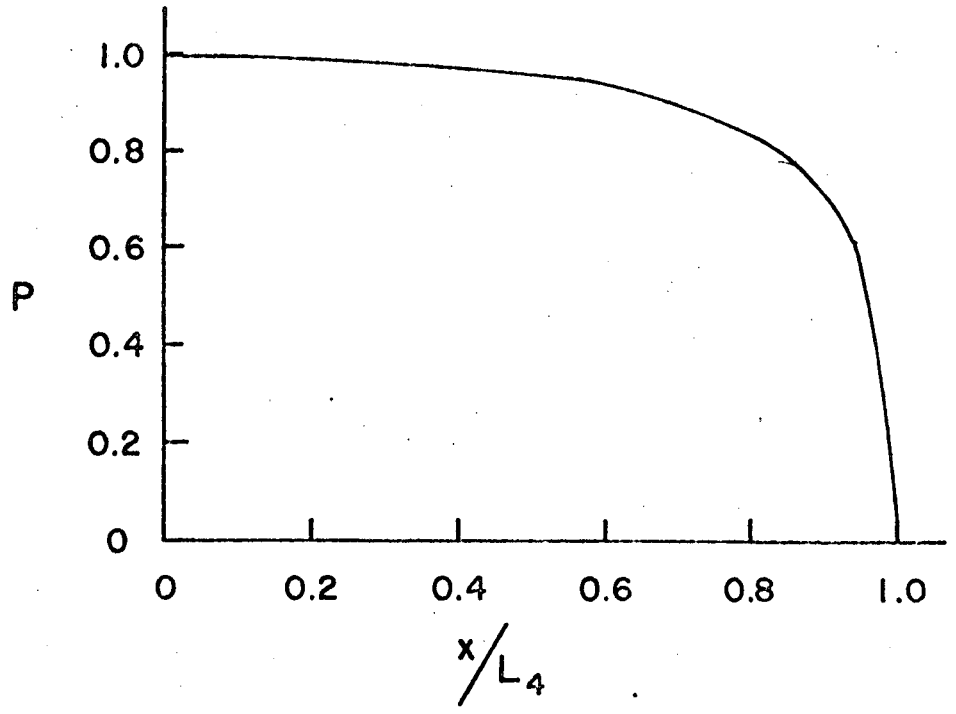

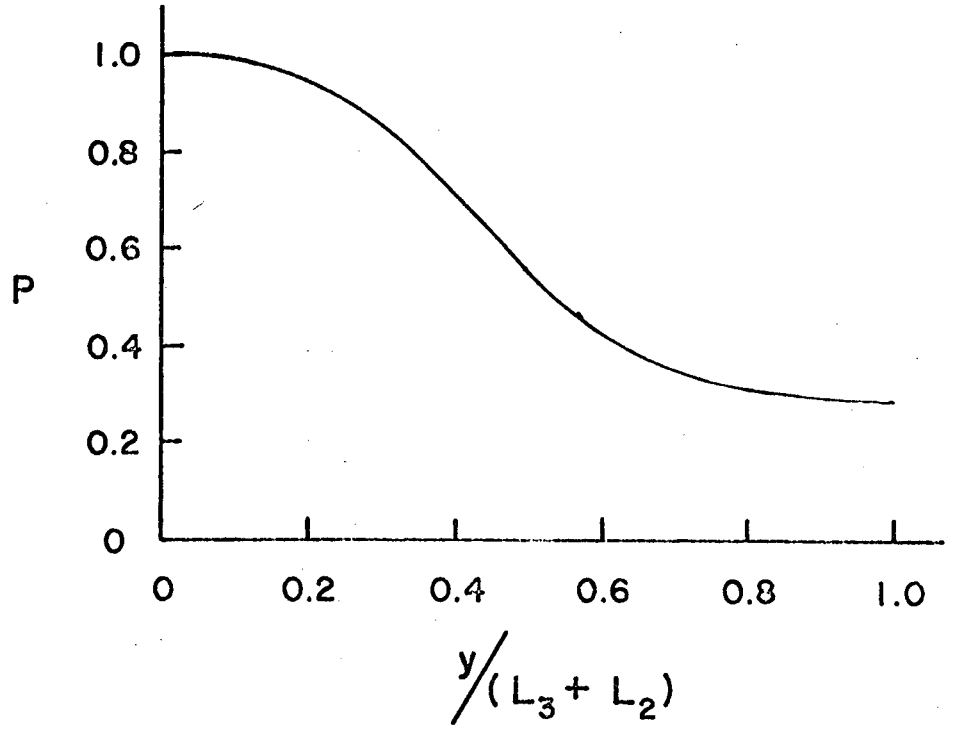

Fig. 4.6. Pressure Distributions for Case A-6

Fig. 4.7. Summary of Analytical Results

CIRCULAR JET CASES

Case	L_2/L_1	L_3/L_1	L_4/L_1	h/L_1	$\theta(°)$	η_T	η
A-1	1.0	1.0	1.5	.5	45	.60	.40
A-2	1.0	1.5	1.5	.5	45	.54	.44
A-3	1.0	2.0	1.5	.5	45	.48	.45
A-4	1.0	2.5	1.5	.5	45	.44	.43
A-5	1.0	1.0	1.75	.5	45	.64	.45
A-6	1.0	1.5	1.75	.5	45	.60	.51
A-7	.10	2.0	1.75	.5	45	.56	.53
A-8	1.0	3.0	1.75	.5	45	.43	.42
A-9	1.0	1.0	2.0	.5	45	.66	.49
A-10	1.0	1.5	2.0	.5	45	.63	.55
A-11	1.0	2.0	2.0	.5	45	.59	.57
A-12	1.0	3.0	2.0	.5	45	.55	.54
A-13	2.0	1.0	2.0	.5	45	.66	.49
A-14	1.0	1.5	1.75	.5	60	.75	.64
A-15	1.0	1.5	1.75	.5	30	.42	.36
A-16	1.0	1.5	1.75	.5	75	.86	.73

PLANE JET CASES

B-1	2.0	2.0	2.0	.34	15	.19	.13
B-2	2.0	2.0	2.0	.34	30	.38	.28
B-3	2.0	2.0	2.0	.34	45	.53	.39
B-4	2.0	2.0	3.0	.80	30	.47	.34
B-5	2.0	3.0	3.0	.80	30	.45	.40
B-6	2.0	4.0	3.0	.80	30	.43	.41
B-7	2.0	5.0	3.0	.80	30	.41	.40

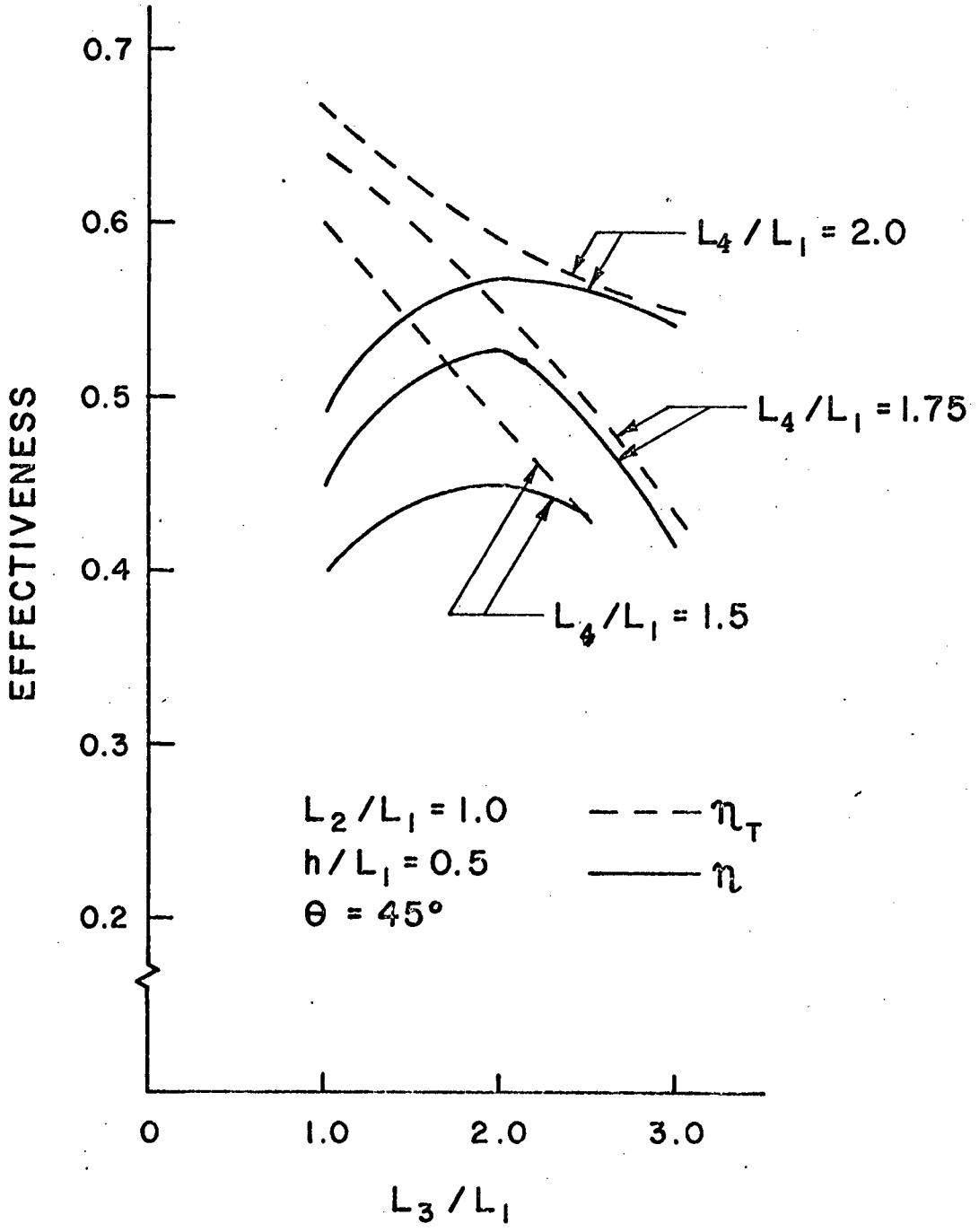

Fig. 4.8. The Effect of Jet Exit to Deflector Spacing on Reverser Performance

spacing occurs at a deflector to jet spacing of approximately two. Povolny, et al [13] experimentally investigated the effect of jet to deflector spacing for the case of a round jet impinging on a hemisphere ($\theta = 90°$). Although their case is not identical to the one considered here it is quite similar. They found an optimum spacing of about 1.8 diameters.

The effect of varying deflector width is shown in Figure 4.9. Note that there is little to be gained by increasing deflector width above about 1.75 diameters. This result also agrees quite well with Povolny's experimental results. Figure 4.9 clearly illustrates the effect of back pressuring. A jet to deflector spacing of one diameter gives much better turning effectiveness than a spacing of two diameters but the higher back pressuring causes the reverser effectiveness to be lower.

The effect of turning angle is illustrated in Figure 4.10. As θ increases both the turning effectiveness and reverser effectiveness increase monotonically. The back pressuring loss shows essentially no increase with turning angle for the geometry considered here.

The purpose of including a length of duct L_2 was to investigate the effect of back pressuring. Since the resulting straight section of duct may not be representative of practical cases, the effect of L_2/L_1 was not studied exhaustively. It was assumed that increasing L_2/L_1 beyond 1.0 would have little effect on the predicted performance. The validity of this assumption is demonstrated by comparison of cases A-9 and A-13 in Figure 4.7.

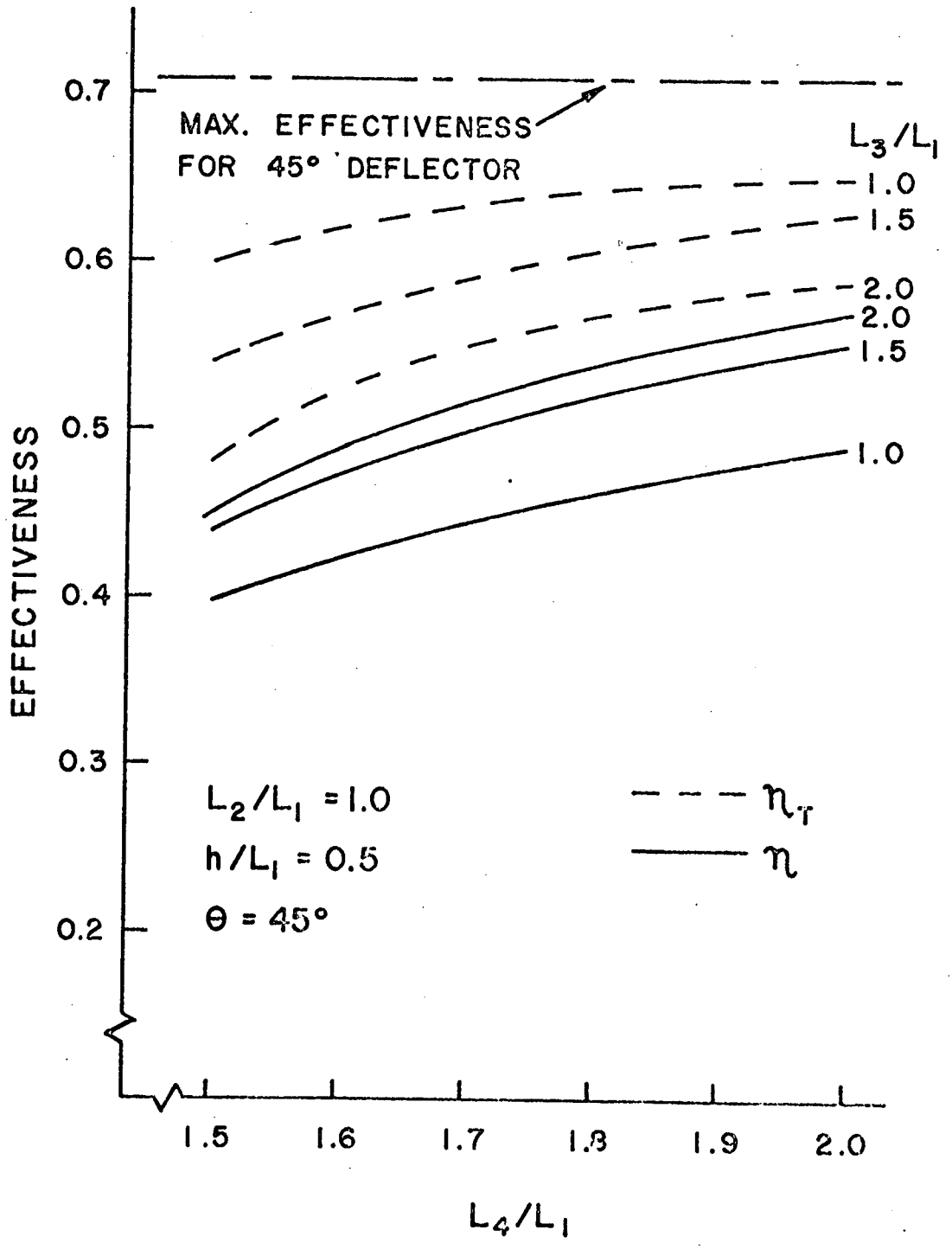

Fig. 4.9. The Effect of Deflector Width on Reverser Performance

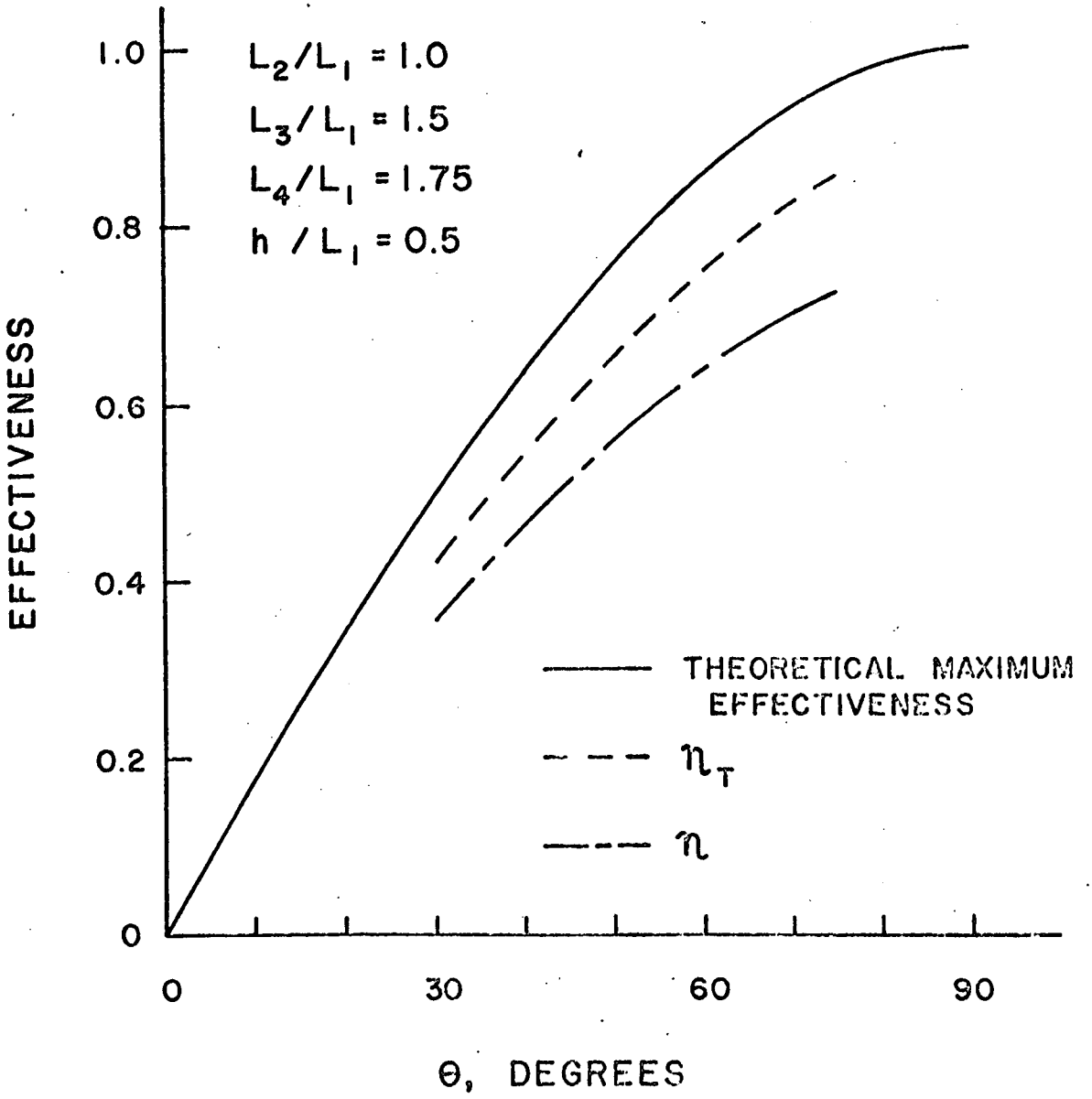

Fig. 4.10. The Effect of Turning Angle on Reverser Performance

4.2 EXPERIMENTAL INVESTIGATION

Two experimental investigations of impinging jets have been made since the last report [1]. The first of these was a brief examination and extension of the results obtained on the two-dimensional cascade reverser/blown-flap thrust reverser model previously reported. The second investigation, and the main experimental effort was that of a round jet impinging on the interior surface of a wedge whose included angle could be varied from 45° to 180°. This simple, three-dimensional geometry was selected with the hope that through these studies a method of extending the analytical techniques developed thus far would evolve. The results of both investigations are presented in the following sections.

4.2.1. Experimental Results of the Cascade Reverser/Blown-Flap Model

Previous studies of the cascade reverser/blown-flap reverser model [1] revealed large discrepancies between the analytical and the experimental results. The experimental thrust measurements and surface static pressures were much less than that predicted by the analysis (see Fig. 4.11). This experimental result was further verified by making a velocity traverse at the edge of the deflector where it was found that the actual flow velocity was inclined at an angle of 25°. (This angle is indicated in Fig. 4.12 which illustrates the geometry of the system.) If the flow had been completely turned by the deflector, the exit angle would have been 54°. The measured exit flow direction corresponds to a reverser effectiveness equal to that obtained in the previous reverse thrust measurements.

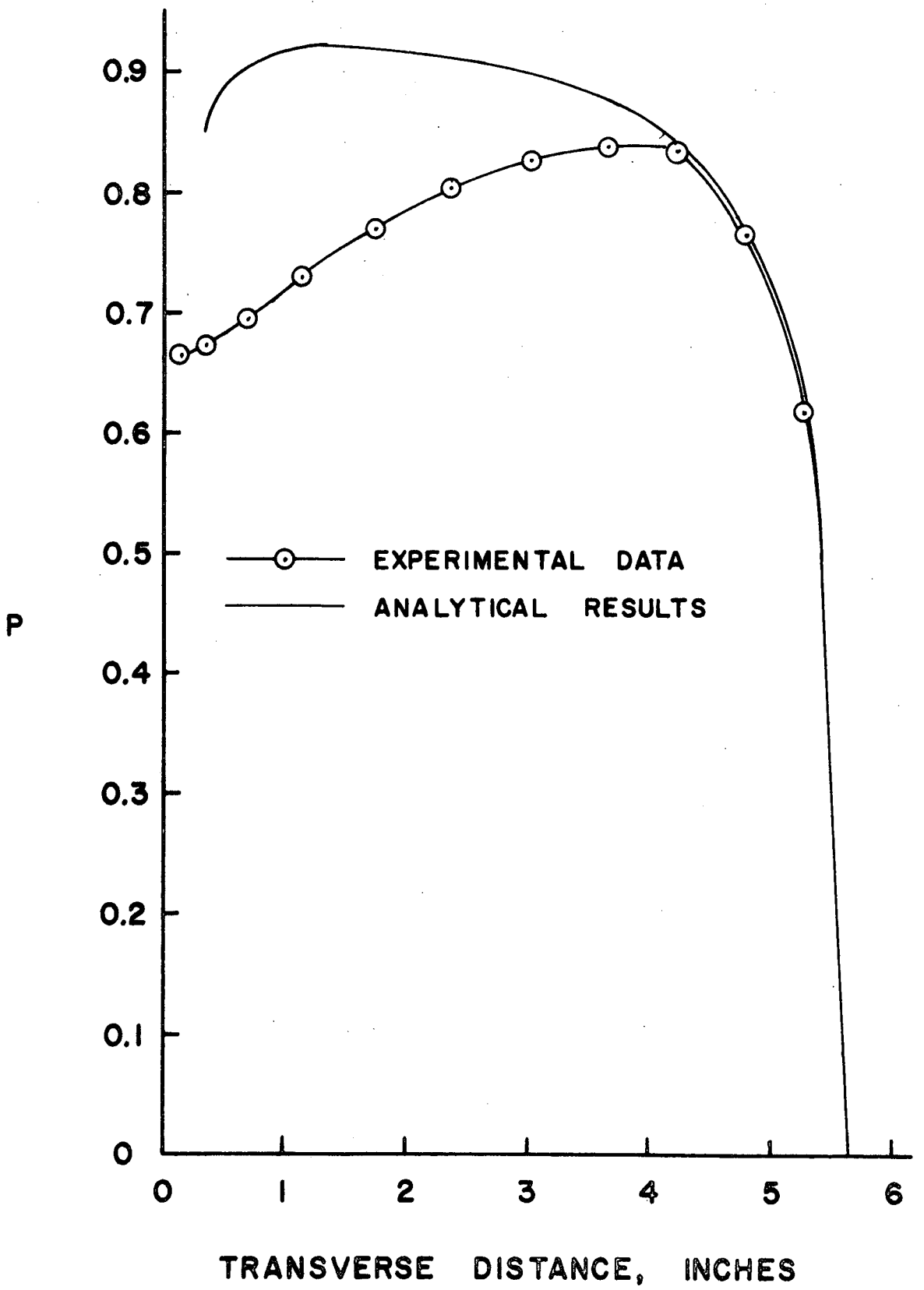

Fig. 4.11. Comparison of Analytical and Experimental Results for the Blown Flap Thrust Reverser

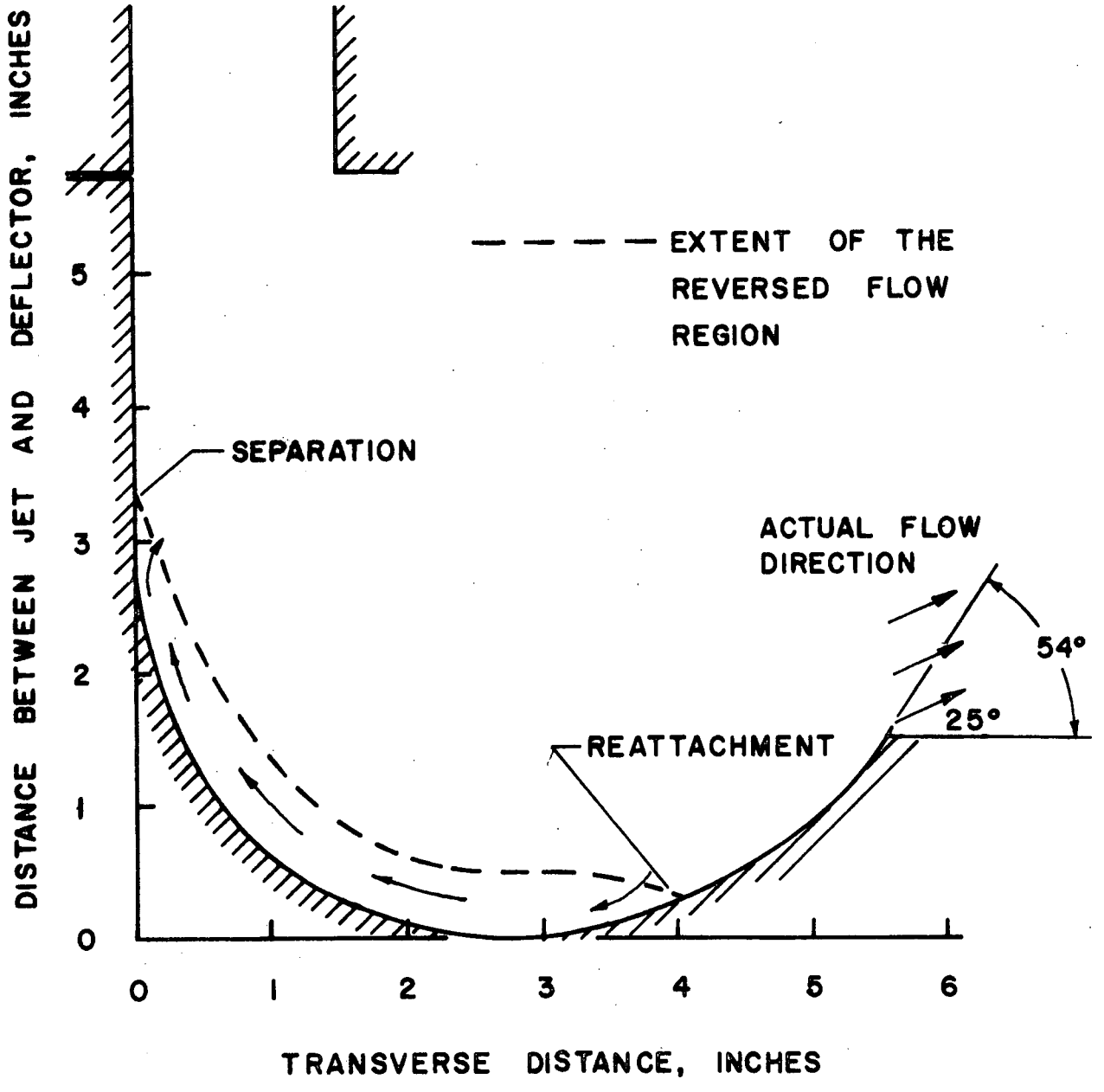

Fig. 4.12. Schematic Diagram of the Blown Flap Thrust Reverser

It was speculated that the flow must be greatly influenced by the adverse pressure gradient existing within the interior flow, and that separation of the flow was a distinct possibility. Separation was confirmed by making flow visualization tests. Fig. 4.12 also shows the area of the separated zone. The zone is extensive; it covers roughly 65% of the curved portion of the deflector.

Obviously, the analytical methods based upon potential flow theory will be inappropriate to this type geometry. In general, it is believed that any thrust reverser exhibiting very extensive areas of adverse pressure gradients along solid surfaces cannot be modeled by potential flow theory. Presently, an attempt is being made to adopt the methods of Patankar-Spalding [16] to the problem of predicting those cases when separation will occur and to predict the location of the point of separation. As analytical methods of this type of flow become available, additional experimental work will be conducted to determine their overall suitability.

4.2.2 Experimental Results of the Wedge-Shaped Deflector Model

The nozzle of the existing jet apparatus was redesigned and constructed so that a circular jet would be available for these studies. The nozzle was constructed in two sections in order that different axisymmetric jets could be investigated. The first section converged from a 16 in. square to a flanged 6 in. square. A circular 3-3/4 in. I.D. plexiglas tube 14 in. long was connected to the first section of the

flange. The jet exiting from this tube at up to 250 feet per second impinged upon the wedge shaped deflector, which was 16 in. on a side when in the flat position. The wedge was hinged along the center-line. It was constructed of plywood with 1/16 in. plexiglas covering the jet impingement side. The included angle of the wedge-shaped deflector could be varied from 45° to 180°.

The instrumentation consisted primarily of a 3/32 in. O.D. stagnation probe with a pressure opening of 1/32 in. and a manometer system. The probe was mounted so that it could be moved along the edge of the deflector at the top and at the side so that one quadrant of the flow could be examined. The probe could also be moved in a transverse direction with respect to the surface of the deflector in increments as small as 0.05 in. To map the exiting flow, it was necessary to be able to measure the angular orientation of the flow besides locating the x, y, z coordinates of the probe tip. To do this correctly, two angles should have been measured, i.e. the angle flow made with respect to the surface tangent and the angle the flow made with respect to the plane of symmetry. This was not possible with the apparatus; instead only the latter angle could be determined. It is felt that it is the most important one since the angle that the flow made with respect to the surface tangent in most cases was small. Besides the exit velocity measurements, the total force acting on the deflector as well as the flow rate issuing from the jet were determined.

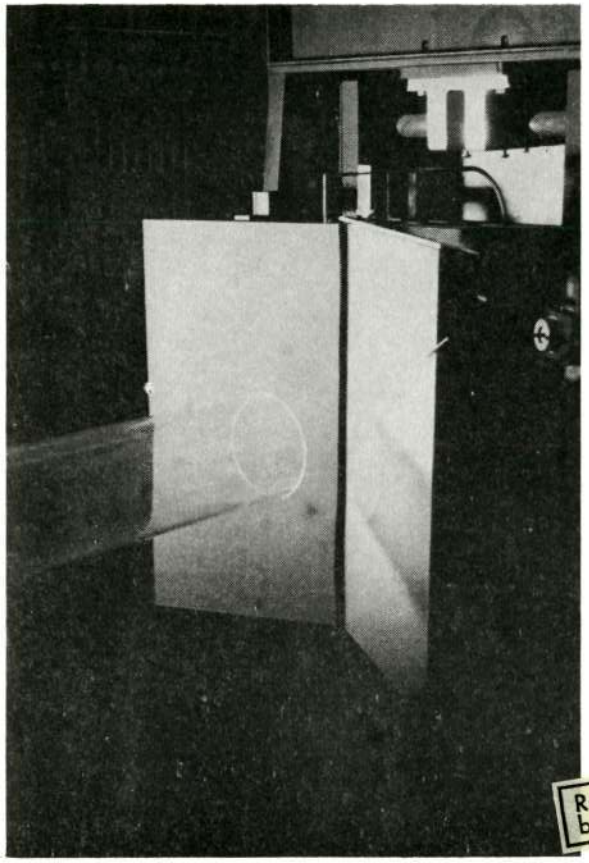

Figure 4.13a. Three-Dimensional
Jet Impingement Rig

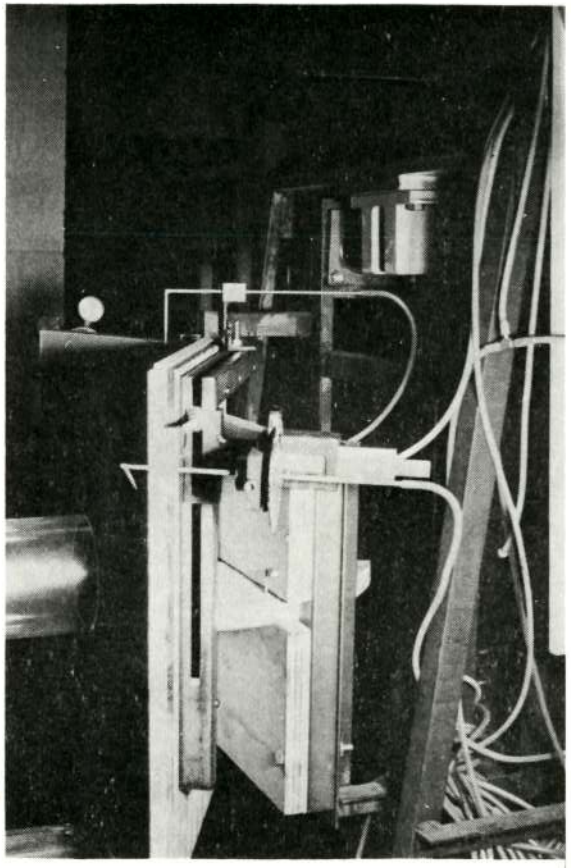

Figure 4.13b. Instrumentation
for Jet Impingement Rig

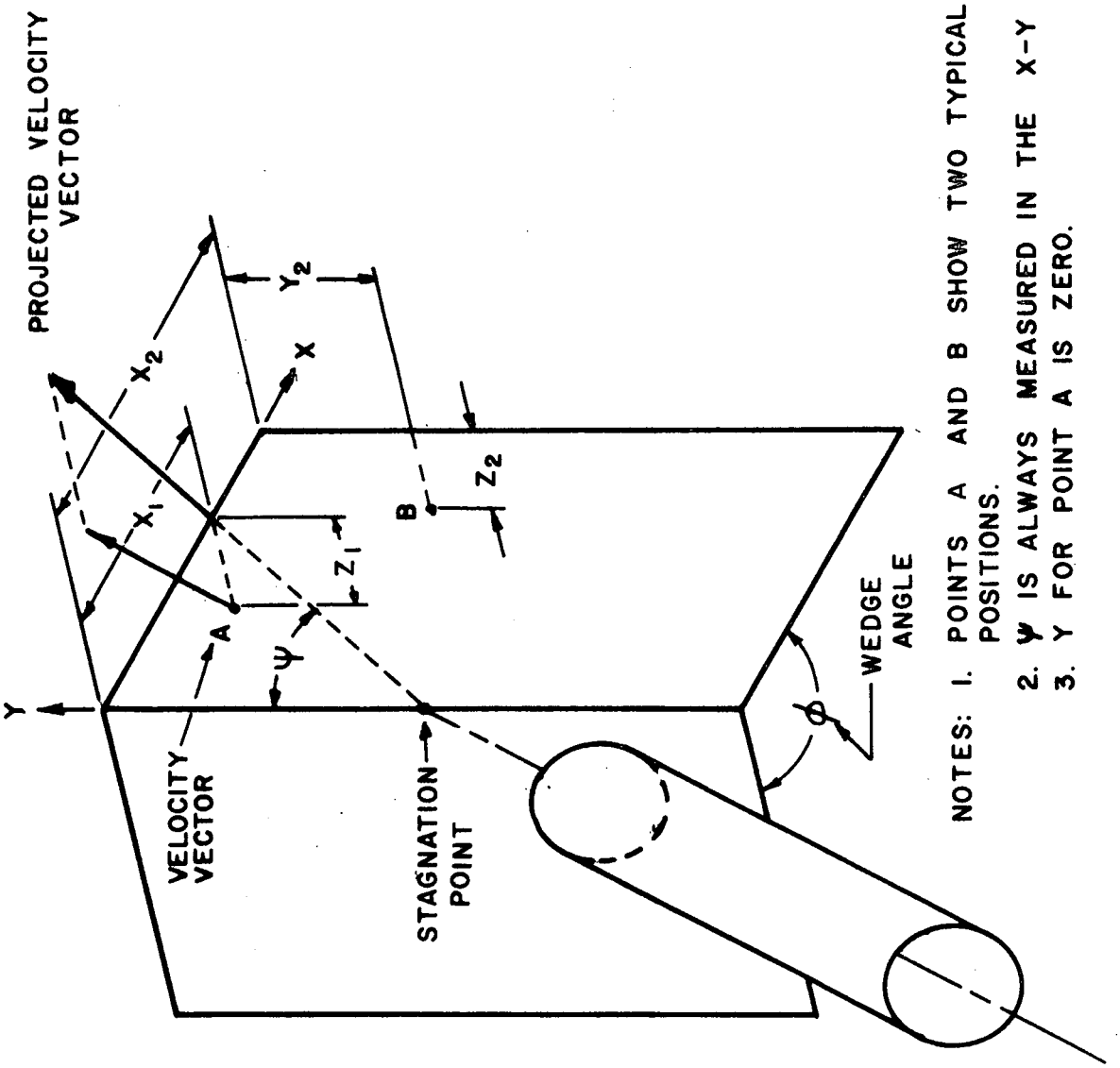

Fig. 4.14. Positioning Variables for the Three-Dimensional Impingement Jet Apparatus

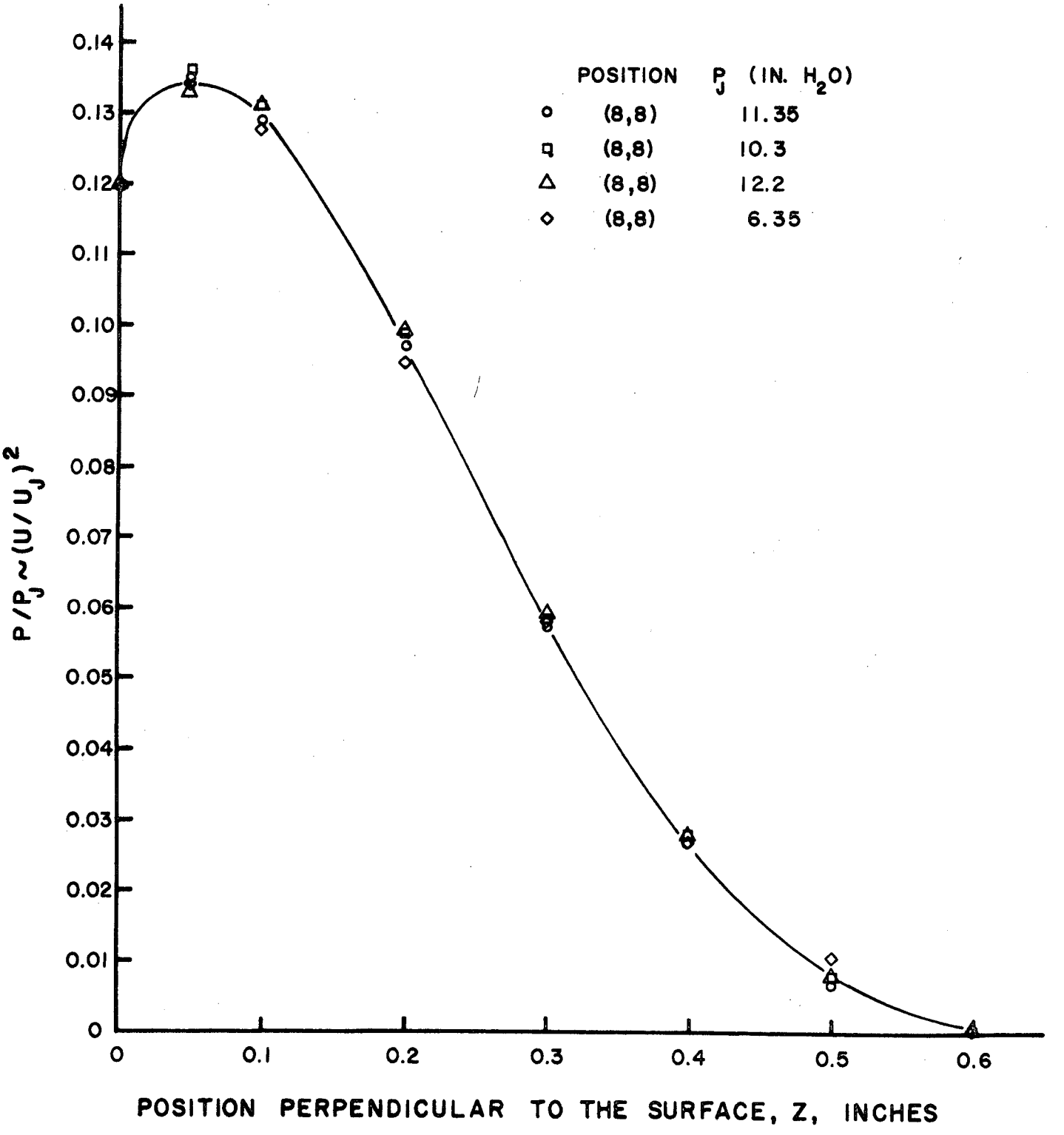

Fig. 4.15. Repeatability of Experimental Measurements Obtained from the Three-Dimensional Jet Apparatus

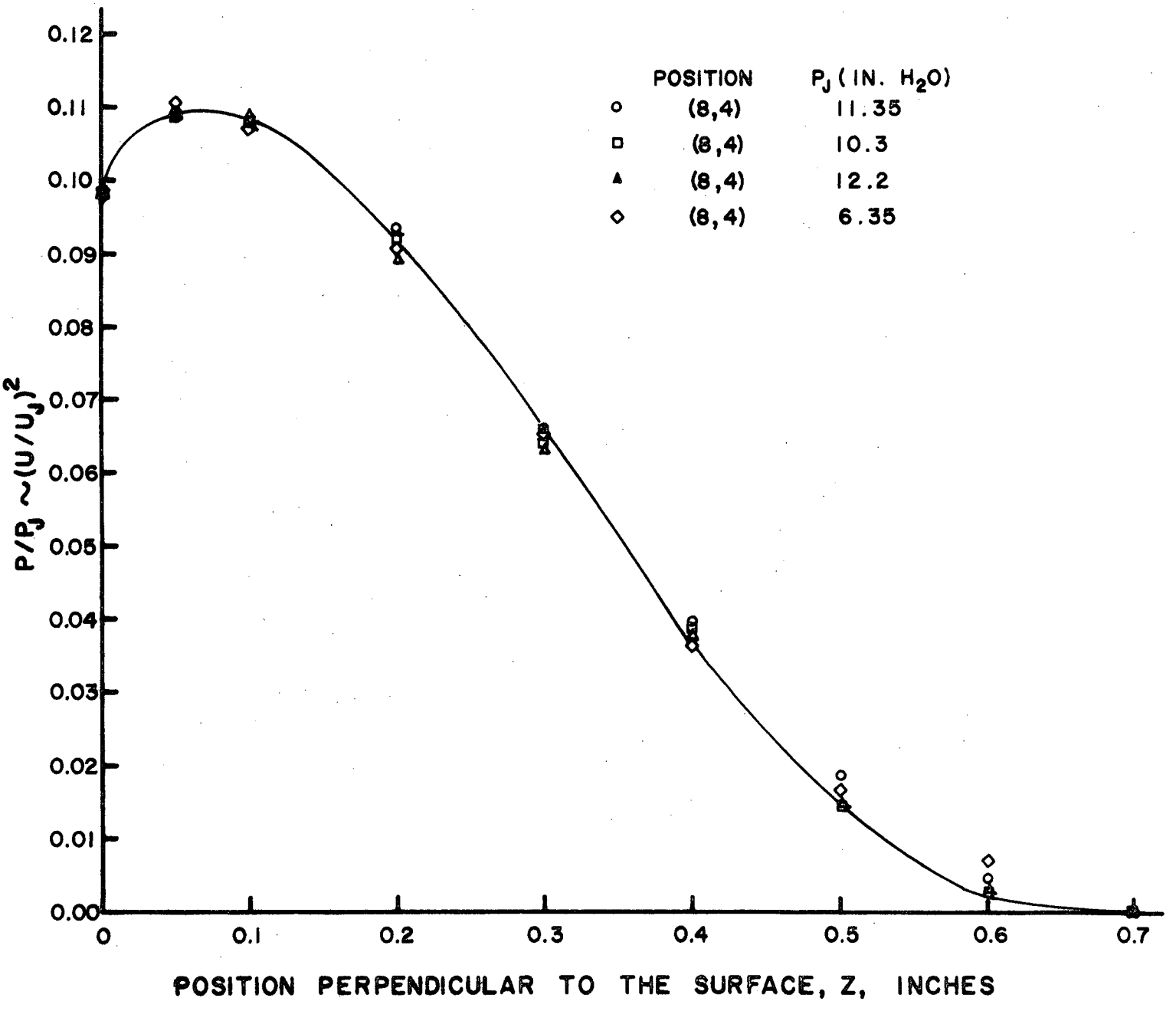

Fig. 4.16. Effect of Jet Exit Velocity on the Velocity Measurements Obtained from the Three-Dimensional Jet Apparatus

Next, velocity traverses were made at included wedge angles of 60°, 90°, 120°, 150°, and 180°. Normalized stagnation pressure profiles for the 90° included angle case are shown in Fig. 4.17. It is obvious that the velocity and the extent of the wall jet leaving the apex of the deflector are much larger than those leaving the side of the deflector, position 8, 8 (x = 8, y = 8). (See Fig. 4.14.) Flow from the sides of the deflector was relatively small and most was entrained back into the jet and finally left the deflector at the apex position. This was verified by flow visualization tests. The boundary layer thickness was estimated at each x, y location. The results for all cases of included angle are shown in Fig. 4.18. Consider the extreme positions of included angle. It is seen that for the 60° deflector, the boundary layer thickness was 3.2 in. at the apex and only 0.5 in. thick at the side. For the 180° case, symmetrical boundary layer thicknesses and velocity profiles for the quadrant were obtained. The boundary layer thickness at the top and the side was 1.0 in. Since the boundary layer thickness was symmetrical about the 45° angle, it was judged that the jet and deflector were well aligned.

With the thrust load measurements available, it was possible to determine directly the effect of included angle on the thrust load. The results are shown in Fig. 4.19. Thrust increased as the included angle was decreased from 180° to a value of approximately 135°. Below this the thrust fell off appreciably. Two factors caused this drop in

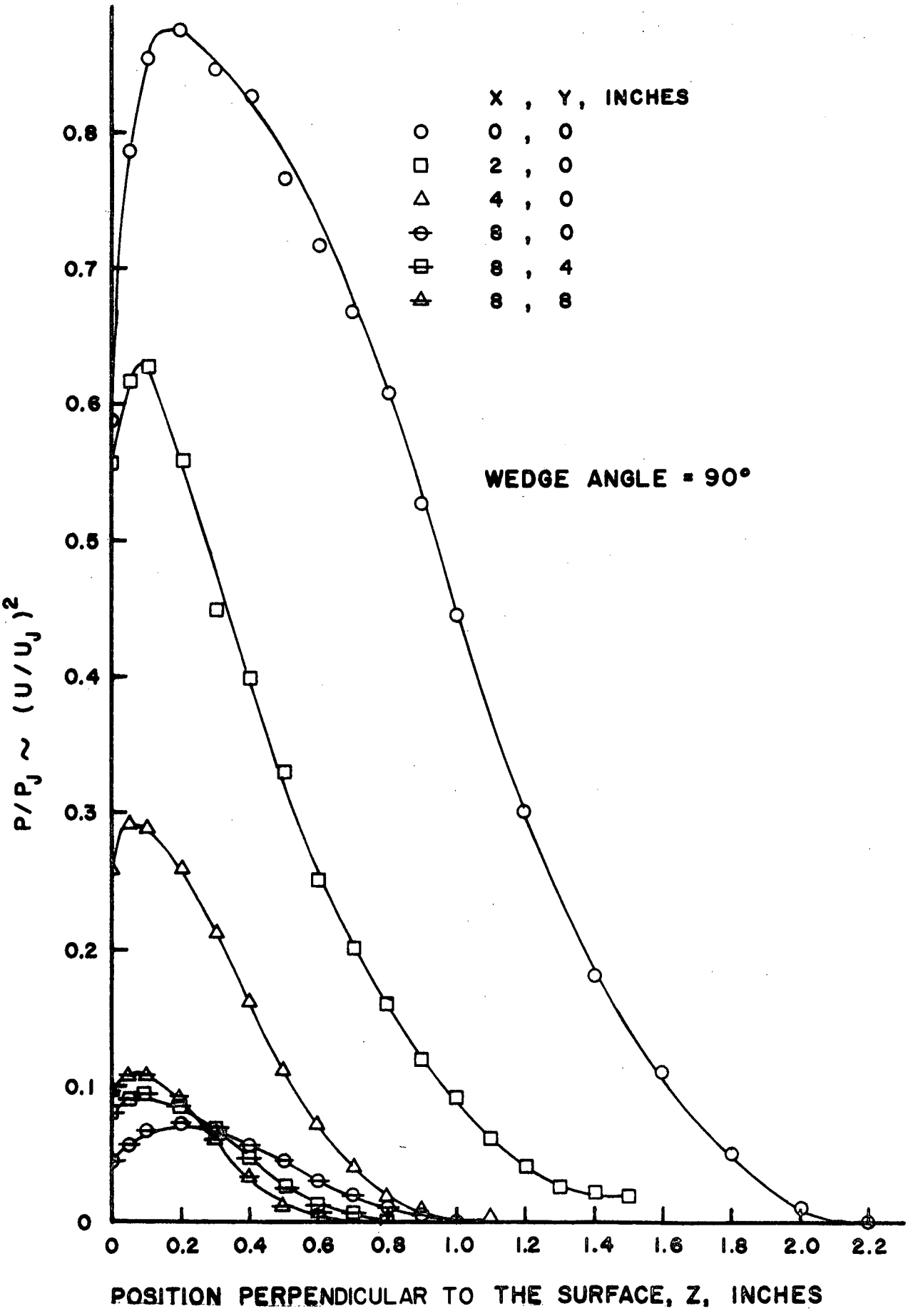

Fig. 4.17. Stagnation Pressure Profiles for the Thrust Reverser with a 90° Included Wedge Angle

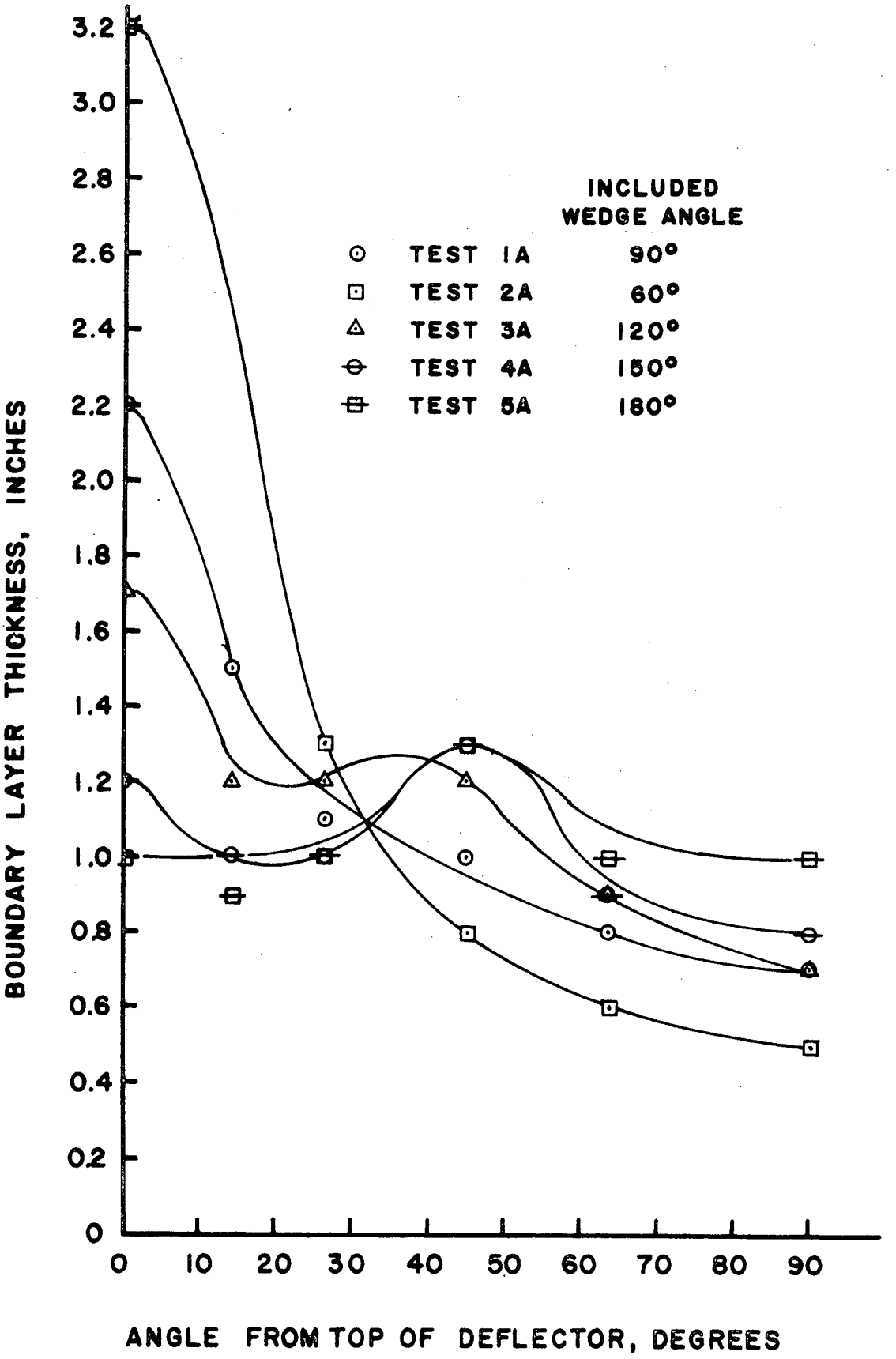

Fig. 4.18. Variation of Boundary Layer Thickness as a Function of Included Wedge Angle

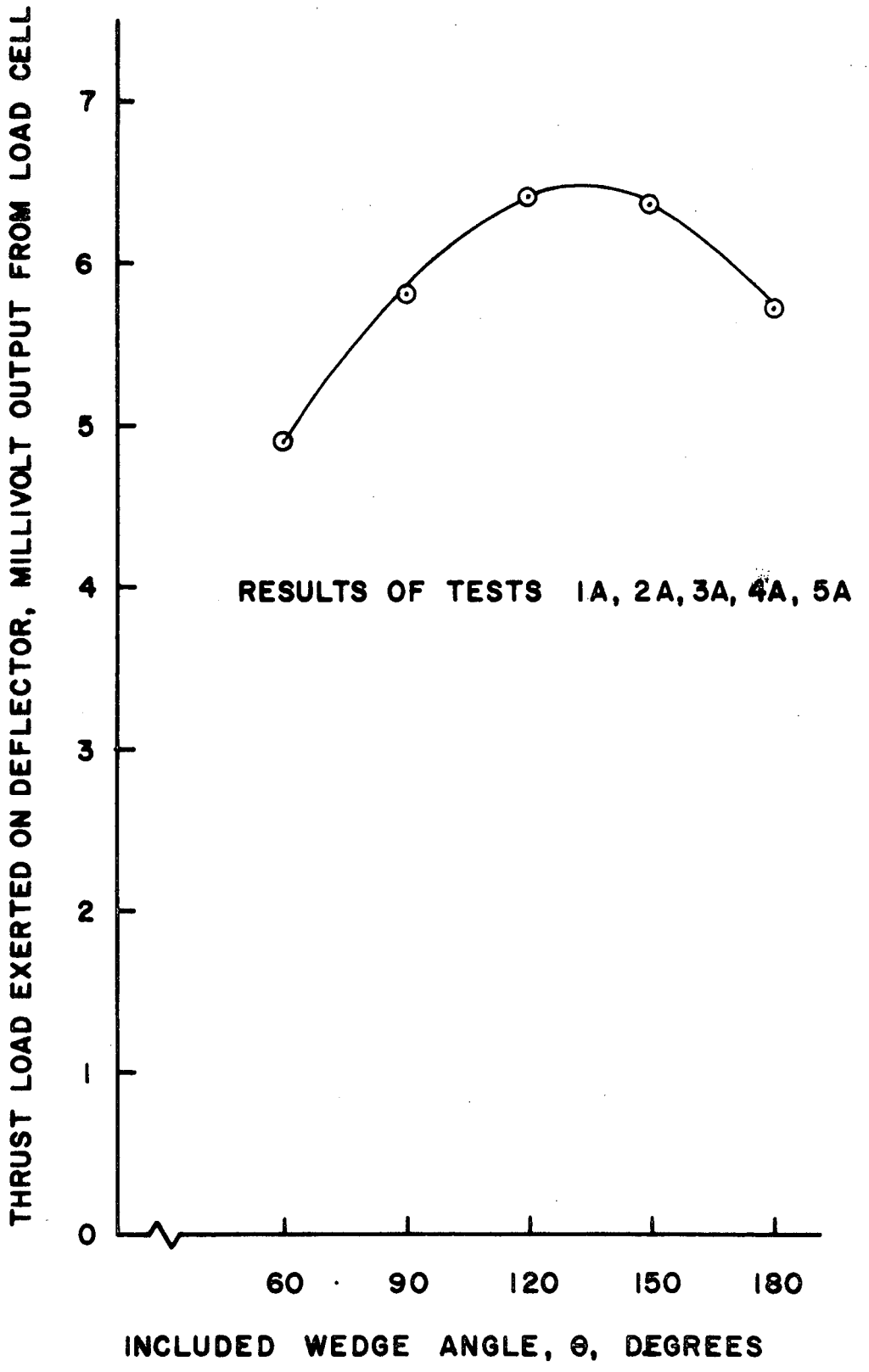

Fig. 4.19. Reverse Thrust as a Function of Included Wedge Angle

performance. First, no entrainment of the jet flow occurred at 180°, but as the angle was reduced more and more jet flow from the sides of the deflector was entrained by flow from the apex of the deflector. Secondly, as the included angle was made smaller, the deflector tended to shut off the flow from the jet, due to back pressuring, even though the apex of the deflector was not moved. As a result, at 60° included angle the load was even less than that which would be measured by impingement on a flat plate at the reference flow rate.

Finally, to investigate possible similarity of the velocity data, the results from typical velocity traverses were plotted in the usual form for a wall jet. The total pressure results were non-dimensionalized by forming the ratio of total pressure to the maximum total pressure measured at any single (x,y) position. The z - coordinate was normalized by using the "half jet" thickness measured at each (x, y) position. These results are shown in Fig. 4.20. While the data points tend to fall close to a single curve, there are clearly differences. To illustrate these differences several curves have been drawn to show clearly the amount of variation between the various traverses. Thus, there is some doubt whether similarity of the velocity profiles is present, although there is good reason to expect it. This study should be extended to determine whether or not there are logical ways of modeling this type of flow based on the findings presented here.

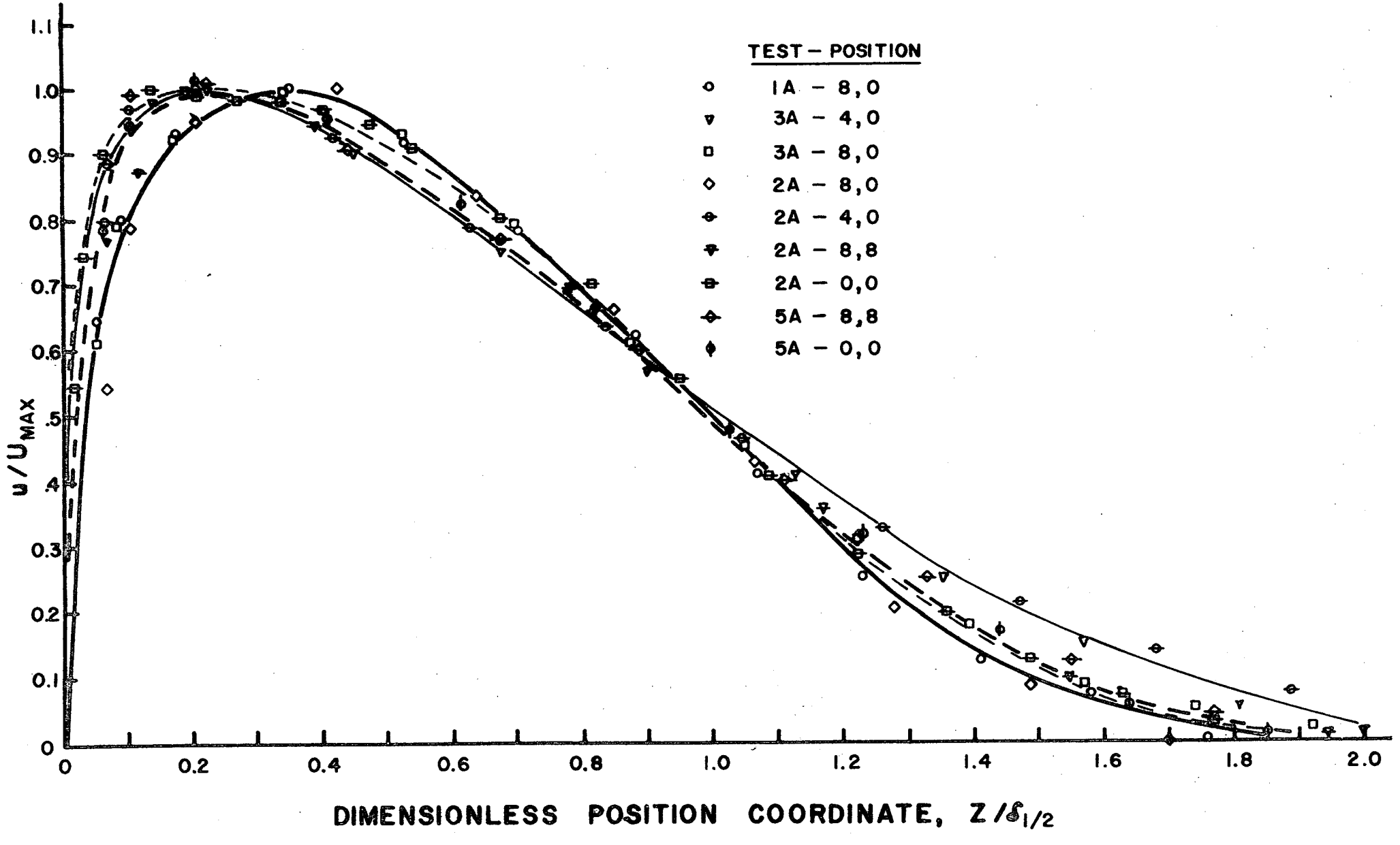

Fig. 4.20. Similarity of the Normalized Velocity Profiles Obtained from the Three-Dimensional Jet Apparatus

5. PLANNED FURTHER WORK

During the next reporting period, the principal theme will be consolidation and completion of work already initiated, however, some new work will be begun. The planned projects are listed below:

(1) The mathematical model of the flow field near an aircraft engine operating in reverse thrust will be completed.

(2) An analysis of the (180°) opposing circular jet will be conducted and the results compared with those from a brief experimental study.

(3) A turbulent flow solution (including prediction of the separation point) for the two-dimensional jet deflected by an arbitrary surface will be completed.

(4) Round jet impingement testing on three-dimensional surfaces will be completed.

(5) The study of the use of flaps as thrust reversers will be completed.

APPENDIX A

TRANSVERSE JET TEMPERATURE AND VELOCITY DATA

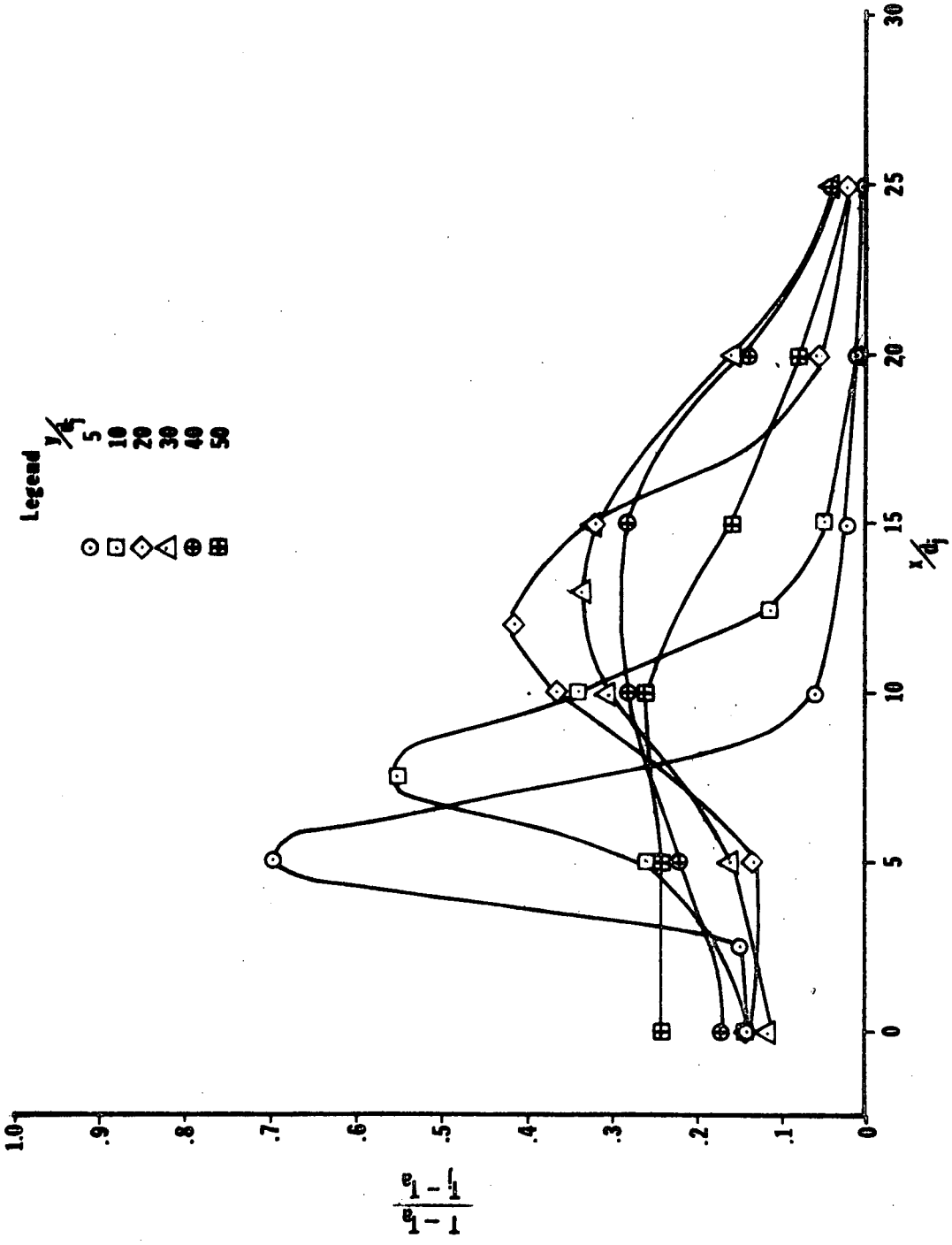

Fig. A-1. Non-dimensional Temperature Plots for Test 24

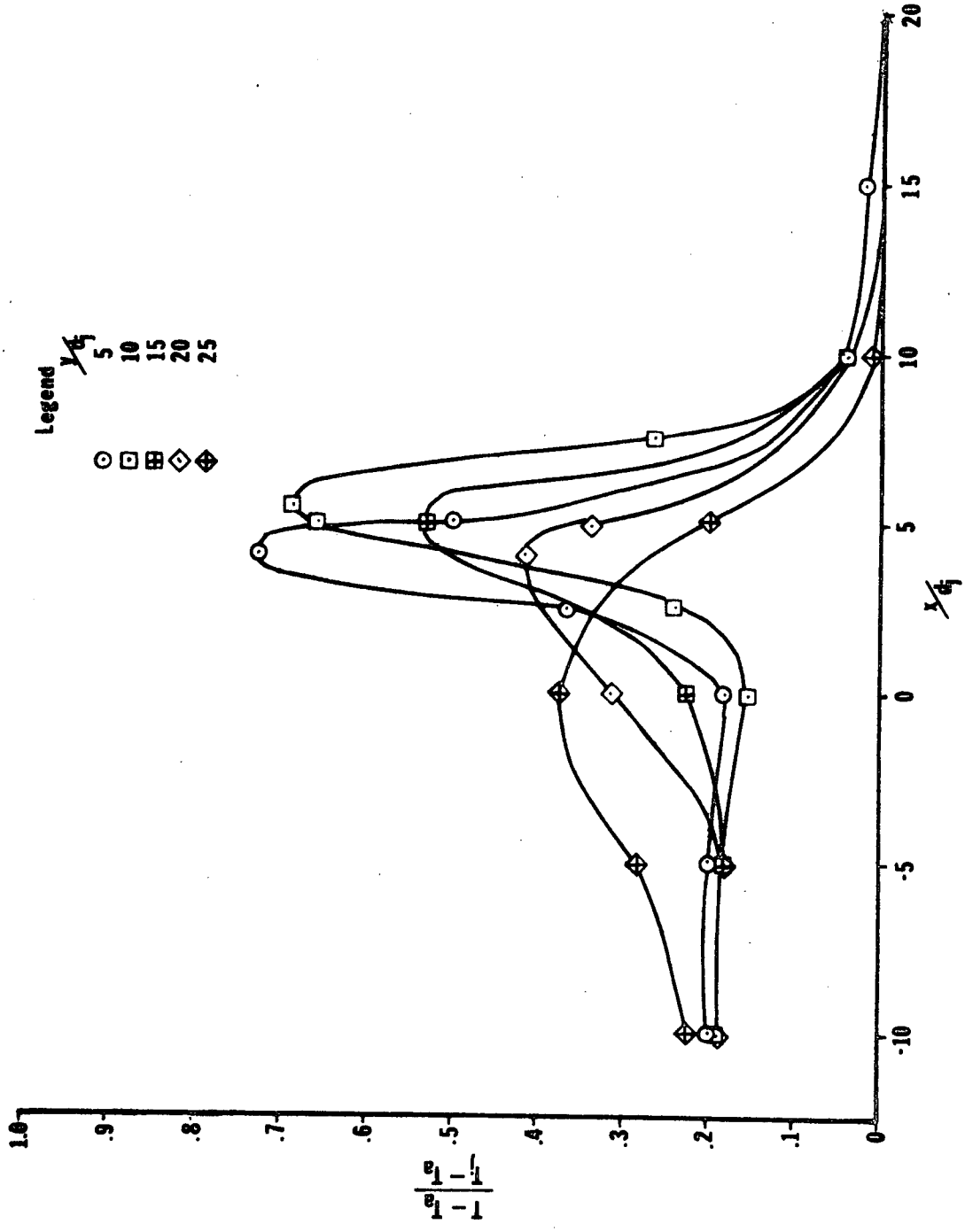

Fig. A-2. Non-dimensional Temperature Plots for Test 25

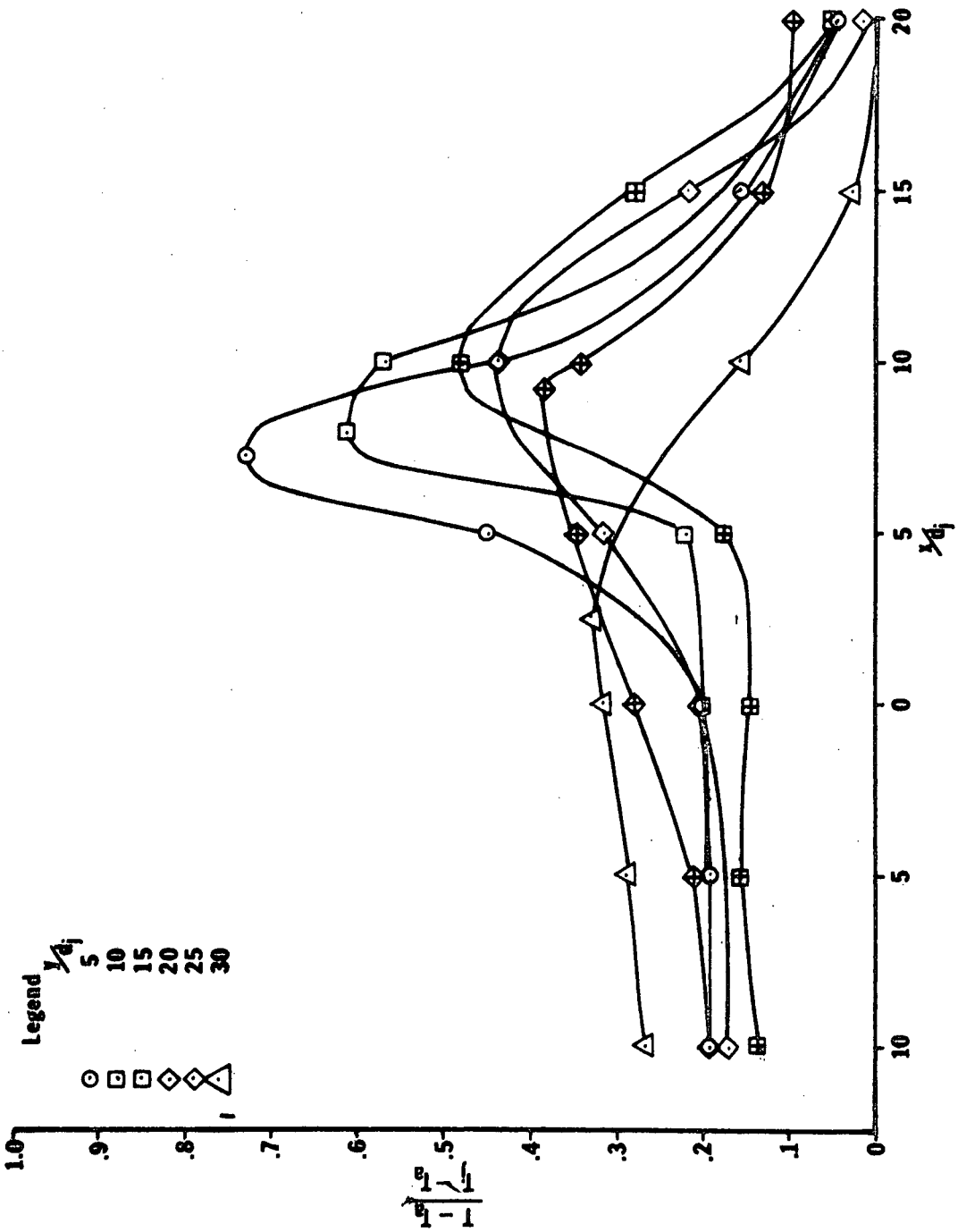

Fig. A-3. Non-dimensional Temperature Plots for Test 30

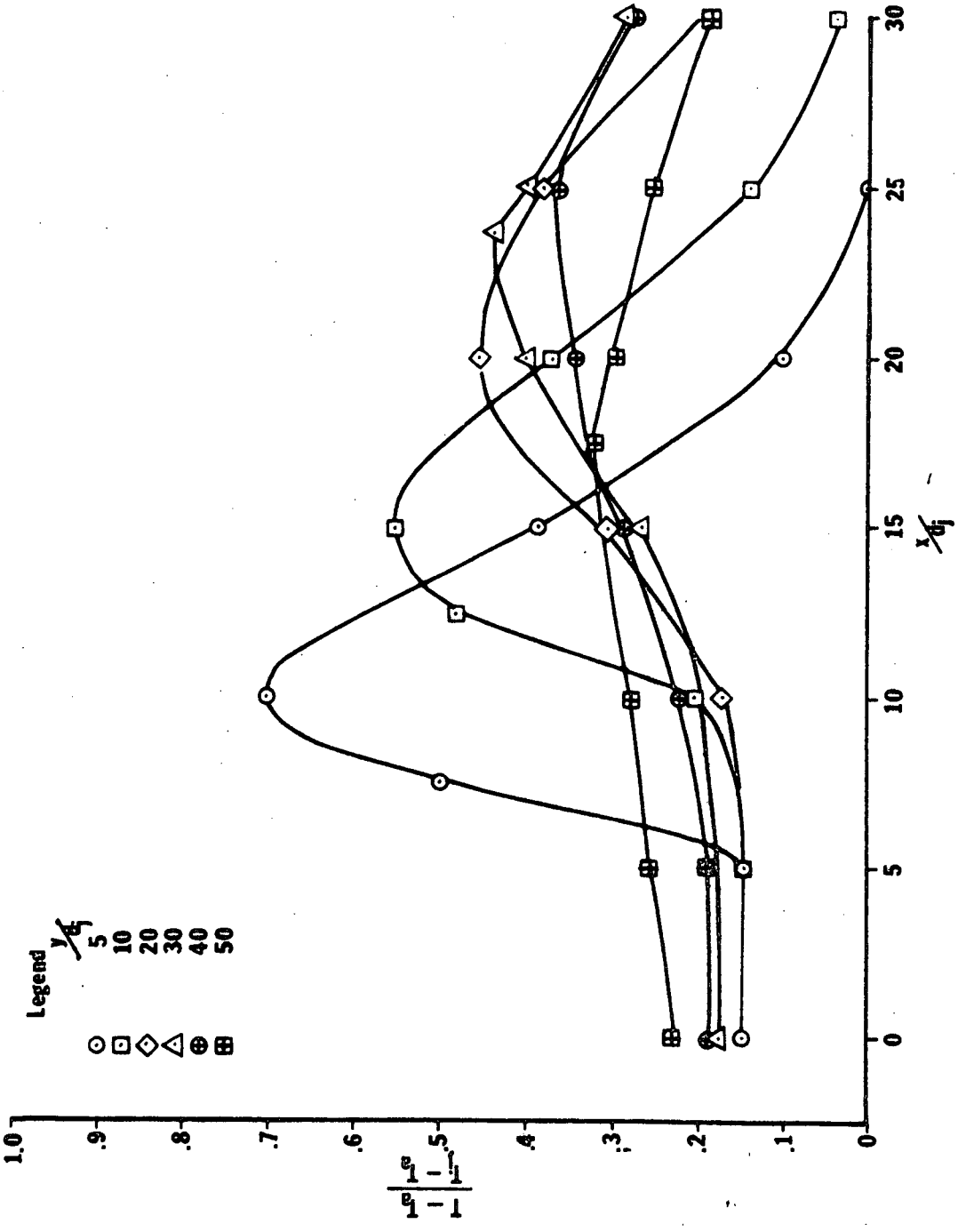

Fig. A-4. Non-dimensional Temperature Plots for Test 31

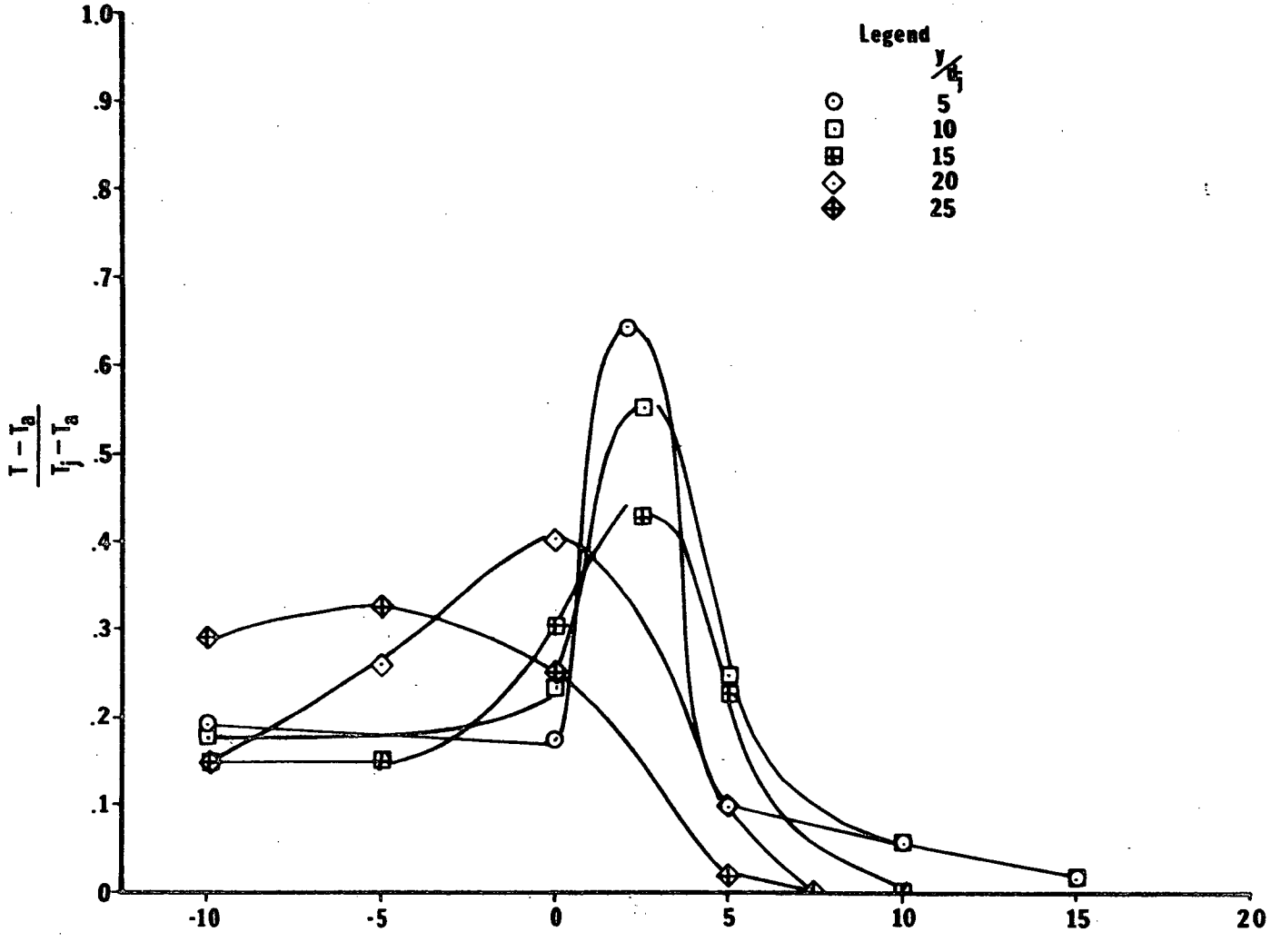

Fig. A-5. Non-dimensional Temperature Plots for Test 35

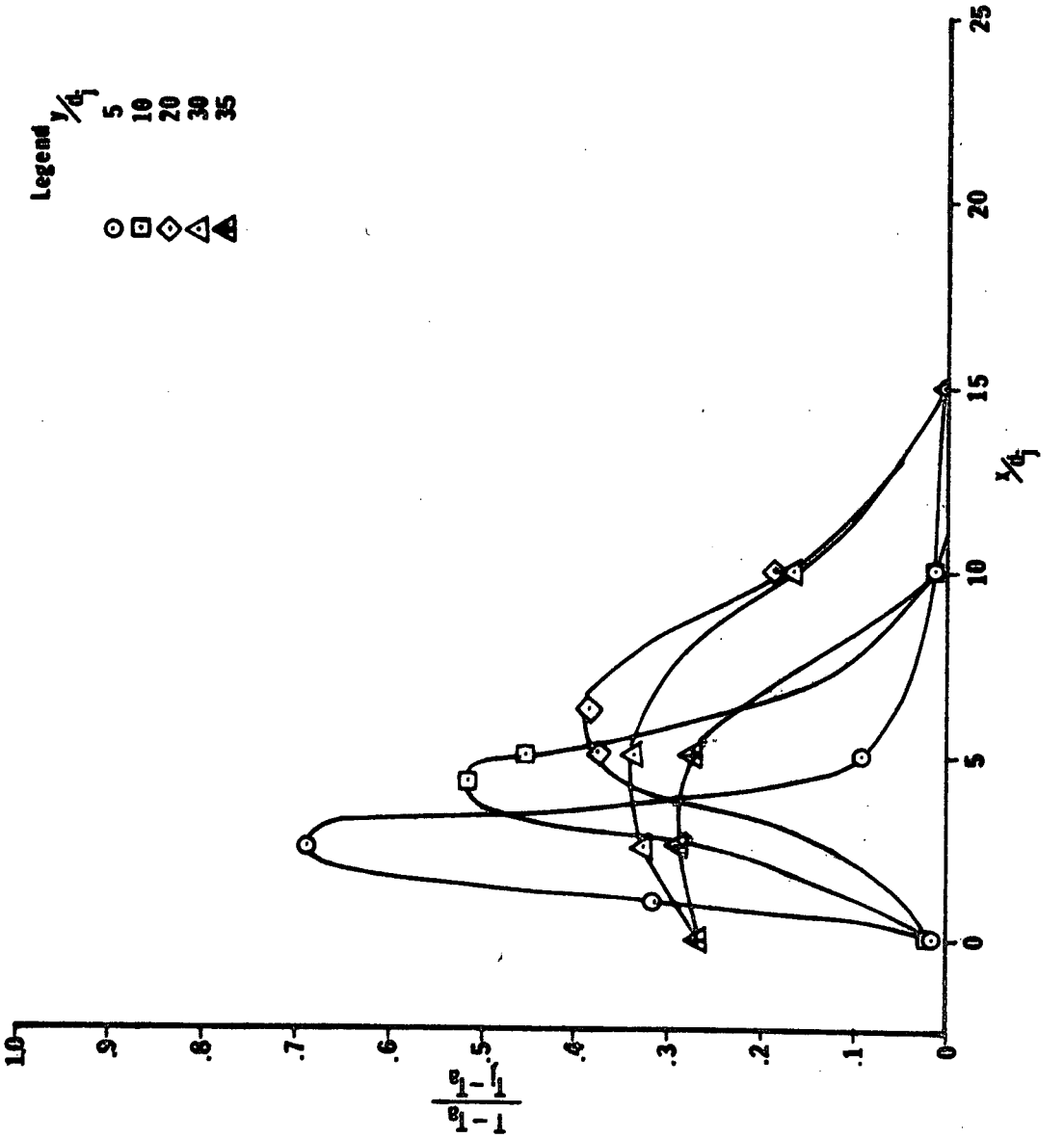

Fig. A-6. Non-dimensional Temperature Plots for Test 36

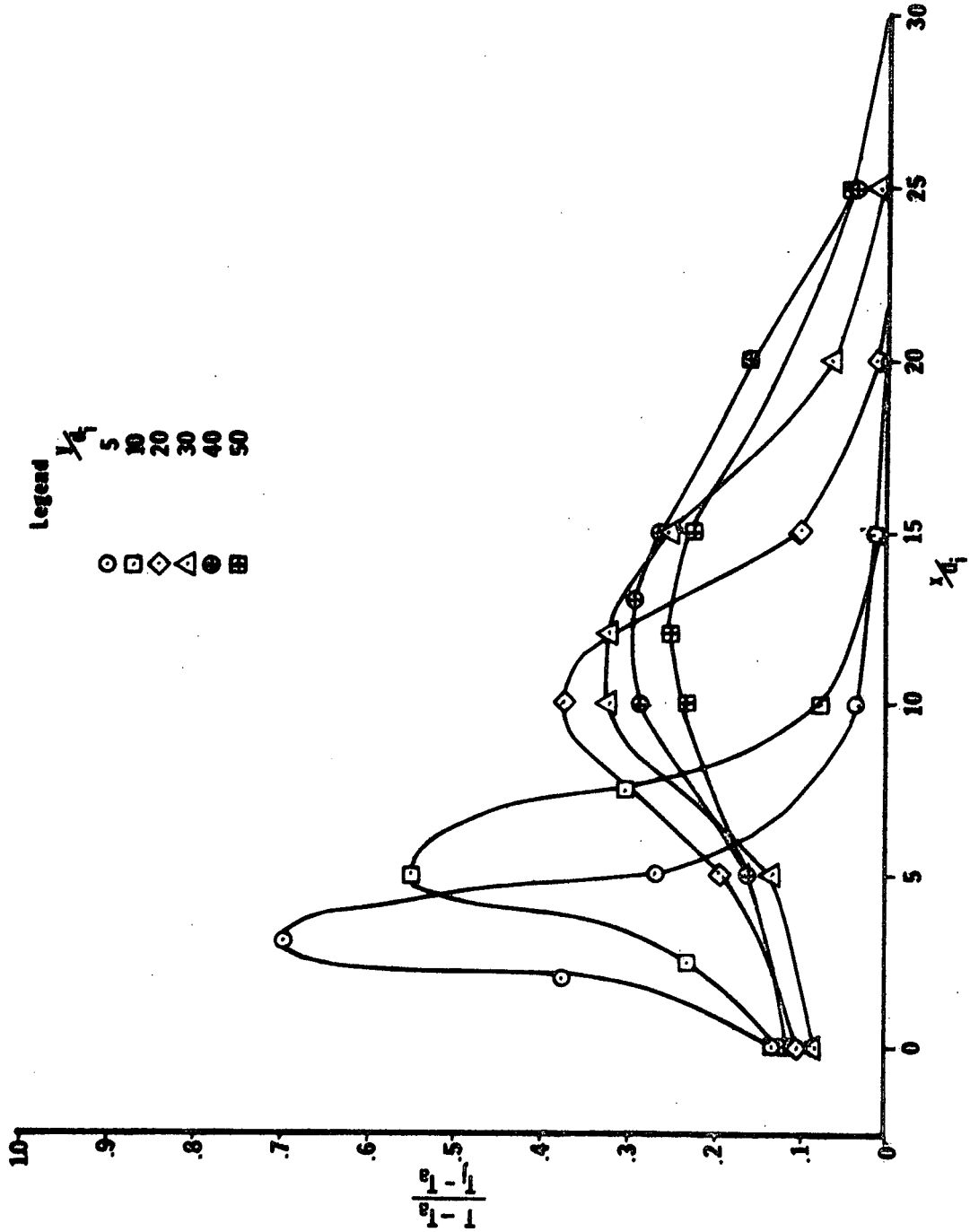

Fig. A-7. Non-dimensional Temperature Plots for Test 37

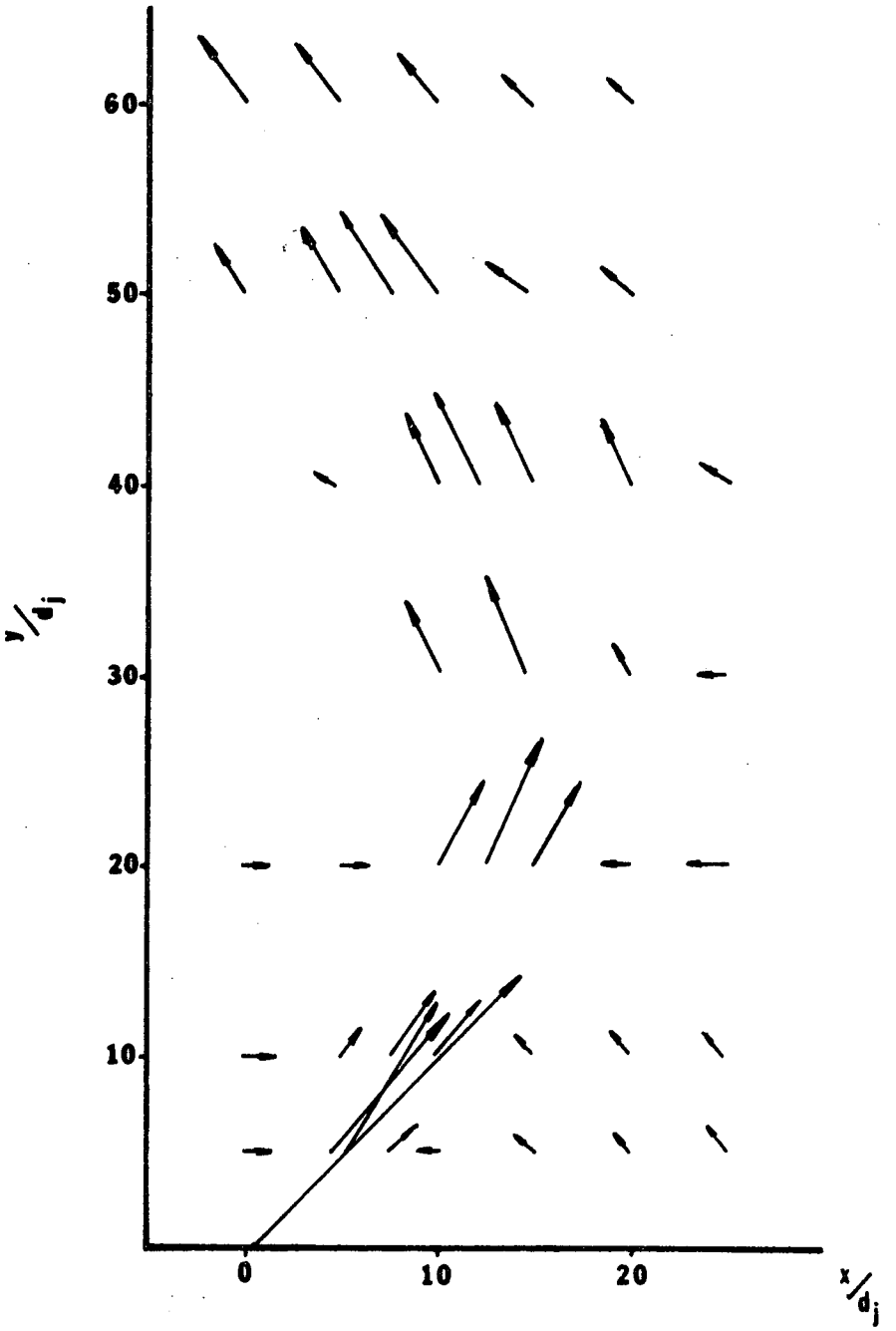

Fig. A-8. Velocity Vector Field for Test 24

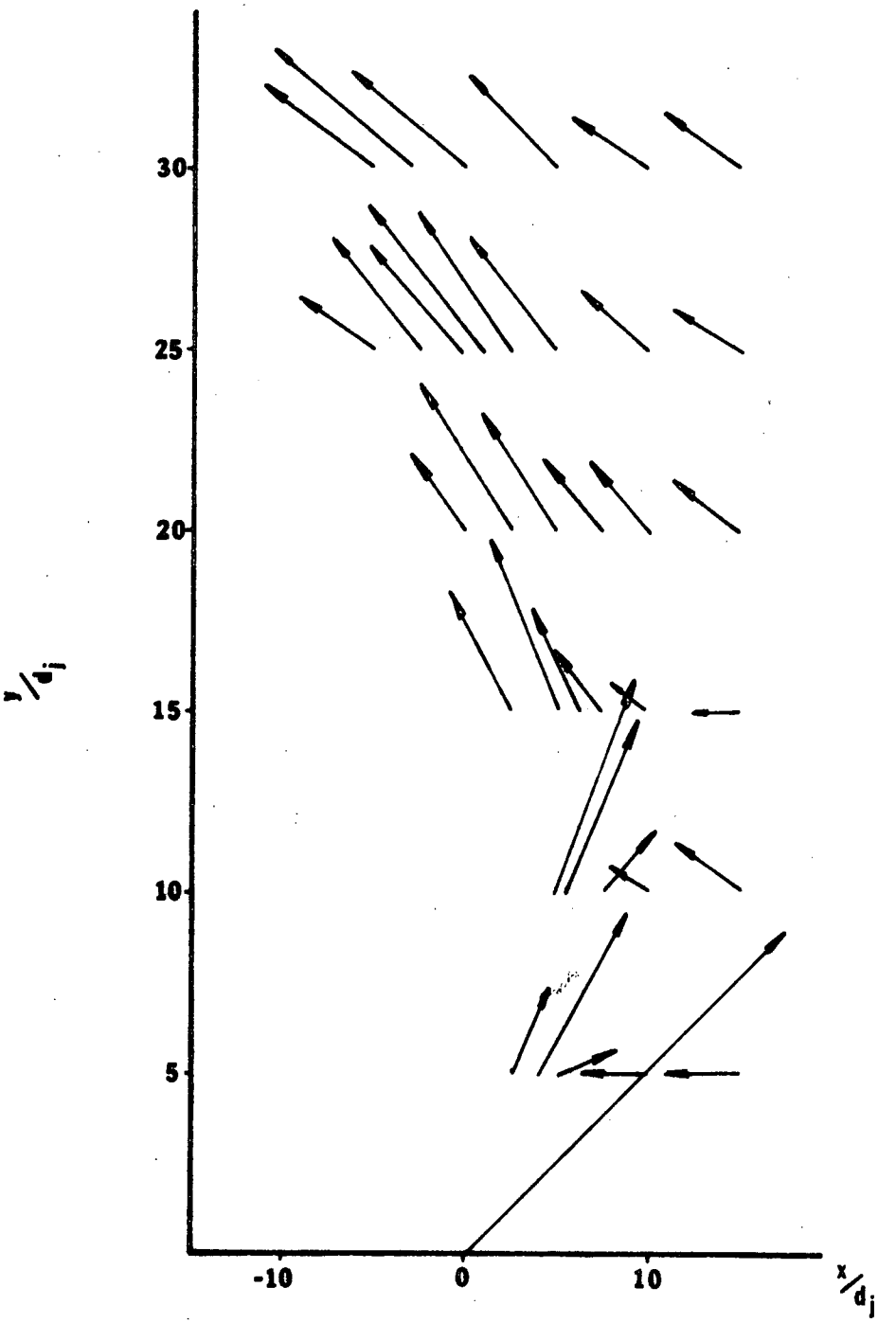

Fig. A-9. Velocity Vector Field for Test 25

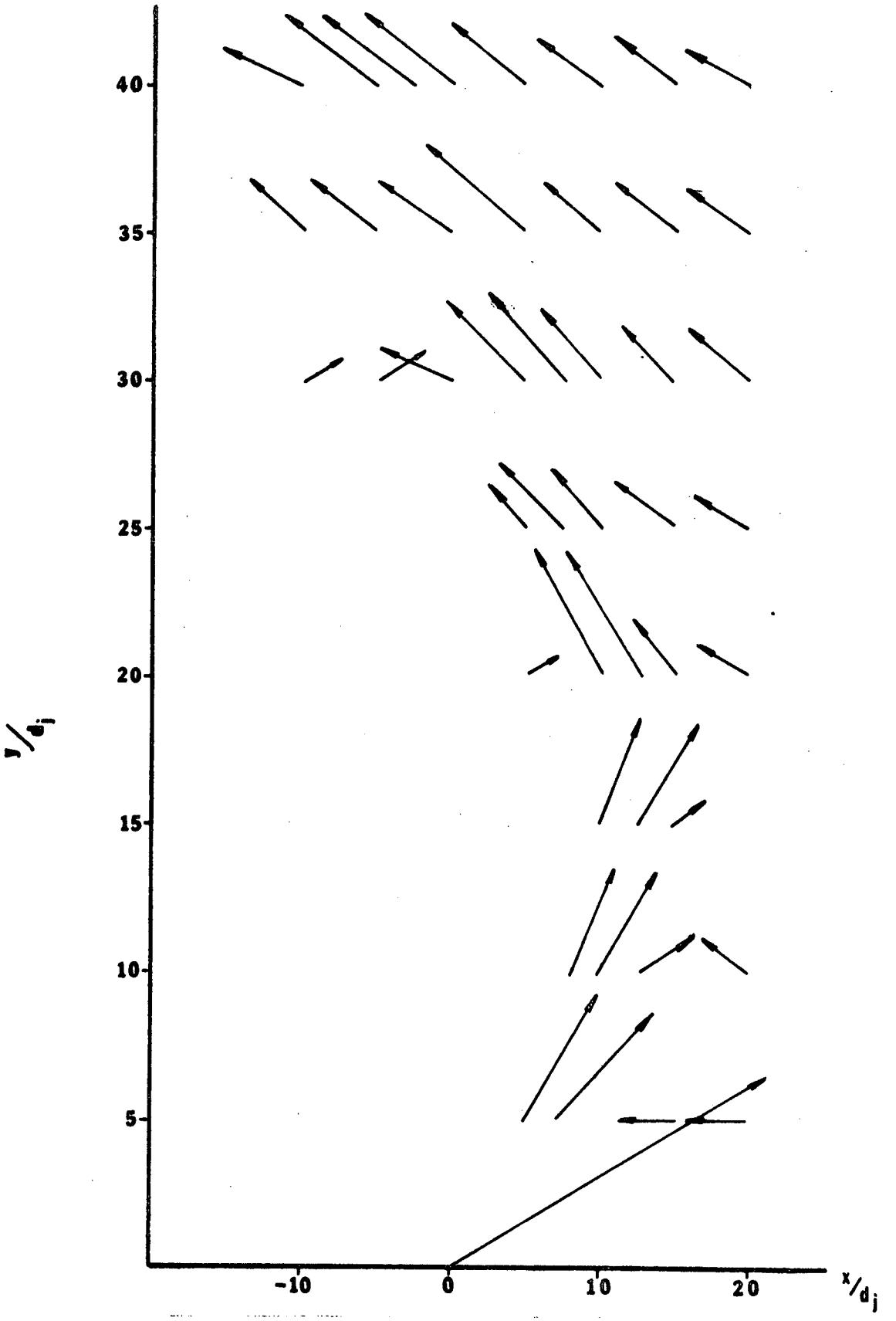

Fig. A-10. Velocity Vector Field for Test 30

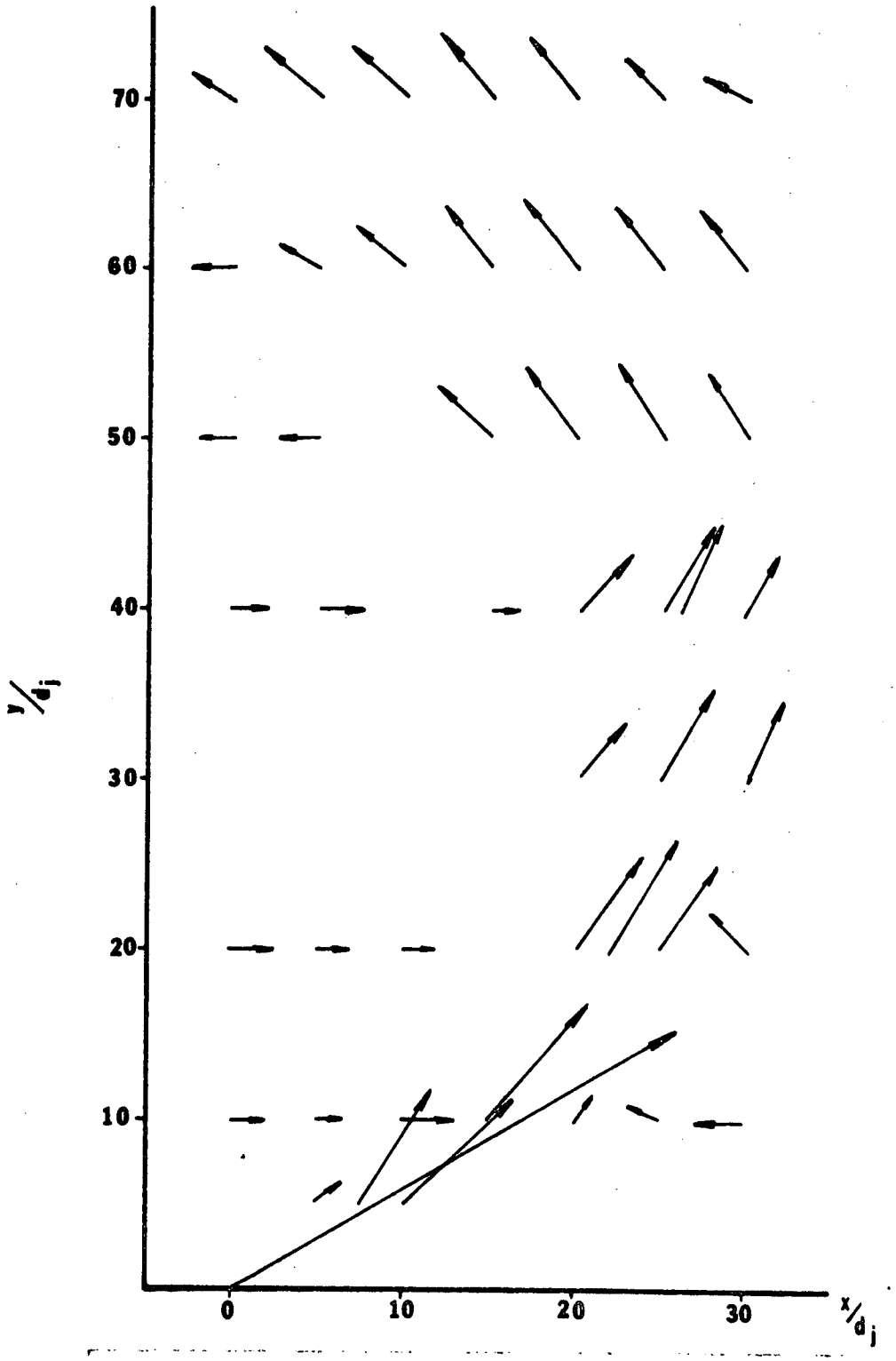

Fig. A-11. Velocity Vector Field for Test 31

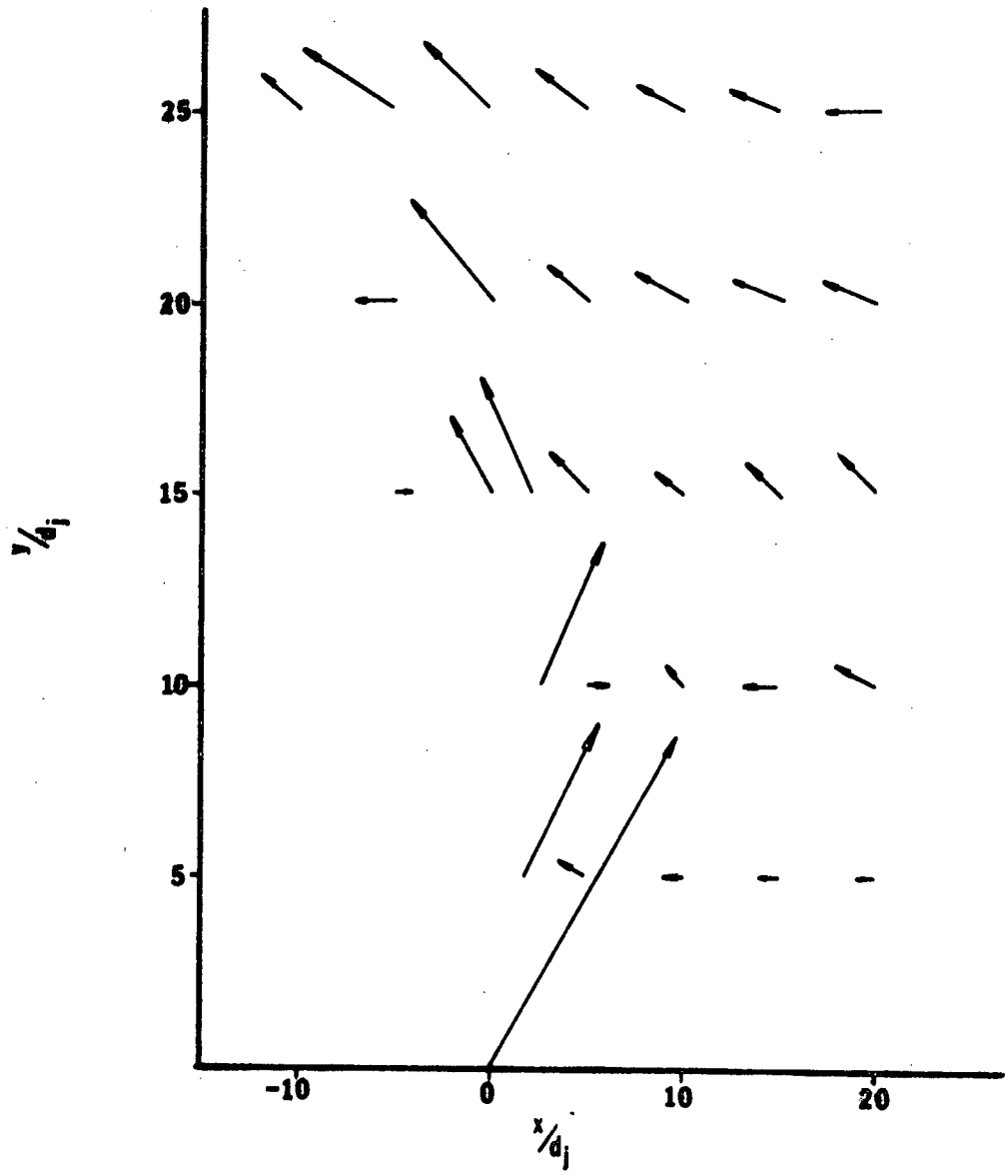

Fig. A-12. Velocity Vector Field for Test 35

3-3

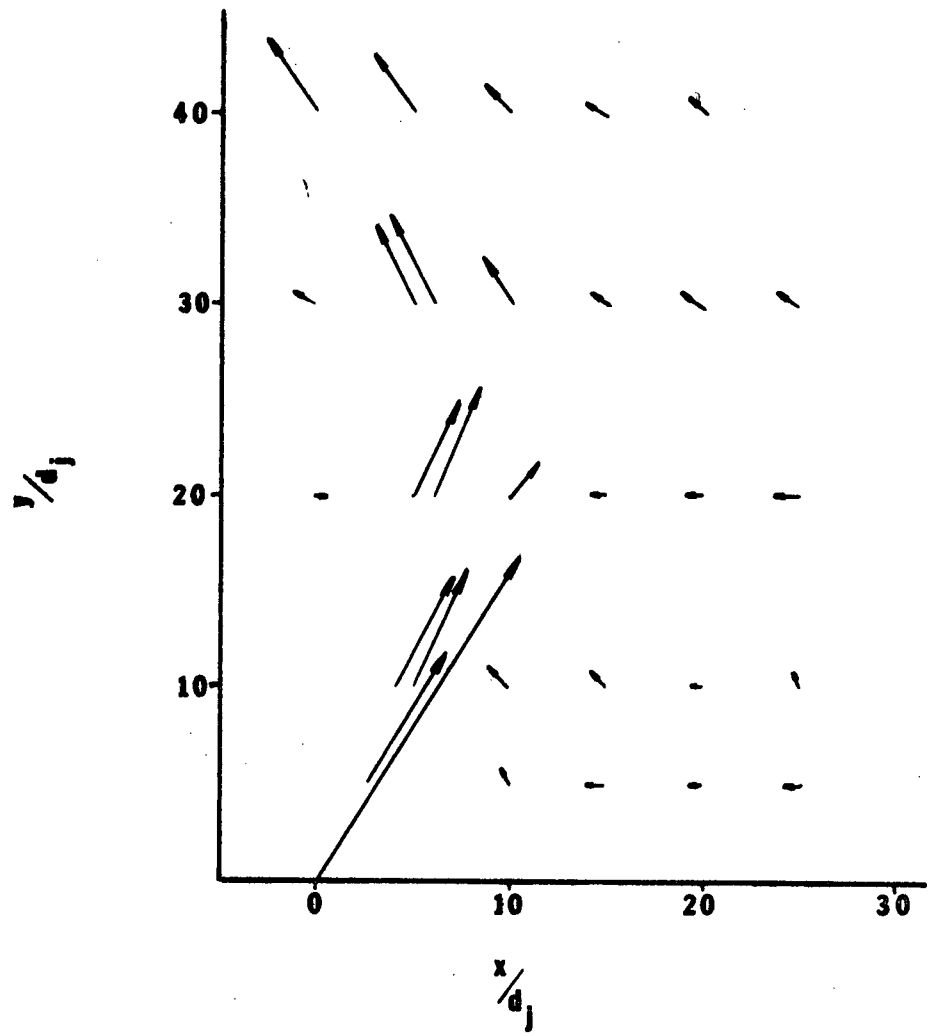

Fig. A-13. Velocity Vector Field for Test 36

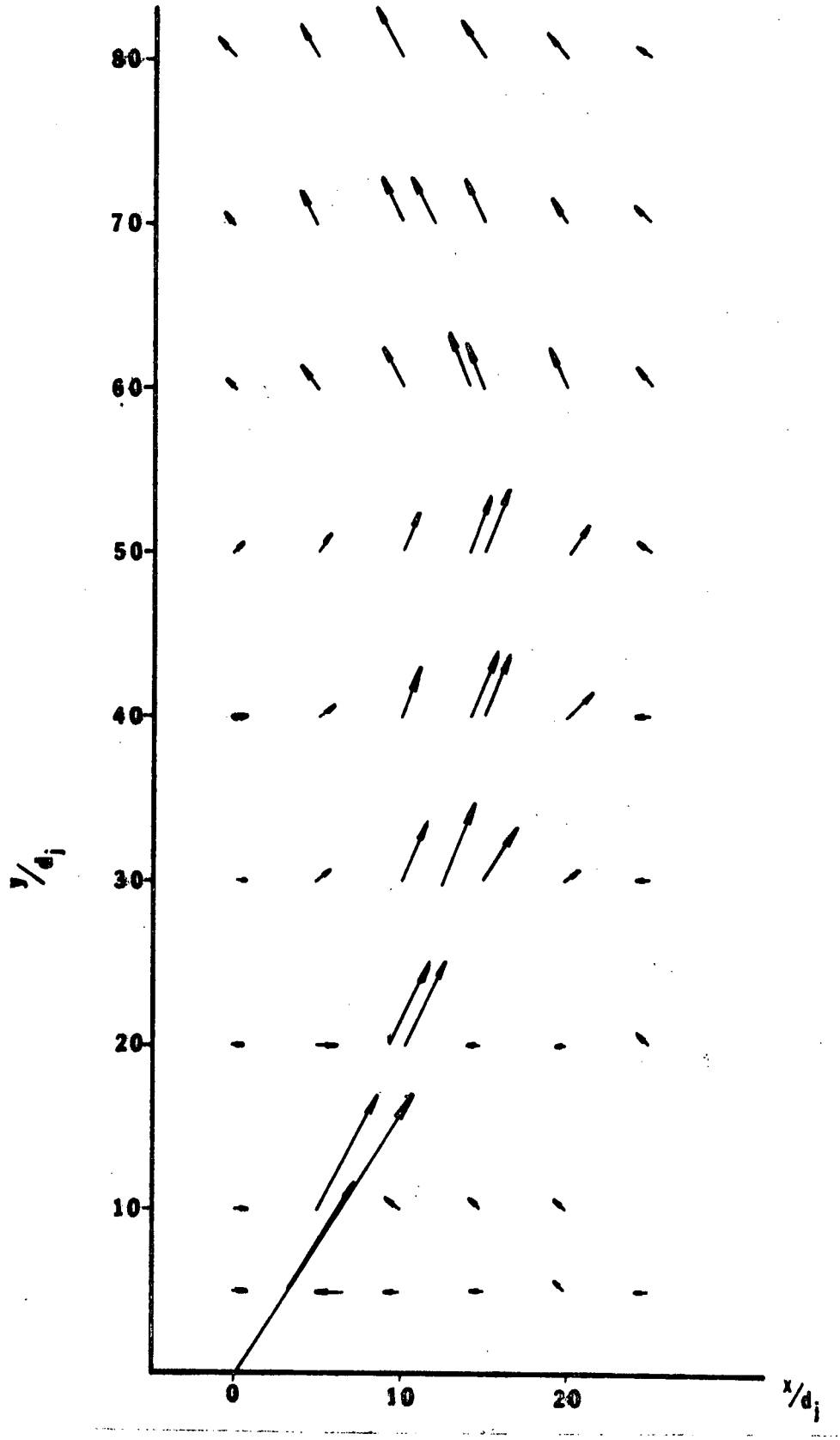

Fig. A-14. Velocity Vector Field for Test 37

TABLE A-1, TEST 24
VR = 10, $\alpha_J = 135°$

x/d_J	y/d_J	$\lvert u/V_\infty \rvert$	$\lvert u+v/V_\infty \rvert$	α
0	5	0.33	0.33	180
4.4		2.75	04.32	129
5.0		2.49	4.55	123
7.5		0.50	0.66	139
10		0.50	0.50	0
15		0.42	0.50	34
20		0.33	0.50	48
25		0.50	0.75	48
0	10	0.25	0.25	180
5		0.50	0.83	127
8		1.90	3.90	123
10		1.16	1.82	129
15		0.50	0.58	31
20		0.42	0.58	44
25		0.42	0.58	44
0	20	0.25	0.25	180
5		0.25	0.25	180
10		1.0	2.16	118
12.5		1.24	3.15	113
15		1.0	2.16	118
20		0.42	0.42	0
25		0.42	0.42	0
10	30	0.66	1.75	112
15		1.0	2.66	112
20		0.50	1.0	120
25		0.33	0.33	0
5	40	.50	0.58	31
10		0.91	1.99	63
12		1.0	2.49	66
15		0.91	2.32	67
20		0.66	1.40	62
25		0.42	0.50	34
0	50	1.0	1.33	41
5		1.16	2.07	56
7.5		1.24	2.16	55
10		1.16	2.16	58
15		0.83	1.40	54
20		0.66	0.83	26
25		0.50	0.66	41
0	60	1.24	1.99	51
5		1.16	1.83	50
10		1.0	1.49	48
15		0.66	1.0	48
20		0.58	0.83	46

TABLE A-2, TEST 25
VR = 5, $\alpha_J = 135°$

x/d_J	y/d_J	$\lvert u/V_\infty \rvert$	$\lvert u+v/V_\infty \rvert$	α
2.5	5	0.41	0.99	115
4		1.04	1.99	121
5		0.91	0.95	163
10		0.29	0.29	0
15		0.33	0.33	0
5	10	0.75	2.11	111
6		0.79	1.82	116
7.5		0.41	0.66	129
10		0.29	0.33	29
15		0.33	0.41	37
2.5	15	0.58	1.16	60
5		0.70	1.90	68
6.4		0.75	1.49	60
7.5		0.66	0.95	46
10		0.37	0.46	35
15		0.41	0.41	0
0	20	0.54	0.87	52
2.5		0.95	1.78	58
5		0.91	1.58	55
7.5		0.66	0.99	48
1.0		0.50	0.75	48
15		0.50	0.62	37
-5	25	0.58	0.66	29
-2.5		0.91	1.24	43
0		1.12	1.62	46
1.0		1.16	1.74	48
2.5		1.04	1.74	53
5		0.83	1.325	51
10		0.58	0.79	43
15		0.58	0.66	29
-10	30	1.08	1.16	22
-5		1.33	1.58	33
-3		1.33	1.70	39
0		1.16	1.49	39
5		0.79	1.08	43
10		0.66	.79	33
15		0.62	.75	33

TABLE A-3, TEST 30
VR = 5 , α_J = 150°

x/d_J	y/d_J	$\lvert u/V_\infty \rvert$	$\lvert u+v/V_\infty \rvert$	α
5	5	0.63	1.35	118
7		1.10	1.69	131
10		0.59	0.59	180
15		0.42	0.42	0
20		0.34	0.34	0
8.2	10	0.72	1.69	115
10		0.76	1.47	121
12.5		0.63	0.76	146
15		0.46	0.46	180
20		0.34	0.42	26
10	15	0.59	1.39	115
12.5		0.67	1.18	125
15		0.55	0.67	144
5	20	0.34	0.42	143
10		0.63	1.39	63
12.5		0.67	1.35	60
15		0.59	0.84	46
20		0.51	0.59	31
5	25	0.67	0.93	43
7.5		0.84	1.14	42
10		0.80	1.27	51
15		0.87	0.84	37
20		0.59	0.63	21
-10	30	0.38	0.42	154
-5		0.46	0.55	148
0		0.80	0.84	18
5		0.93	1.35	47
7.5		0.93	1.43	50
10		0.89	1.35	49
15		0.76	0.89	39
20		0.67	0.84	37
-10	35	0.67	0.84	37
-5		0.93	1.10	32
0		1.10	1.26	30
5		1.05	1.35	39
10		0.89	1.18	41
15		0.76	1.01	41
20		0.72	0.89	36
-10	40	1.05	1.14	22
-5		1.14	1.39	35
-2.5		1.18	1.39	32
0		1.10	1.39	38
5		1.01	1.26	37
10		0.89	1.10	36
15		0.76	0.97	38
20		0.76	0.84	26

TABLE A-4, TEST 31
VR = 10, $\alpha_J = 150°$

x/d_J	y/d_J	$\lvert u/V_\infty \rvert$	$\lvert u+v/V_\infty \rvert$	α
5	5	0.34	0.42	137
7.5		1.43	2.94	119
10		2.35	3.28	136
0	10	0.34	0.34	180
5		0.34	0.34	180
10		0.50	0.50	180
15		1.77	2.85	132
20		1.01	1.68	127
25		0.50	0.59	31
30		0.50	0.50	0
0	20	0.34	0.34	180
5		0.34	0.34	180
10		0.34	0.34	180
20		1.09	1.93	124
22		1.18	2.26	121
25		1.01	1.93	121
30		0.59	0.84	46
20	30	0.67	1.01	132
25		0.92	1.85	120
30		0.67	1.68	114
0	40	0.34	0.34	180
5		0.34	0.34	180
15		0.50	0.50	180
20		0.76	1.18	130
25		0.84	1.77	118
26		0.84	1.85	117
30		0.67	1.51	116
0	50	0.34	0.34	0
5		0.42	0.42	0
15		0.84	1.18	44
20		0.84	1.51	56
25		0.84	1.68	60
30		0.67	1.34	60
0	60	0.67	0.67	0
5		0.76	0.84	26
10		1.01	1.18	51
15		1.01	1.51	48
20		1.01	1.51	48
25		0.84	1.34	51
30		0.67	1.09	52
0	70	1.01	1.09	23
5		1.09	1.34	36
10		1.09	1.43	40
15		1.01	1.51	48
20		0.92	1.34	47
25		0.84	1.18	44
30		0.76	0.84	26

TABLE A-5, TEST 35
VR = 5, $\alpha_J = 120°$

x/d_J	y/d_J	$\lvert u/V_\infty \rvert$	$\lvert u+v/V_\infty \rvert$	α
1.8	5	0.94	2.23	115
5.0		0.30	0.34	29
10		0.24	0.24	0
15		0.26	0.26	0
20		0.26	0.26	0
2.5	10	0.73	1.98	112
5		0.34	0.34	180
10		0.26	0.34	42
15		0.43	0.43	0
20		0.47	0.51	33
-5	15	0.17	0.17	180
0		0.51	1.11	61
2		0.69	1.71	66
5		0.47	0.69	47
10		0.43	0.51	34
15		0.51	0.69	42
20		0.56	0.77	44
-5	20	0.51	0.51	0
0		1.03	1.63	51
5		0.56	0.73	40
10		0.60	0.69	29
15		0.64	0.69	20
20		0.69	0.73	19
-10	25	0.56	0.69	36
5		1.28	1.50	31
0		0.94	1.28	43
5		0.69	0.86	37
10		0.69	0.77	27
15		0.69	0.73	20
20		0.69	0.69	0

TABLE A-6, TEST 36
VR = 10, $\alpha_J = 120°$

x/d_J	y/d_J	$\lvert u/V_\infty \rvert$	$\lvert u+v/V_\infty \rvert$	α
2.5	5	1.97	3.95	120
10		0.34	0.43	66
15		0.26	0.26	0
20		0.26	0.26	0
25		0.26	0.26	0
4	10	1.46	3.35	115
5		1.37	3.42	114
10		0.43	0.60	44
15		0.34	0.52	48
20		0.34	0.34	0
25		0.34	0.43	66
0	20	0.34	0.34	180
5		0.94	2.81	114
6		1.03	2.91	111
10		0.69	1.11	128
15		0.43	0.43	0
20		0.52	0.52	0
25		0.60	0.60	0
0	30	0.69	0.77	27
5		1.03	2.40	65
6		1.03	2.49	66
10		0.69	1.37	60
15		0.43	0.52	34
20		0.52	0.6	31
25		0.60	0.69	29
0	40	1.29	2.23	55
5		1.11	1.89	54
10		0.69	0.94	43
15		0.60	0.69	29
20		0.52	0.69	42

TABLE A-7, TEST 37
VR = 20, $\alpha_J = 120°$

x/d_J	y/d_J	$\lvert u/V_\infty \rvert$	$\lvert u+v/V_\infty \rvert$	α
0	5	0.69	0.69	180
3		4.95	7.53	121
5		1.37	1.37	180
10		0.69	0.86	0
15		0.69	0.69	0
20		0.69	0.69	0
25		0.69	0.69	0
0	10	0.69	0.69	180
5		3.25	7.53	116
10		0.86	1.03	34
15		0.69	0.86	37
20		0.69	0.86	37
0	20	.51	0.51	180
5		1.03	1.03	180
9		2.39	5.80	114
10		2.39	5.30	117
15		1.03	1.03	0
20		0.69	0.69	0
25		0.51	0.69	42
0	30	0.34	0.34	180
5		0.51	0.69	138
10		1.54	3.97	113
12.4		1.71	4.80	111
15		1.71	3.43	120
20		0.69	0.86	143
25		0.51	0.51	0
0	40	0.34	0.34	180
5		0.69	0.86	143
10		1.03	3.08	110
14		1.54	4.14	112
15		1.54	3.97	113
20		1.20	1.71	134
25		0.69	0.69	0
0	50	0.34	0.51	132
5		0.69	1.03	132
10		1.03	2.74	112
14		1.37	3.76	111
15		1.37	3.97	110
20		1.20	2.07	126
25		0.69	0.86	137

TABLE A-7, TEST 37
VR = 20, $\alpha_J = 120°$
(Continued)

x/d_J	y/d_J	$\lvert u/V_\infty \rvert$	$\lvert u+v/V_\infty \rvert$	α
0	60	0.51	0.69	42
5		0.86	1.37	51
10		1.2	2.74	64
14		1.2	3.43	70
15		1.2	3.08	67
20		1.03	2.39	65
25		0.69	1.2	55
0	70	0.69	1.03	48
5		1.03	2.07	60
10		1.20	2.91	66
12		1.37	3.08	64
15		1.20	2.74	64
20		1.03	1.88	57
25		0.69	1.03	48
0	80	1.03	1.71	53
5		1.2	2.57	62
10		1.37	3.08	64
15		1.20	2.39	60
20		1.03	1.71	53
25		0.86	1.03	34

APPENDIX B

COMPUTER LISTING AND SAMPLE OUTPUT - CIRCULAR JET IMPINGING ON CURVED SURFACE

```
C   CIRCULAR JET IMPINGING ON A CURVED SURFACE
      DIMENSION F(33,33),DXR(33,33),DXL(33,33),DYU(33,33),DYD(33,33),
     1  X(33),Y(33),F1(33,15),NVP(33),NHP(33),Y1(33,15)
      DIMENSION YS(33),XS(33),PP(33),PSL(33)
      DIMENSION IS(33),JS(33),DXS(33),X1(33,15)
      DIMENSION FS(33),FSX(33),FO(33,33),NHP2(33),YN(33,15)
      DIMENSION NHS(33),XSL(33),FSXL(33),NHPP(33)
      DIMENSION V(33,33),ANGLE(33,33)
      DIMENSION LCASE(33,33),DYUR(33,33),DYDR(33,33),DXRR(33,33),
     1  DXLR(33,33)
      DIMENSION VSS(33,33)
C   FLUID PROPERTIES AND MACH NUMBER
      AMACH=.5
      AK=1.4
      RCON=53.3
      TSTAT=530.
      PSTAT=14.696*144.
      RHOS=PSTAT/RCON/TSTAT
      TTOT=TSTAT*(1.+(AK-1.)*.5*AMACH**2)
      PTOT=PSTAT*(TTOT/TSTAT)**(AK/(AK-1.))
      RHOT=RHOS*(TTOT/TSTAT)**(1./(AK-1.))
      CZERO=SQRT(32.16*AK*RCON*TTOT)
      CNORM=SQRT(32.16*AK*RCON*TSTAT)
      VNORM=AMACH*CNORM
      CZERO=CZERO/VNORM
      OUTPUT PSTAT,PTOT,TTOT,RHOS,RHOT,AMACH,CNORM,CZERO,VNORM
  INPUT OF INITIAL INFORMATION
      LS=0
      ICOM=20
      ISTOP=10
      NSP=5
      NH=12
      NJV=16
      NV=23
      AL1=1.
      AL2=1.
      AL3=1.5
      AL4=1.5
      ANH=NH
      ANV=NV
      ANSP=NSP
      ANJV=NJV
      NSPP1=NSP+1
      NSPM1=NSP-1
      NSP2=(NSP+1)/2
      NHP1=NH+1
      NHM1=NH-1
      NVP1=NV+1
      NJVM1=NJV-1
      NJVP1=NJV+1
      NTRY=0
      FACTOR=.00002
```

```
      TMAX=2.*3.1415926*AL1*AL1
      DX1=AL1/(ANSP-1.)
      DX2=(AL4-AL1)/(ANH-ANSP+1.)
      DY1=AL3/(ANJV-1.)
      DY2=AL2/(ANV+1.-ANJV)
C     DETERMINATION OF GRID POINT LOCATIONS
      DO 501 J=1,NSPM1
      AJ=J-1
  501 X(J)=AJ*DX1
      DO 502 J=NSP,NHP1
      AJ=J-NSP
      X(J)=AL1+AJ*DX2
  502 X1(J,1)=X(J)
      DO 503 I=1,NJV
      AI=I-1
  503 Y(I)=AI*DY1
      DO 504 I=NJVP1,NVP1
      AI=I-NJV
  504 Y(I)=AL3+AI*DY2
C     SPECIFICATION OF PLATE LOCATION
      ZETAE=45.
      ZETAE=ZETAE*3.1415926/180.
      A1=.5
      A2=TAN(ZETAE)*TAN(ZETAE)
      A3=X(NHP1)*X(NHP1)
      A=A3*A2-4.*A1*A1
      B=4.*A1**3.-2.*A1*A3*A2
      C=A1*A1*A3*A2-A1**4.
      GP1=(-B+SQRT(B*B-4.*A*C))/2./A
      GP2=(-B-SQRT(B*B-4.*A*C))/2./A
      GP=GP1
      G=GP*GP
      FF=A3*G/(2.*A1*SQRT(G)-A1*A1)
      OUTPUT ZETAE,A1,A2,A3,A,B,C,GP1,GP2,G,FF
      DO 320 J=1,NHP1
      GP=ABS(GP)
  320 YS(J)=GP-SQRT((1.-X(J)*X(J)/FF)*G)
      WRITE(6,4500)(YS(J),J=1,NHP1)
 4500 FORMAT(E10.4)
C     INITIAL FREE STREAMLINE LOCATION
      Y1(NSP,1)=AL3+.75
      Y2=YS(NHP1)
      Y33=Y2+AL1**2/AL4
      DO 301 J=NSPP1,NHP1
  301 Y1(J,1)=.5*((Y1(NSP,1)+(Y33-Y1(NSP,1))*(J-NSP)/(NHP1-NSP))+YS(J))
      Y3=Y1(NHP1,1)
      Y1(NSP,1)=AL3
C     LOCATION OF PLATE
      DO 4 I=2,NV
      IF(Y(I).GT.Y2.AND.Y(I-1).LT.Y2)I1=I
    4 CONTINUE
      I1M1=I1-1
   72 CONTINUE
C     SPECIFICATION OF NODE SPACING
      DO 505 I=1,NJVM1
      DO 505 J=1,NSPM1
      DXR(I,J)=DX1
      DXL(I,J)=DX1
      DYU(I,J)=DY1
  505 DYD(I,J)=DY1
      DO 506 I=1,NVP1
      DO 506 J=NSPP1,NHP1
      DXL(I,J)=DX2
      DXR(I,J)=DX2
      DYU(I,J)=DY1
  506 DYD(I,J)=DY1
```

```
      DO 507 I=1,NJV
      DXR(I,NSP)=DX2
      DXL(I,NSP)=DX1
      DYU(I,NSP)=DY1
507   DYD(I,NSP)=DY1
      DO 508 I=NJVP1,NVP1
      DO 508 J=1,NSP
      DXL(I,J)=DX1
      DXR(I,J)=DX1
      DYU(I,J)=DY2
508   DYD(I,J)=DY2
      DO 509 J=1,NSP
      DXL(NJV,J)=DX1
      DXR(NJV,J)=DX1
      DYU(NJV,J)=DY2
509   DYD(NJV,J)=DY1
      DO 400 I=1,NVP1
      DO 400 J=1,NHP1
      V(I,J)=0.
400   ANGLE(I,J)=0.
C     DETERMINE XS(I) AND NHP(I)
      DO 14 I=1,NVP1
      NHP(I)=NH
 14   NHS(I)=2
      I1L=1
      DO 200 I=2,NV
      IF(Y(I).GE.YS(1).AND.Y(I-1).LT.YS(1))I1L=I
200   CONTINUE
      I1LM1=I1L-1
      I1LP2=I1L+2
      I1MAX=I1
      IF(I1L.GT.I1)I1MAX=I1L
C     DETERMINE XS(I), XSL(I), NHS(I), NHP(I), DXR(I,J),DXL(I,J), AND
C     DYD(I,J)
      DO 201 I=2,I1MAX
      DO 201 J=1,NH
      IF(YS(J).GT.Y(I).AND.YS(J+1).LT.Y(I))GO TO 203
      IF(YS(J).LT.Y(I).AND.YS(J+1).GT.Y(I))GO TO 204
      GO TO 202
203   NHS(I)=J+1
      XSL(I)=X(J)+DXR(I,J)*(YS(J)-Y(I))/(YS(J)-YS(J+1))
      DXL(I,J+1)=X(J+1)-XSL(I)
      GO TO 202
204   NHP(I)=J
      NHPP(I)=NHP(I)
      XS(I)=X(J)+DXR(I,J)*(Y(I)-YS(J))/(YS(J+1)-YS(J))
      DXR(I,J)=XS(I)-X(J)
202   CONTINUE
      DYDD=Y(I)-YS(J)
      IF(DYDD.LT.DY)DYD(I,J)=DYDD
201   CONTINUE
C     DETERMINE INTERCEPTS FOR CONSTANT POTENTIALS AT PLATE
      DO 205 J=1,NHP1
      I=1
207   I=I+1
      IF(Y(I-1).LE.YS(J).AND.Y(I).GT.YS(J))GO TO 206
      GO TO 207
206   IS(J)=I
      IF(J.EQ.1)SL10=(YS(2)-YS(1))/DX1
      IF(J.EQ.1)GO TO 209
      IF(J.EQ.NHP1)SL10=(YS(NHP1)-YS(NH))/DX2
      IF(J.EQ.NHP1)GO TO 208
      DX=DX1
      IF(J.GE.NSPP1)DX=DX2
      IF(J.EQ.NSP)DX=.5*(DX1+DX2)
      SL10=(YS(J+1)-YS(J-1))*.5/DX
```

```
  208      CONTINUE
           IF(YS(J).LE..000001)GO TO 405
           ISJ=IS(J)
           XTEMP=X(J)+(Y(ISJ)-YS(J))*(-SL10)
           L=0
  211      L=L+1
           IF(XTEMP.LT.X(L+1).AND.XTEMP.GT.X(L))GO TO 210
           GO TO 211
  210      JS(J)=L
           DX=DX1
           IF(J.GT.NSP)DX=DX2
           DXS(J)=(XTEMP-X(L))/DX
           GO TO 205
  405      DXS(1)=0.
           JS(1)=1
  205      CONTINUE
C     DETERMINE NVP(J)
           DO 21 J=1,NHP1
           IF(J.LT.NSP)NVP(J)=NV
           IF(J.LT.NSP)GO TO 21
           IF(J.EQ.NSP)NVP(J)=NJV-1
           IF(J.EQ.NSP)GO TO 21
           I=0
   22      I=I+1
           IF(Y(I).LT.Y1(J,1))NVP(J)=I
           IF(Y(I).LT.Y1(J,1))GO TO 22
   21      CONTINUE
           DO 38 J=NSPP1,NHP1
           I=NVP(J)
   38      DYU(I,J)=Y1(J,1)-Y(I)
C     DETERMINE NVPMIN
           NVPMIN=NVP(1)
           DO 28 J=2,NHP1
           IF(NVP(J).LE.NVPMIN)NVPMIN=NVP(J)
   28      CONTINUE
C     DETERMINE LOCATION OF SPECIAL BOUNDARY POINTS
           DO 37 I=1,NVP1
   37      NHP2(I)=0
           DO 23 J=NSP,NH
           IF(NVP(J).GE.NVP(J+1))KMAX=1+NVP(J)-NVP(J+1)
           IF(NVP(J).LT.NVP(J+1))KMAX=1-NVP(J)+NVP(J+1)
           IF(KMAX.LE.1)GO TO 23
           DO 25 K=2,KMAX
           I=NVP(J)+2-K
           IF(NVP(J).LT.NVP(J+1))I=NVP(J)-1+K
           Y1(J,K)=Y(I)
           DX=DX2
           X1(J,K)=X(J)+DX*(Y1(J,1)-Y(I))/(Y1(J,1)-Y1(J+1,1))
           IF(NVP(J).LT.NVP(J+1))DXL(I,J+1)=X(J+1)-X1(J,K)
           IF(NVP(J).GE.NVP(J+1))DXR(I,J)=X1(J,K)-X(J)
           IF(NVP(J).LT.NVP(J+1))GO TO 35
           M=0
   26      M=M+1
           IF(X(M).LT.X1(J,K))NHP(I)=M
           IF(X(M).LT.X1(J,K))GO TO 26
           GO TO 702
   35      M=0
   36      M=M+1
           IF(X(M).LT.X1(J,K))NHP2(I)=M+1
           IF(X(M).LT.X1(J,K))GO TO 36
  702      CONTINUE
   25      CONTINUE
   23      CONTINUE
           IF(I1.GT.NVPMIN)GO TO 704
           DO 27 I=I1,NVPMIN
   27      NHP(I)=NH
```

```
  704     CONTINUE
          NST=NJVM1
          DO 520 J=NSP,NHP1
  520     IF(NVP(J).GT.NST)NST=NVP(J)                                    126
          NSTP1=NST+1
          DO 29 I=NSTP1,NVP1
   29     NHP(I)=NSPM1
C     CALCULATION OF VELOCITY POTENTIAL AT BOUNDARY POINTS
          F1(NSP,1)=0.
          DO 30 J=NSP,NH
          KMAX=1+NVP(J)-NVP(J+1)
          IF(NVP(J).LT.NVP(J+1))KMAX=1+NVP(J+1)-NVP(J)
          IF(KMAX.EQ.1)GO TO 31
          DO 32 K=2,KMAX
          F1(J,K)=F1(J,K-1)+SQRT((X1(J,K)-X1(J,K-1))**2+(Y1(J,K)-Y1(J,K-1))
         1 **2)
   32     CONTINUE
          FLAST=F1(J,KMAX)
          YLAST=Y1(J,KMAX)
          XLAST=X1(J,KMAX)
          GO TO 33
   31     FLAST=F1(J,1)
          XLAST=X1(J,1)
          YLAST=Y1(J,1)
   33     CONTINUE
          F1(J+1,1)=FLAST+SQRT((Y1(J+1,1)-YLAST)**2+ (X1(J+1,1)-XLAST)**2)
   30     CONTINUE
          DO 34 I=1,NV
   34     F(I,NHP1)=F1(NHP1,1)
C     INPUT OF INITIAL VALUES OF F(I,J)
          IF(NTRY.GT.0)GO TO 39
          DO 40 I=1,NVP1
          DO 40 J=1,NHP1
   40     F(I,J)=0.
          DO 41 J=NSP,NHP1
          DO 41 I=1,NV
   41     F(I,J)=F1(J,1)
          DO 42 I=NJV,NVP1
          DO 42 J=1,NSP
          AI=I
   42     F(I,J)=-(AI-ANJV)*DY2
          DO 43 J=1,NHP1
   43     FS(J)=F(1,J)
   39     CONTINUE
          L=0
          IF(NTRY.LT.ICOM)GO TO 521
C     DETERMINATION OF LCASE(I,J)
          EPS=1.E-7
          DO 531 I=1,NVP1
          DO 531 J=1,NHP1
          LCASE(I,J)=9
          DIFX=ABS(DXR(I,J)-DXL(I,J))
          DIFY=ABS(DYD(I,J)-DYU(I,J))
          IF(DIFX.LT.EPS.AND.DIFY.LT.EPS)GO TO 522
          IF(DIFX.GE.EPS.AND.DIFY.GE.EPS)GO TO 554
          IF(DYU(I,J).LE.DYD(I,J)-EPS)LCASE(I,J)=1
          IF(DYD(I,J).LE.DYU(I,J)-EPS)LCASE(I,J)=5
          IF(DXR(I,J).LE.DXL(I,J)-EPS)LCASE(I,J)=3
          IF(DXL(I,J).LE.DXR(I,J)-EPS)LCASE(I,J)=7
          GO TO 522
  554     IF(DYU(I,J).LE.DYD(I,J)-EPS)GO TO 555
          IF(DXR(I,J).LE.DXL(I,J)-EPS)LCASE(I,J)=4
          IF(DXL(I,J).LE.DXR(I,J)-EPS)LCASE(I,J)=6
          GO TO 522
  555     IF(DXR(I,J).LE.DXL(I,J)-EPS)LCASE(I,J)=2
          IF(DXL(I,J).LE.DXR(I,J)-EPS)LCASE(I,J)=8
```

```
  522      CONTINUE
C     DETERMINATION OF SPACING FOR COMPRESSIBLE CASE
         LCIJ=LCASE(I,J)
         GO TO (523,524,525,526,527,528,529,530,531),LCIJ
  523    DYUR(I,J)=DYU(I,J)/DYD(I,J)
         DYD(I,J)=DYU(I,J)
         GO TO 531
  524    DYUR(I,J)=DYU(I,J)/DYD(I,J)
         DXRR(I,J)=DXR(I,J)/DXL(I,J)
         DYD(I,J)=DYU(I,J)
         DXL(I,J)=DXR(I,J)
         GO TO 531
  525    DXRR(I,J)=DXR(I,J)/DXL(I,J)
         DXL(I,J)=DXR(I,J)
         GO TO 531
  526    DYDR(I,J)=DYD(I,J)/DYU(I,J)
         DXRR(I,J)=DXR(I,J)/DXL(I,J)
         DYU(I,J)=DYD(I,J)
         DXL(I,J)=DXR(I,J)
         GO TO 531
  527    DYDR(I,J)=DYD(I,J)/DYU(I,J)
         DYU(I,J)=DYD(I,J)
         GO TO 531
  528    DYDR(I,J)=DYD(I,J)/DYU(I,J)
         DXLR(I,J)=DXL(I,J)/DXR(I,J)
         DYU(I,J)=DYD(I,J)
         DXR(I,J)=DXL(I,J)
         GO TO 531
  529    DXLR(I,J)=DXL(I,J)/DXR(I,J)
         DXR(I,J)=DXL(I,J)
         GO TO 531
  530    DYUR(I,J)=DYU(I,J)/DYD(I,J)
         DXLR(I,J)=DXL(I,J)/DXR(I,J)
         DYD(I,J)=DYU(I,J)
         DXR(I,J)=DXL(I,J)
  531    CONTINUE
  521    CONTINUE
C     SAVE VALUES OF F(I,J)
   53    CONTINUE
         DO 54 I=1,NVP1
         DO 54 J=1,NHP1
   54    FO(I,J)=F(I,J)
C     ITERATION ON F(I,J)
C     POINTS ON THE PLATE
         DO 212 J=1,NHP1
         ISJ=IS(J)
         JSJ=JS(J)
  212    FS(J)=F(ISJ,JSJ)+DXS(J)*(F(ISJ,JSJ+1)-F(ISJ,JSJ))
         IF(I1L.EQ.2)GO TO 213
         DO 214 I=2,I1LM1
         JL=NHS(I)-1
  214    FSXL(I)=FS(JL)+(XSL(I)-X(JL))/(X(JL+1)-X(JL))*(FS(JL+1)-FS(JL))
  213    IF(I1.EQ.2)GO TO 216
         DO 215 I=2,I1M1
         JL=NHPP(I)
  215    FSX(I)=FS(JL)+(XS(I)-X(JL))/(X(JL+1)-X(JL))*(FS(JL+1)-FS(JL))
  216    CONTINUE
C     INTERIOR POINTS
         DO 47 I=2,NV
         F(I,1)=F(I,2)
         IF(LS.EQ.0)GO TO 330
         DY=DY1
         IF(I.EQ.NJV)DY=.5*(DY1+DY2)
         IF(I.GT.NJV)DY=DY2
         VY=(F(I+1,1)-F(I-1,1))/(2.*DY)
         IF(I.EQ.I1L)VY=((F(I+1,1)-F(I,1))/DY1)
```

```
      ANGLE(I,1)=-90.
      V(I,1)=ABS(VY)
330   CONTINUE
      JLAST=NHP(I)
      IF(I.EQ.NJV)JLAST=NSPM1-1                                          128
      IF(NHP2(I).NE.0)JLAST=NH
      JFIRST=NHS(I)
      DO 48 J=JFIRST,JLAST
      IF(I.LT.NJV.OR.I.GE.NSTP1)GO TO 580
      IF(J.GT.NSPM1.AND.J.LT.NHP2(I))GO TO 48
580   CONTINUE
      IF(I.EQ.NJV.AND.J.EQ.NSPM1)GO TO 48
      FR=F(I,J+1)
      FL=F(I,J-1)
      FU=F(I+1,J)
      FD=F(I-1,J)
      FUR=F(I+1,J+1)
      FUL=F(I+1,J-1)
      FDR=F(I-1,J+1)
      FDL=F(I-1,J-1)
      IF((Y(I)-YS(J)).LT.DY1)FD=FS(J)
      IF(J.EQ.NHS(I).AND.I.LT.I1L)FL=FSXL(I)
      IF(NHP2(I).EQ.0)GO TO 49
      K=I-NVP(J-1)+1
      IF(J.EQ.NHP2(I))FL=F1(J-1,K)
49    CONTINUE
      IF(I.EQ.NV)GO TO 75
      IF(I.EQ.NVP(J))FU=F1(J,1)
75    CONTINUE
      IF(I.GT.I1)GO TO 50
      IF(J.GT.NHPP(I-1).AND.J.LE.NHPP(I))FD=FS(J)
      IF(I.EQ.2.AND.J.LE.NHPP(I))FD=FS(J)
      IF(I.EQ.I1)GO TO 59
      IF(J.EQ.NHPP(I))FR=FSX(I)
50    CONTINUE
      IF(J.EQ.NH)GO TO 59
      IF(I.GE.NJV)GO TO 59
      K=NVP(J)+2-I
      IF(J.EQ.NHP(I).AND.I.GT.NVPMIN)FR=F1(J,K)
59    CONTINUE
      IF(NTRY.LT.ICOM)GO TO 551
C     DETERMINE SURROUNDING POTENTIALS FOR COMPRESSIBLE CASE
      LCIJ=LCASE(I,J)
      GO TO (533,534,535,536,537,538,539,540,532),LCIJ
533   FD=FD+(1.-DYUR(I,J))*(F(I,J)-FD)
      FDL=FDL+(1.-DYUR(I,J))*(FL-FDL)
      GO TO 532
534   FTEMP=FDL+(1.-DXRR(I,J))*(FD-FDL)
      FD=FD+(1.-DYUR(I,J))*(F(I,J)-FD)
      FL=FL+(1.-DXRR(I,J))*(F(I,J)-FL)
      FDL=FTEMP+(1.-DYUR(I,J))*(FL-FTEMP)
      GO TO 532
535   FL=FL+(1.-DXRR(I,J))*(F(I,J)-FL)
      FUL=FUL+(1.-DXRR(I,J))*(FU-FUL)
      GO TO 532
536   FTEMP=FUL+(1.-DXRR(I,J))*(FU-FUL)
      FU=FU+(1.-DYDR(I,J))*(F(I,J)-FU)
      FL=FL+(1.-DXRR(I,J))*(F(I,J)-FL)
      FUL=FTEMP+(1.-DYDR(I,J))*(FL-FTEMP)
      GO TO 532
537   FU=FU+(1.-DYDR(I,J))*(F(I,J)-FU)
      FUR=FUR+(1.-DYDR(I,J))*(FR-FUR)
      GO TO 532
538   FTEMP=FUR+(1.-DXLR(I,J))*(FU-FUR)
      FU=FU+(1.-DYDR(I,J))*(F(I,J)-FU)
      FR=FR+(1.-DXLR(I,J))*(F(I,J)-FR)
```

```
      FUR=FTEMP+(1.-DYDR(I,J))*(FR-FTEMP)
      GO TO 532
  539 FR=FR+(1.-DXLR(I,J))*(F(I,J)-FR)
      FDR=FDR+(1.-DXLR(I,J))*(FD-FDR)
      GO TO 532
  540 FTEMP=FDR+(1.-DXLR(I,J))*(FD-FDR)
      FR=FR+(1.-DXLR(I,J))*(F(I,J)-FR)
      FD=FD+(1.-DYUR(I,J))*(F(I,J)-FD)
      FDR=FTEMP+(1.-DYUR(I,J))*(FR-FTEMP)
  532 CONTINUE
C     CALCULATION OF POTENTIALS FOR COMPRESSIBLE CASE
      FER=.5*(FR-FL)/DXR(I,J)
      FEZ=.5*(FU-FD)/DYD(I,J)
      VS=CZERO**2-(AK-1.)*.5*(FER**2+FEZ**2)
      VSS(I,J)=VS
      G1=1.-FER*FER/VSS(I,J)
      G2=1.-FEZ*FEZ/VSS(I,J)
      G3=2.*FER*FEZ/VSS(I,J)
      G4=FER/X(J)
      T1=G1*(FR+FL)/DXR(I,J)**2+G2*(FU+FD)/DYD(I,J)**2+G4
      T2=G1*2./DXR(I,J)**2+G2*2./DYD(I,J)**2
      DXDDY=1./DXR(I,J)/DYD(I,J)
      LCIJ=LCASE(I,J)
      GO TO (542,543,544,545,546,547,548,549,550),LCIJ
  542 CONTINUE
  543 T1=T1-G3*(FDL-FL-FD)*DXDDY
      T2=T2+G3*DXDDY
      GO TO 541
  544 CONTINUE
  545 T1=T1-G3*(FU-FUL+FL)*DXDDY
      T2=T2-G3*DXDDY
      GO TO 541
  546 CONTINUE
  547 T1=T1-G3*(FUR-FU-FR)*DXDDY
      T2=T2+G3*DXDDY
      GO TO 541
  548 CONTINUE
  549 T1=T1-G3*(FR+FD-FDR)*DXDDY
      T2=T2-G3*DXDDY
      GO TO 541
  550 T1=T1-G3*(FUR-FUL+FDL-FDR)/4.*DXDDY
  541 CONTINUE
      F(I,J)=T1/T2
      GO TO 552
  551 CONTINUE
      T=2./(DXL(I,J)+DXR(I,J))*(1./DXR(I,J)+1./DXL(I,J))+2./(DYU(I,J)+
     1 DYD(I,J))*(1./DYU(I,J)+1./DYD(I,J))+.5*(1./DXR(I,J)-1./DXL(I,J))
     1 /X(J)
      F(I,J)=(2./(DXL(I,J)+DXR(I,J))*(FR/DXR(I,J)+FL/DXL(I,J))+2./
     1 (DYU(I,J)+DYD(I,J))*(FU/DYU(I,J)+FD/DYD(I,J))+.5*(FR/DXR(I,J)-
     1 FL/DXL(I,J))/X(J))/T
  552 CONTINUE
      IF(LS.EQ.0)GO TO 48
      VX=(FR-FL)/(DXR(I,J)+DXL(I,J))
      VY=(FU-FD)/(DYU(I,J)+DYD(I,J))
      ANGT=ATAN2(VY,VX)
      ANGLE(I,J)=ANGT*180./3.1415926
      V(I,J)=SQRT(VX*VX+VY*VY)
   48 CONTINUE
      IF(Y(I).GT.Y2.AND.Y(I).LT.Y3)GO TO 52
      IF(I.LE.NJV)GO TO 47
      F(I,NSP)=F(I,NSPM1)
      IF(LS.EQ.0)GO TO 331
      DY=DY1
      IF(I.EQ.NSP)DY=.5*(DY1+DY2)
      IF(I.GT.NSP)DY=DY2
```

```
      VY=(F(I+1,NSP)-F(I-1,NSP))/(2.*DY)
      ANGLE(1,NSP)=-90.
      V(I,NSP)=ABS(VY)
  331 CONTINUE
      GO TO 47
   52 SL1=(Y2-YS(NH))/DX2
      SL2=(Y1(NHP1,1)-Y1(NH,1))/DX2
      SL3=SL1+(SL2-SL1)*(Y(I)-Y2)/(Y1(NHP1,1)-Y2)
      SLAV=(SL1+SL2)*.5
      REFF2=(1.+SLAV/SQRT(1.+SLAV**2))/(1.+SL1/SQRT(1.+SL1**2))
      VEL=SQRT(1./(1.+SL3*SL3))
      IF(LS.EQ.0)GO TO 332
      V(1,NHP1)=1.
      ANG=ATAN(SL3)
      ANGLE(I,NHP1)=ANG*180./3.1415926
  332 CONTINUE
      F(I,NHP1)=F(I,NH)+VEL*DX2
      IF(NHP1.NE.NHP2(I))GO TO 47
      K=I-NVP(NH)+1
      F(I,NHP1)=F1(NH,K)+VEL*DXL(I,NHP1)
   47 CONTINUE
      DO 76 J=1,NSP
   76 F(NV,J)=F(NV,NSP2)
      SUM=0.
      DY=.5*(DY1+DY2)
      DO 73 J=2,NSP
   73 SUM=SUM+(F(NJVM1,J)-F(NJVP1,J)+F(NJVM1,J-1)-F(NJVP1,J-1))*.25/DY
     1*3.1415926*(X(J)*X(J)-X(J-1)*X(J-1))
      VAV=SUM/X(NSP)**2/3.1415926
      TMAX=2.*3.1415926*X(NSP)**2*VAV*VAV
      IF(NTRY.LT.ICOM)GO TO 594
      VS=CZERO**2-(AK-1.)*.5*VAV**2
      AMS=VAV**2/VS
      RHO=RHOT/(1.+(AK-1.)*.5*AMS)**(1./(AK-1.))
      TMAX=2.*3.1415926*X(NSP)**2*(VAV*VNORM)**2*RHO/32.2
  594 CONTINUE
      VAVJ=VAV
      FTOP=F(NV,NSP2)-VAV*DY2
      DO 74 J=1,NSP
   74 F(NVP1,J)=FTOP
      IF(LS.EQ.0)GO TO 334
      DO 333 J=1,NSP
      ANGLE(NVP1,J)=-90.
  333 V(NVP1,J)=(F(NV,J)-F(NVP1,J))/DY2
      IF(LS.EQ.1)GO TO 401
  334 CONTINUE
C     CRITERION FOR CONVERGENCE
      DO 55 I=1,NVP1
      DO 55 J=1,NHP1
      DIF=ABS(FO(I,J)-F(I,J))
      IF(DIF.GE.(FACTOR*F1(NH,1)))GO TO 56
   55 CONTINUE
      GO TO 57
   56 L=L+1
      GO TO 53
   57 CONTINUE
      WRITE(6,131)
  131 FORMAT(1H1,///,5X,'ROUND JET IMPINGING ON CURVED DEFLECTOR')
      WRITE(6,134)AL1,AL2
  134 FORMAT(5X,'JET RADIUS =',F5.3,18X,'DUCT LENGTH =',F5.3)
      WRITE(6,135)AL3,AL4
  135 FORMAT(5X,'JET CLEARANCE =',F5.3,15X,'PLATE RADIUS =',F5.3)
      WRITE(6,6100)AMACH
 6100 FORMAT(5X,'MACH NUMBER =', F4.2)
      WRITE(6,133)
  133 FORMAT(/,27X,'VALUES OF VELOCITY POTENTIAL',/)
```

```
      WRITE(6,2000)
2000  FORMAT(7X,'Y')
 401  IF(LS.EQ.0)GO TO 321
      V(NJV,NSP)=1.
      ANGLE(NJV,NSP)=-90.
      NL=NSP-2
      DX=DX1
      VX=(F(NJV,NSP)-F(NJV,NL))/2./DX
      DY=.5*(DY1+DY2)
      VY=(F(NJVP1,NSPM1)-F(NJVM1,NSPM1))/2./DY
      ANGT=ATAN2(VY,VX)
      ANGLE(NJV,NSPM1)=ANGT*180./3.1415926
      V(NJV,NSPM1)=SQRT(VX*VX+VY*VY)
      WRITE(6,322)
 322  FORMAT(1H1,///,10X,'LOCAL VELOCITIES',/)
      DO 560 I=1,NVP1
      DO 560 J=1,NHP1
 560  V(I,J)=V(I,J)*VNORM
      WRITE(6,2000)
 321  CONTINUE
      DO 58 I=1,NV
      M=NVP1-I+1
      NLAST=NHP(M)
      IF(M.LE.NVP(NHP1).AND.M.GE.I1)NLAST=NHP1
      IF(M.LT.I1.AND.M.GT.NVPMIN)NLAST=NHPP(M)
      IF(M.GE.NJV)NLAST=NHP(M)+1
      IF(M.EQ.1)NLAST=1
      NFIRST=1
      IF(M.LT.I1L)NFIRST=NHS(M)
      N9=NFIRST-1
      IF(NHP2(M).NE.0)GO TO 79
      IF(LS.EQ.1)GO TO 323
      WRITE(6,126)Y(M),N9,(F(M,J),J=NFIRST,NLAST)
 126  FORMAT(5X,F5.3,3X,N(5X),21F5.2)
      GO TO 58
 323  WRITE(6,324)Y(M),N9,(V(M,J),J=NFIRST,NLAST)
 324  FORMAT(5X,F5.3,3X,N(6X),19F6.0)
      WRITE(6,325)N9,(ANGLE(M,J),J=NFIRST,NLAST)
 325  FORMAT(13X,N(6X),19F6.1)
      GO TO 58
  79  N5=NHP(M)
      N10=NHP(M)
      IF(M.LT.I1L)N10=NHP(M)-N9
      N6=NHP2(M)
      N7=N6-N5-1
      N8=NLAST-N6+1
      IF(LS.EQ.1)GO TO 326
      IF(N7.LT.0.OR.N8.LT.0)GO TO 58
      IF(N9.LT.0.OR.N10.LT.0)GO TO 58
      WRITE(6,138)Y(M),N9,N10,(F(M,J),J=NFIRST,N5),N7,N8,(F(M,J),J=N6,
     1 NLAST)
 138  FORMAT(5X,F5.3,3X,N(5X),NF5.2,N(5X),NF5.2)
      GO TO 58
 326  WRITE(6,327)Y(M),N9,N10,(V(M,J),J=NFIRST,N5),N7,N8,(V(M,J),J=N6,
     1 NLAST)
 327  FORMAT(5X,F5.3,3X,N(6X),NF6.0,N(6X),NF6.0)
      WRITE(6,328)N9,N10,(ANGLE(M,J),J=NFIRST,N5),N7,N8,(ANGLE(M,J),
     1 J=N6,NLAST)
 328  FORMAT(13X,N(6X),NF6.1,N(6X),NF6.1)
  58  CONTINUE
      IF(LS.EQ.1)GO TO 2003
      WRITE(6,2001)(X(I),I=1,NHP1)
2001  FORMAT(/,7X,'X',5X,21F5.2)
      GO TO 2004
2003  WRITE(6,2002)(X(I),I=1,NHP1)
2002  FORMAT(/,7X,'X',5X,19F6.3)
```

```
      IF(LS.EQ.1)GO TO 999
 2004 CONTINUE
      WRITE(6,101)
  101 FORMAT(//,10X,'LOCATION OF FREE STREAMLINE')
      WRITE(6,102)                                                    132
  102 FORMAT(//,13X,'X',13X,'Y')
      WRITE(6,103)(X(J),Y1(J,1),J=NSP,NHP1)
  103 FORMAT(11X,F5.3,8X,F6.3)
C     CALCULATION OF BOUNDARY PRESSURES
C     PRESSURE ALONG PLATE
      IF(NTRY.LT.ICOM)GO TO 595
      PP(1)=PTOT
      DO 596 J=2,NH
      DX=DX1
      IF(J.EQ.NSP)DX=.5*(DX1+DX2)
      IF(J.GT.NSP)DX=DX2
      DIST=SQRT(DX**2+((YS(J+1)-YS(J-1))*.5)**2)
      V1S=((FS(J+1)-FS(J-1))*.5/DIST)**2
      VS=CZERO**2-(AK-1.)*.5*V1S
      AMS=V1S/VS
  596 PP(J)=PTOT/(1.+(AK-1.)*.5*AMS)**(AK/(AK-1.))
      PP(NHP1)=PSTAT
      GO TO 597
  595 CONTINUE
      PP(1)=1.
      DO 60 J=2,NH
      DX=DX1
      IF(J.EQ.NSP)DX=.5*(DX1+DX2)
      IF(J.GT.NSP)DX=DX2
      DIST=SQRT(DX**2+((YS(J+1)-YS(J-1))*.5)**2)
   60 PP(J)=1.-((FS(J+1)-FS(J-1))*.5/DIST)**2
      PP(NHP1)=0.
  597 CONTINUE
      SUM=0.
      IF(NTRY.LT.ICOM)GO TO 593
      DO 601 J=2,NHP1
  601 SUM=SUM+((PP(J)+PP(J-1))*.5-PSTAT)*3.1415926*(X(J)*X(J)-X(J-1)*
     1 X(J-1))
      GO TO 602
  593 CONTINUE
      DO 77 J=2,NHP1
   77 SUM=SUM+(PP(J)+PP(J-1))*.5*3.1415926* (X(J)*X(J)-X(J-1)*X(J-1))
  602 CONTINUE
      TIDEAL=1.+1./SQRT(1.+(1./SL1)**2)
C     PRESSURE ALONG SYMMETRY LINE
      I1LP1=I1L+1
      IF(NTRY.LT.ICOM)GO TO 598
      DO 599 I=I1LP1,NV
      DY=DY1
      IF(I.EQ.NJV)DY=.5*(DY1+DY2)
      IF(I.GT.NJV)DY=DY2
      V1S=((F(I-1,1)-F(I+1,1))*.5/DY)**2
      VS=CZERO**2-(AK-1.)*.5*V1S
      AMS=V1S/VS
  599 PSL(I)=PTOT/(1.+(AK-1.)*.5*AMS)**(AK/(AK-1.))
      TACT=SUM-(PSL(NV)-PSTAT)*3.1415926*X(NSP)*X(NSP)
      GO TO 600
  598 CONTINUE
      DO 61 I=I1LP1,NV
      DY=DY1
      IF(I.EQ.NJV)DY=.5*(DY1+DY2)
      IF(I.GT.NJV)DY=DY2
   61 PSL(I)=1.-((F(I-1,1)-F(I+1,1))/2./DY)**2
      TACT=SUM-PSL(NV)*3.1415926*X(NSP)*X(NSP)
      TACT=TACT*.5
  600 CONTINUE
```

```
      REFF=TACT*2./TMAX/TIDEAL
      WRITE(6,128)
  128 FORMAT(1H1,//,10X,'LOCATION OF PLATE',15X,'PRESSURE ALONG PLATE')
      WRITE(6,129)
  129 FORMAT(//,11X,'X',13X,'Y',18X,'X',12X,'PRESSURE')                  133
      IF(NTRY.LT.ICOM)GO TO 592
      DO 590 J=1,NHP1
  590 PP(J)=(PP(J)-PSTAT)/(PTOT-PSTAT)
  592 CONTINUE
      WRITE(6,130)(X(J),YS(J),X(J),PP(J),J=1,NHP1)
  130 FORMAT(8X,F5.3,7X,F7.5,14X,F5.3,12X,F5.3)
      WRITE(6,113)
  113 FORMAT(///,10X,'PRESSURE ALONG SYMMETRY LINE')
      WRITE(6,124)
  124 FORMAT(/,14X,'Y',10X,'PRESSURE')
      IF(NTRY.LT.ICOM)GO TO 603
      DO 591 I=I1LP2,NV
  591 PSL(I)=(PSL(I)-PSTAT)/(PTOT-PSTAT)
  603 CONTINUE
      WRITE(6,114)(Y(I),PSL(I),I=I1LP2,NV)
  114 FORMAT(11X,F5.3,10X,F5.3)
      WRITE(6,127)REFF,REFF2
  127 FORMAT(//,10X,'TURNING EFFECTIVENESS 1 =',F5.3,10X,
     1 'TURNING EFFECTIVENESS 2 =',F5.3)
      WRITE(6,152)L
  152 FORMAT(////,10X,'L = ',I4)
C     ADJUSTMENT OF FREE BOUNDARY
      SL2P=-100.
      YN(NSP,1)=AL3
      DO 62 J=NSPP1,NH
      FB=F1(J,1)
      SL1=(Y1(J+1,1)-Y1(J-1,1))*.5/DX2
      NVPJ=NVP(J)
      NVPJ1=NVPJ+1
      FL=F(NVPJ1,J-1)
      FR=F(NVPJ1,J+1)
      DY3=DY1
      DY4=DY1
      IF(FB.GT.F(NVPJ,J))GO TO 63
      IF(NVP(J-1).NE.NVP(J))GO TO 64
      FL=F1(J-1,1)
      DY3=Y1(J-1,1)-Y(NVPJ)
   64 CONTINUE
      IF(FB.GT.F(NVPJ,J-1))GO TO 65
      YT=DY3*(F(NVPJ,J-1)-FB)/(F(NVPJ,J-1)-FL)
      DYY=Y1(J,1)-Y(NVPJ)-YT
      DXX=DX2
      GO TO 66
   65 CONTINUE
      DYY=Y1(J,1)-Y(NVPJ)
      X11=DX2*(FB-F(NVPJ,J-1))/(F(NVPJ,J)-F(NVPJ,J-1))
      DXX=DX2-X11
      GO TO 66
   63 CONTINUE
      IF(NVP(J+1).NE.NVP(J))GO TO 67
      FR=F1(J+1,1)
      DY4=Y1(J+1,1)-Y(NVPJ)
   67 CONTINUE
      IF(FB.LT.F(NVPJ,J+1))GO TO 68
      YT=DY4*(F(NVPJ,J+1)-FB)/(F(NVPJ,J+1)-FR)
      DYY=Y1(J,1)-Y(NVPJ)-YT
      DXX=-DX2
      GO TO 66
   68 DYY=Y1(J,1)-Y(NVPJ)
      X11=DX2*(FB-F(NVPJ,J))/(F(NVPJ,J+1)-F(NVPJ,J))
      DXX=-X11
```

```
 66     CONTINUE
        SL2=-DXX/DYY
        IF(SL2.LT.SL2P)SL2=SL2P
        SL2P=SL2
        IF(J.LE.(NSP+2))GO TO 69
        YN(J,1)=YN(J-1,1)+SL2*DX2
        GO TO 62
 69     YN(J,1)=YN(J-1,1)+SL2/SL1*(Y1(J,1)-Y1(J-1,1))
        YN(J,1)=(YN(J,1)+Y1(J,1))*.5
        IF(YN(J,1).GT.YN(J-1,1))YN(J,1)=YN(J-1,1)
 62     CONTINUE
        YN(NHP1,1)=YN(NH,1)+(YN(NH,1)-YN(NHM1,1))
        SL3=(YS(NHP1)-YS(NH))/DX2
        SL4=(YN(NHP1,1)-YN(NH,1))/DX2
        IF(SL4.LT.0.)SL4=0.
        SL5=.5*(SL3+SL4)
        V3=(FS(NHP1)-FS(NH))/SQRT(DX2**2+(YS(NHP1)-YS(NH))**2)
        VAV=(1.+V3)*.5
        VAV=VAV*DX2/SQRT(DX2**2*(1.+SL5*SL5))
        Y3=Y2+.5*VAVJ*X(NSP)*X(NSP)/VAV/X(NHP1)
        DO 70 J=NSPP1,NHP1
 70     YN(J,1)=YN(J,1)+(Y3-YN(NHP1,1))*(J-NSP)/(NHP1-NSP)
        DO 71 J=NSPP1,NHP1
 71     Y1(J,1)=YN(J,1)
        NTRY=NTRY+1
        IF(NTRY.GE.ISTOP) GO TO 99
        L=0
        GO TO 72
 99     CONTINUE
        LS=1
        GO TO 53
999     STOP
        END
```

ROUND JET IMPINGING ON CURVED DEFLECTOR
JET RADIUS =1.000 DUCT LENGTH =1.000
JET CLEARANCE =1.000 PLATE RADIUS =2.000
MACH NUMBER = .50

VALUES OF VELOCITY POTENTIAL

Y											
2.000	-.76	-.76	-.76	-.76	-.76						
1.875	-.67	-.67	-.67	-.67	-.67						
1.750	-.58	-.58	-.58	-.58	-.58						
1.625	-.49	-.49	-.49	-.48	-.48						
1.500	-.40	-.40	-.39	-.39	-.39						
1.375	-.31	-.31	-.30	-.30	-.30						
1.250	-.22	-.22	-.21	-.20	-.20						
1.125	-.13	-.13	-.12	-.10	-.10						
1.000	-.05	-.05	-.04	.00	.00						
.933	-.01	-.01	.01	.04	.07						
.867	.03	.03	.05	.09	.13						
.800	.06	.06	.08	.13	.19						
.733	.09	.09	.12	.17	.24						
.667	.13	.13	.15	.20	.28	.37					1.23
.600	.15	.15	.18	.23	.32	.41				1.06	1.20
.533	.18	.18	.21	.26	.35	.45	.57	.73	.89	1.03	1.17
.467	.20	.20	.23	.29	.38	.47	.59	.73	.88	1.01	
.400	.22	.22	.25	.31	.40	.49	.60	.73	.86	.98	
.333	.24	.24	.27	.32	.41	.50	.60	.72	.84		
.267	.25	.25	.28	.34	.42	.50	.60	.71			
.200	.26	.26	.29	.34	.43	.51	.60				
.133	.26	.26	.29	.35	.43	.50					
.067	.27	.27	.30	.35							
X	.00	.25	.50	.75	1.00	1.17	1.33	1.50	1.67	1.83	2.00

LOCATION OF FREE STREAMLINE

X	Y
1.000	1.000
1.167	.674
1.333	.571
1.500	.567
1.667	.600
1.833	.665
2.000	.730

LOCATION OF PLATE

X	Y
.000	.00000
.250	.00523
.500	.02113
.750	.04844
1.000	.08856
1.167	.12361
1.333	.16667
1.500	.21967
1.667	.28602
1.833	.37269
2.000	.50000

PRESSURE ALONG PLATE

X	PRESSURE
.000	1.000
.250	.997
.500	.974
.750	.932
1.000	.870
1.167	.770
1.333	.670
1.500	.553
1.667	.455
1.833	.336
2.000	.000

PRESSURE ALONG SYMMETRY LINE

Y	PRESSURE
.200	.987
.267	.973
.333	.955
.400	.932
.467	.905
.533	.874
.600	.840
.667	.804
.733	.766
.800	.728
.867	.689
.933	.652
1.000	.602
1.125	.560
1.250	.519
1.375	.492
1.500	.475
1.625	.465
1.750	.459
1.875	.454

TURNING EFFECTIVENESS 1 = 1.116 TURNING EFFECTIVENESS 2 = .933

L = 68

LOCAL VELOCITIES

Y											
2.000	418.	418.	418.	418.	418.						
	-90.0	-90.0	-90.0	-90.0	-90.0						
1.875	417.	417.	418.	420.	420.						
	-90.0	-90.0	-90.0	-90.0	-90.0						
1.750	415.	415.	416.	422.	422.						
	-90.0	-89.9	-89.8	-89.9	-90.0						
1.625	413.	413.	418.	423.	423.						
	-90.0	-89.7	-89.5	-89.7	-90.0						
1.500	409.	409.	416.	426.	426.						
	-90.0	-89.5	-89.0	-89.5	-90.0						
1.375	402.	402.	413.	430.	430.						
	-90.0	-89.2	-88.3	-89.1	-90.0						
1.250	391.	391.	408.	438.	438.						
	-90.0	-88.7	-87.0	-88.4	-90.0						
1.125	374.	374.	396.	452.	452.						
	-90.0	-87.9	-84.8	-87.2	-90.0						
1.000	356.	356.	381.	428.	564.						
	-90.0	-86.9	-80.9	-84.6	-90.0						
.933	332.	333.	355.	368.	547.						
	-90.0	-86.3	-79.8	-79.3	-83.3						
.867	314.	315.	337.	368.	513.						
	-90.0	-85.6	-78.4	-75.5	-77.2						
.800	294.	296.	318.	360.	483.						
	-90.0	-85.0	-76.6	-71.6	-71.1						
.733	273.	274.	298.	345.	454.						
	-90.0	-84.1	-74.4	-67.6	-64.6						
.667	250.	252.	276.	325.	424.	476.					564.
	-90.0	-83.2	-71.8	-63.3	-57.3	-49.3					27.0
.600	225.	228.	253.	302.	387.	483.				540.	564.
	-90.0	-82.1	-68.9	-58.8	-51.3	-40.7				19.8	31.4
.533	200.	203.	229.	277.	350.	445.	504.	531.	524.	513.	564.
	-90.0	-80.7	-65.4	-53.8	-45.1	-32.7	-17.3	-1.6	10.5	21.0	35.5
.467	174.	177.	204.	252.	316.	397.	454.	484.	487.	477.	
	-90.0	-79.1	-61.4	-48.4	-38.5	-26.3	-13.6	.6	12.1	22.2	
.400	147.	151.	179.	228.	285.	359.	413.	448.	443.	478.	
	-90.0	-76.9	-56.5	-42.3	-31.5	-19.7	-8.1	4.0	13.6	31.9	
.333	119.	124.	156.	205.	259.	328.	381.	409.	436.		
	-90.0	-74.0	-50.4	-35.3	-23.9	-12.8	-2.4	8.1	24.3		
.267	92.	98.	134.	185.	237.	304.	350.	389.			
	-90.0	-69.6	-42.5	-27.2	-15.7	-5.4	4.3	17.8			
.200	65.	73.	115.	168.	219.	281.	327.				
	-90.0	-62.4	-32.4	-18.0	-3.9	2.4	12.5				
.133	38.	51.	98.	154.	208.	256.					
	-90.0	-48.7	-14.1	-6.6	4.4	8.3					
.067	25.	35.	93.	137.							
	-90.0	-21.6	-4.8	.2							
X	.000	.250	.500	.750	1.000	1.167	1.333	1.500	1.667	1.833	2.000

TOP

REFERENCES

1. Tatom, J. W., et al. "A Study of Jet Impingment on Curved Surfaces Followed by Oblique Introduction Into a Freestream Flow," First Annual Progress Report under NASA Grant NGR 43-002-034, Vanderbilt University, April 15, 1971.

2. Cooper, M.A. Temperature Field of the Two-Dimensional Transverse Hot Air Jet In a Freestream Flow, Masters Thesis, Vanderbilt University, December, 1971.

3. Hayden, T.K. Velocity Field of the Two-Dimensional Transverse Hot Air Jet in a Freestream Flow, Masters Thesis, Vanderbilt University, Spring, 1972.

4. Tatom, Frank B. Interaction of a Two-Dimensional Compressible, Turbulent Free Jet with a Crossflowing Freestream, Ph.D. Thesis, Georgia Institute of Technology, 1971.

5. Ivanov, Yu V. Effective Combustion of Overfire Fuel Gases in Furnaces, Estonian State Publishing House, Talling, 1959, English Translation recently completed by A. D. Little.

6. Heyser, A. and Maurer, F. "Experimental Investigation of Solid Spoilers and Jet Spoilers at Mach Numbers of 0.6 to 2.8," Zertshrift fur Flugwissenschaften, Vol. 10, No. 45, 1962; issued by Jet Propulsion Laboratory as Astronautics Information Translation No. 32, February 21, 1964.

7. Schlichting, H. Boundary-Layer Theory, McGraw-Hill Book Co., Inc., New York, 6th Edition, 1968, pp. 176-178 and 367-369.

8. Vizel, Ya M. and Mostinskii, I. L. "Deflection of a Jet Injected Into a Stream," Inzhenerno-Fizicheskii Zhurnal, Vol. 8, No. 2, pp. 238-242, 1965.

9. Abramovich, G. N. The Theory of Turbulent Jets, MIT Press, Cambridge, Massachusetts, 1963.

10. Keffer, J. F. and Baines, W. D. "The Round Turbulent Jet in a Cross-Wind," Journal of Fluid Mechanics, Vol. 15, 1963, pp. 481-496.

11. Robertson, J. M. Hydrodynamics in Theory and Application, Prentice Hall, 1965, pp. 299-309.

12. Smith, A.M.O., and Pierce, J. "Exact Solution of the Neumann Problem. Calculation of Non-Circulatory Plane and Axially Symmetric Flows About or Within Arbitrary Boundaries," Proc. Third U.S. National Congress on Applied Mechanics.

13. Tatom, F. B., et al. "Study Effect of Engine Ignition on Airflow Over Vehicle," Northrop Space Laboratories, Research and Analysis Section Tech. Memo #43, December, 1964.

14. Ledwith, Drew, Analysis of the Flow Field Generated Near an Aircraft Engine Operating in Reverse Thrust, Masters Thesis, Vanderbilt University, Spring, 1972.

15. Povolny, J. H., Steffen, Fred W., and McArdle, J. G. "Summary of Scale-Model Thrust-Reverser Investigation, NACA Report 1314, 1957.

16. Patankar, S. V. Heat and Mass Transfer in Turbulent Boundary Layers, Ph.D. Thesis, University of London, June, 1967.